ISSN 1925-542X [Print]
ISSN 1925-5438 [Online]

APED

Advances in Petroleum Exploration and Development

Volume 3
Number 1
31 March 2012

Peer Reviewed Journal

Canadian Research & Development Center of Sciences and Cultures
www.cscanada.net www.cscanada.org

Subscription Rates

Single Issue Prices (Institutions and Individuals)

In Canada	$80.00 (CAD)
Outside Canada	$80.00 (USD)

Advances in Petroleum Exploration and Development

ISSN 1925-542X [Print]
ISSN 1925-5438 [Online]

Frequency: Quarterly

First published on June 30th, 2011, ***Advances in Petroleum Exploration and Development*** is devoted to promoting the development of petroleum exploration and development, and builds the bridge between the geology and the engineering of petroleum and natural gas. APED covers the fields of petroleum geology, petroleum exploration and development in its broadest possible sense. It publishes peer-reviewed original scholarly high-quality work such as analytical, numerical, or experimental results and physical analysis of processes of lasting scientific value. Those pertaining to modeling, theory, analysis, simulations, technology development, experiments, visualization and measurement techniques are also appropriate for the journal. High-quality research papers are solicited in, but are not limited to.

Authors could send manuscripts by E-mail:
aped@cscanada.org aped@cscanada.net caooc@hotmail.com

Or send paper by post office to:
758, 77e AV, Laval, Quebec, H7V 4A8, Canada

For citation format, we require parenthetical citations within the text rather than endnotes or footnotes. Citation in the text provides information, usually the name of the author, the date of publication (the Author-Date System), and if need, the page number(s), to lead the reader to the accompanying full bibliographical entry in the reference list which is placed at the end of the research paper. We only accept the APA (American Psychological Association) style.

For details on manuscripts submissions, please see the Author Guidelines in our website:
Http://www.cscanada.org Http://www.cscanada.net

CSCanada
Advances in Petroleum Exploration and Development
Vol. 3, No. 1
March 31, 2012

ISSN 1925-542X [Print]
ISSN 1925-5438 [Online]
www.cscanada.net
www.cscanada.org

CONTENTS

CSCanada
Advances in Petroleum Exploration and Development
Vol. 3, No. 1, 2012, pp. 1-10
DOI:10.3968/j.aped.1925543820120301.152

ISSN 1925-542X [Print]
ISSN 1925-5438 [Online]
www.cscanada.net
www.cscanada.org

Hybrid Forecasting Methods for Multi-Fractured Horizontal Wells: EUR Sensitivities

Morteza Nobakht[1,*]; Christopher Clarkson[1]

[1]University of Calgary, 2500 University Dr. NW, Calgary, Alberta, T2N 1N4, Canada.
*Corresponding author.

Received 16 January 2012; accepted 28 February 2012

Abstract

In this paper, the sensitivity of expected ultimate recovery (EUR) for horizontal wells with multiple fractures to decline exponent is studied using the simplified forecasting method introduced by Nobakht et al.[1]. This is very important from the reserves evaluation perspective due to uncertainty in decline exponent, *b*. This uncertainty is caused by many factors like desorption and reservoir/completion heterogeneity. It is found that in case of time-based forecast (duration of forecast is specified), the ratio of EURs for two different specified values of decline exponent depends on the ratio of economic life time of a well to the duration of linear flow. On the other hand, this EUR ratio depends on the ratio of rate at the end of linear flow to economic rate limit for economic limit-based forecast (economic rate limit is specified).

Key words: EUR sensitivities; Multi-fractured horizontal wells; Hybrid forecasting methods

Nobakht, M., & Clarkson, C.R. (2012). Hybrid Forecasting Methods for Multi-Fractured Horizontal Wells: EUR Sensitivities. *Advances in Petroleum Exploration and Development*, *3*(1), 1-10. Available from: URL: http://www.cscanada.net/index.php/aped/article/view/j.aped.1925543820120301.152
DOI: http://dx.doi.org/10.3968/j.aped.1925543820120301.152

Nomenclature

A = Drainage area, ft^2
b = Hyperbolic decline exponent, dimensionless
b' = Intercept of inverse gas rate versus square root of time plot, 1/(Mscf/D)
B_g = Gas formation volume factor, ft^3/scf
c_g = Gas compressibility, psi^{-1}
c_t = Total compressibility, psi^{-1}
D_{elf} = Decline rate at the end of linear flow, 1/day
D_i = Decline rate at the start of hyperbolic forecast, 1/day
EUR = Expected ultimate recovery, Mscf
h = Net pay thickness, ft
k = Permeability, mD
m = Slope of inverse gas rate versus square root of time plot, $day^{1/2}$/Mscf
n = The ratio of the rate at the end of linear flow to the economic rate limit
$OGIP$ = Original gas-in-place, Mscf
p = Pressure, psi
p_i = Initial pressure, psi
p_{pi} = Pseudopressure at initial pressure, psi^2/cp
p_{pwf} = Pseudopressure at flowing pressure, psi^2/cp
p_{wf} = Flowing pressure, psi
q = Gas rate, Mscf/D
q_i = Gas rate at the start of hyperbolic forecast, Mscf/D
q_D = Dimensionless rate, dimensionless
q_{Dd} = Dimensionless rate, dimensionless
$(q_{Dye})_{elf}$ = Dimensionless rate at the end of linear flow, dimensionless
q_{elf} = Gas rate at the end of linear flow, Mscf/D
Q = Gas cumulative production, Mscf
Q_{elf} = Gas cumulative production at the end of linear flow, Mscf
ΔQ = Volume of gas produced between the end of linear flow and end of forecast, Mscf
S_g = Gas saturation, fraction
t = Economic life of a well, days
t_{Dye} = Dimensionless time, dimensionless
$(t_{Dye})_{elf}$ = Dimensionless time at the end of linear flow, dimensionless
t_{elf} = Duration of linear flow, days
T = Reservoir temperature, $^\circ R$

x_e = Reservoir width, ft
x_f = Fracture half-length, ft
y_e = Reservoir length, ft
Z = Gas compressibility factor

Greek Symbols

γ_g = Reservoir gas specific gravity (air=1)
ϕ = Porosity, fraction
μ_g = Gas viscosity, cp

INTRODUCTION

Shale gas reservoirs have become a significant source of gas supply in North America owing to the advancement of drilling and stimulation techniques to enable commercial development. Production analysis and forecasting of shale gas wells is difficult due to complex reservoir behavior (ex. ultra-low matrix permeability, dual porosity or dual permeability behavior, heterogeneities at all scales, stress-dependent porosity and permeability etc.) and complex wellbore architectures and stimulation and completion methods. The most popular method for exploiting shale gas reservoirs today is the use of long horizontal wells completed with multiple-fracturing stages; the resulting, often complex, hydraulic fracture network can impart further complexity for production analysis and forecasting. Although rigorous methods to account for reservoir and hydraulic fracture network complexities in production data analysis and forecasting using numerical modeling approaches have been proposed[2], it is desirable to seek simpler methods for analysis and forecasting that can be used more routinely by the reservoir engineer.

Simple empirical methods such as Arps' decline curve method[3] have been used historically to forecast multi-fractured horizontal wells (MFHW). The Arps' method, where the rate profile is described by a constant *b*-value, is limited to cases where operating conditions are not changing and the well is in boundary-dominated flow. For tight formations, the transient flow may continue for a long time and therefore, Arps' decline may not be applicable to these formations. Stright and Gordon[4] studied the production decline curves of three low-permeability gas wells in Piceance basin and found that linear flow equations can be used to approximate long term production in these wells. To forecast rates during boundary-dominated flow, they suggested switching from the forecast based on linear flow projection to exponential decline when decline rate reaches a pre-determined value. Maley[5] studied the linear flow in tight formations and concluded that linear flow can be modeled using Arps decline using $b = 2$. Hale[6] analyzed the monthly production rates of more than 6000 hydraulically fractured gas wells located in low-permeability reservoirs. He compared exponential forecasting, logarithmic forecasting and linear flow forecasting. However, no method was defined on how to forecast rates during boundary-dominated flow. Wattenbarger et al.[7] also focused on linear flow as the flow regime that lasts for a long time in tight gas reservoirs. They used the reservoir geometry shown in Fig.1 and developed general solutions for linear flow. They proposed to use the constant productivity index during boundary-dominated flow. Kupchenko et al.[8] proposed using $b = 2$ to forecast during linear flow and switch to $b = 0.5$ during boundary-dominated flow. They determined the end of linear flow for a hydraulically-fractured (vertical) well, located in square reservoir geometry, based on assumed value for porosity and some assumption for gas properties. The power-law and the stretched exponential decline are new empirical methods introduced by Ilk et al.[9] and Valkó[10], respectively. These methods account for changing *b*-value with time. Due to number of parameters in these techniques, they produce non-unique forecasts[11]. Recently, a semi-empirical method was developed that models changing *b*-value with time in multi-fractured horizontal wells with unequal fracture half-lengths and/or non-uniform fracture spacing along horizontal well[12].

Recognizing that the flow regime most often observed in multi-fractured horizontal wells is linear flow, Nobakht et al.[1] developed a simplified forecasting method for horizontal wells with multiple fractures in tight/shale gas reservoirs. This semi-empirical method was developed assuming that the transient linear flow is the dominant flow-regime in horizontal wells with multiple fractures, which is a reasonable assumption. This flow regime may continue for several years, and will ultimately become boundary-dominated flow at much later times. This method combines the linear flow transient period with hyperbolic decline during boundary-dominated flow. The slope of the inverse gas rate versus square root of time plot is used to yield a forecast for transient linear flow and then applied the Arps' hyperbolic decline for boundary-dominated flow. A method for estimating the start of boundary-dominated flow was provided that does not rely on an estimate of matrix permeability (often elusive for tight formations because of the difficulty in measurement) or fracture half-length.

In this paper, first, the above-mentioned simplified forecasting method is briefly reviewed. Secondly, it is shown that for gas production under constant flowing pressure in a volumetric reservoir, at some point during depletion the decline exponent starts to deviate from 0.5. The time of this transition is correlated to permeability, porosity, gas properties and reservoir width. Thirdly, it is shown that ignoring this transition from $b = 0.5$ for forecasting is not affecting the forecast practically. Finally, the sensitivity of expected ultimate recovery to *b*-value is studied for both time-based and economic-limit based forecasts.

1. REVIEW OF SIMPLIFIED FORECASTING METHOD

The base reservoir geometry, for which the simplified forecasting method was developed, is shown in Fig. 1. The well is at the center of a rectangular reservoir and the fracture extends all the way to the lateral boundaries of the reservoir. This geometry was first used by Wattenbarger et al.[7] for modeling linear flow in tight gas reservoirs. This base geometry was chosen as it is reasonable to assume that drainage beyond the stimulated region is insignificant for ultra-low matrix permeability reservoirs. The constant flowing pressure solution was used by Nobakht et al.[1] for linear flow analysis, as in practice, tight gas and shale gas wells are produced under high drawdown to maximize production. The forecasting procedure using this simplified method of Nobakht et al.[1] follows the 7 steps below:

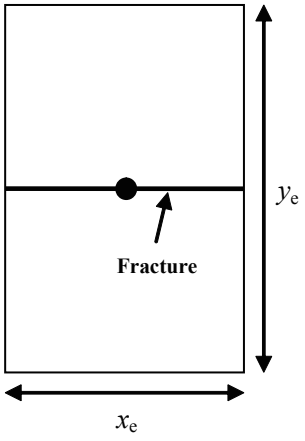

Figure 1
A Hydraulically Fractured Vertical Well in the Center of a Rectangular Reservoir

Step 1. Plot $\frac{1}{q}$ versus $\sqrt{t}$, where q is gas rate and t is time, on Cartesian coordinates and place a line through the data corresponding to linear flow. Determine the slope, *m,* of this line and its intercept, *b'*. Linear flow can be recognized independently using semi-log derivative analysis.

Step 2. Specify a value for drainage area.

Step 3. Calculate the duration of linear flow, t_{elf}.

$$t_{elf} = \left[\frac{Ah\left(\phi\mu_g c_t\right)_i m\ (p_{pi} - p_{pwf})}{200.6T}\right]^2 \quad (1)$$

In this equation, A is the drainage area, h is the net pay thickness, ϕ is the reservoir porosity, μ_g is gas viscosity, c_t is total compressibility, subscript "i" refers to initial reservoir conditions, p_{pi} and p_{pwf} are pseudopressures at initial pressure and flowing pressure, respectively and T is the reservoir temperature. It should be noted that Eq. (1) is derived for field units.

Step 4. Calculate the production rate at the end of the linear flow period, q_{elf}.

$$q_{elf} = \frac{1}{m\sqrt{t_{elf}} + b'} \quad (2)$$

Step 5. Calculate the decline rate at the end of the linear flow period, D_{elf}.

$$D_{elf} = \frac{1}{m\sqrt{t_{elf}} + b'} \times \frac{m}{2\sqrt{t_{elf}}} \quad (3)$$

Step 6. Forecast rates for $t \le t_{elf}$ using the following equation:

$$q = \frac{1}{m\sqrt{t + b'}} \quad (4)$$

Step 7. Assume a value for decline exponent, b, and use Eq. (5) to forecast rates for $t > t_{elf}$.

$$q = \frac{q_{elf}}{\left[1 + bD_{elf}(t - t_{elf})\right]^{1/b}} \quad (5)$$

In the preceding equations, b and b' are in no way related. b' is the intercept of inverse gas rate versus square root of time plot whereas b is the hyperbolic decline exponent. Although this forecasting procedure was developed for the reservoir geometry shown in Fig.1, it can be used to forecast rates for horizontal well with multiple fracture system shown in Fig. 2 using the area of stimulated reservoir volume (SRV) as the input to the simplified method instead of drainage area[1].

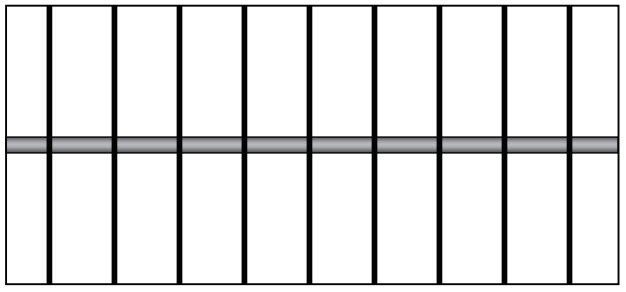

Figure 2
Schematic of a Homogeneous Multi-Fractured Horizontal Well Completion

2. DECLINE EXPONENT (*b*-VALUE)

This forecasting procedure requires a decline exponent to forecast rates during boundary-dominated flow (Step 7). It is well documented in the literature that for volumetric gas reservoirs $b = 0.5$ can be used in hyperbolic decline. Therefore, $b = 0.5$ is a good number to be used for tight gas. However, for shale gas reservoirs, depending on operating conditions and the shape of desorption isotherm, desorption can cause the b value to be above 0.5. b value larger than 0.5 is also expected in multi-layer reservoirs

with no cross flow.

This forecasting method with $b = 0.5$ is only applicable to horizontal wells with homogeneous completions (i.e., the fractures have the same length)[11]. Ambrose et al.[11] proposed that for a heterogeneous completion, where the fracture lengths are not the same (Fig. 3), the system needs to be divided into sub-components and then for each sub-component, the simplified forecasting method of Nobakht et al.[1] can be applied. It was shown that for a volumetric gas reservoir after the first two fractures start to interfere, the decline exponent value starts to deviate from $b = 2$ and when the whole system is in boundary-dominated flow the decline exponent value reaches $b = 0.5$. Using some real data, Ambrose et al.[11] showed that Nobakht et al. method[1] with a decline exponent between 0.5 and 2 (after the end of linear flow) can be used to forecast rates from heterogeneous completions. The decline exponent that should be used depends on the completion geometry. This shows that when using the simplified forecasting method for shale gas reservoirs, there might be uncertainties in decline exponent and therefore, it is important to study the relative impact of b-value used after the end of linear flow on long-term production forecast for linear-flow dominated wells.

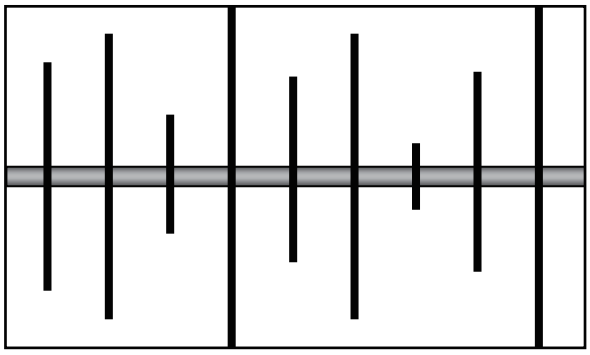

Figure 3
Schematic of a Heterogeneous Multi-Fractured Horizontal Well Completion

2.1 Evolution of Decline Exponent During Depletion

It is observed in the literature that for constant flowing pressure production from a single layer volumetric gas reservoir, the decline exponent during boundary-dominated flow is going to deviate from $b = 0.5$ and eventually reduces to $b = 0$[1,13]. It is important to find the time that this deviation starts and determine if it practically affects the expected ultimate recovery (EUR) calculated from Arps' decline. In this section, this time is determined for the reservoir geometry shown in Fig. 1. First, the constant-pressure type curve for this reservoir geometry was developed using the linear flow solution for a slightly compressible fluid during linear flow[7] and hyperbolic decline with $b = 0.5$ during boundary-dominated flow. The plotting format for this type curve, shown in Fig. 4, is $q_{Dd} = \frac{y_e}{x_e} q_D$ against t_{Dye} [7], where:

$$q_D = \frac{141.2qB\mu}{kh\left(p_i - p_{wf}\right)} \tag{6}$$

$$t_{Dye} = \frac{0.00633kt}{\phi\mu c_t y_e^2} \tag{7}$$

The manner in which the type curve is generated is presented in Appendix A. This plotting format gives only one type curve for geometry shown in Fig. 1 rather than families of type curves with different values of $\frac{x_f}{y_e}$ [7]. As shown in Appendix A, $t_{Dye} = 0.0625$ at the end of the linear flow period (i.e., at $t = t_{elf}$).

To calculate the time that the decline exponent starts to deviate from $b = 0.5$, a total number of 10 simulation cases were generated for constant flowing pressure condition. The input data for the numerical simulation cases are given in Table 1. The blank cells in this table indicate that the value for that parameter is the same as that of Case 1. The rate versus time data points for these cases was transformed to q_{Dd} versus t_{Dye} format and plotted on the type curve. Fig. 4 also shows this data plotted on the type curve for Cases 1–5. This figure shows that for all cases, the b value starts to gradually decrease from $b = 0.5$ around $t_{Dye} = 0.4$. As $t_{Dye} = 0.0625$ at $t = t_{elf}$, it can be concluded that the b value starts to deviate from $b = 0.5$ around $t = 6t_{elf}$. The simulated data during linear flow do not fall on the half-slope part of the type curve in Fig. 4. This is because we simply used time instead of pseudo-time for plotting the data on the type curve[14,15].

Table 1
Input Parameters Used for Numerical Simulation for Different Cases, the Blank Cells in this Table Indicate that the Value for that Parameter is the Same as that of Case 1

Case	1	2	3	4	5	6	7	8	9	10
p_i (psi)	2,000						1,000	4,000		
T (°F)	120									
h (ft)	100									
ϕ(%)	10									
S_g (%)	100									
γ_g	0.65									
p_{wf} (psi)	200								500	1,000
x_f (ft)	250									
x_e (ft)	500									
y_e (ft)	5,000				10,000	2,500				
k (md)	1	0.5	2	4						

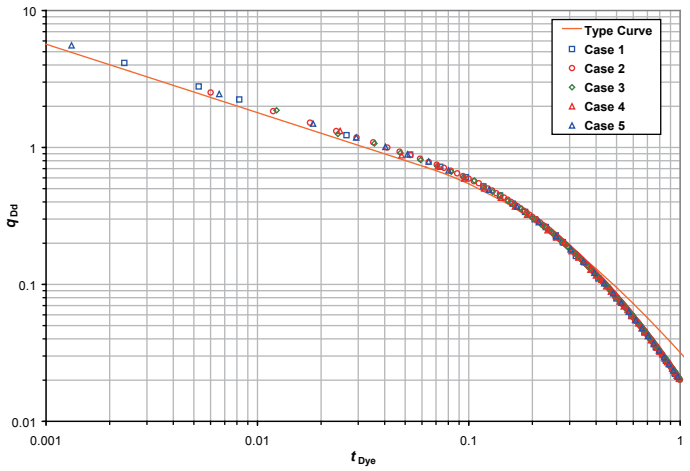

Figure 4
The Rate Versus Time Data Points for Cases 1–5 Plotted on the q_{Dd} Versus t_{Dye} Type Curve

To investigate if the gradual deviation of decline exponent from $b = 0.5$ affects the EUR, the following assumptions are made to simplify the problem:

1. The gas is ideal ($Z = 1$). Using the definition of gas compressibility, this assumption leads to:

$$c_g = \frac{1}{p} - \frac{1}{Z}\frac{dZ}{dp} = \frac{1}{p} \tag{8}$$

2. Gas viscosity is not changing with pressure. Using the definition of pseudopressure and ideal gas assumption,

$$p_{pi} = 2\int \frac{p}{\mu_g Z}dp = \frac{2}{\mu_{gi}}\int pdp = \frac{p_i^2}{\mu_{gi}} \tag{9}$$

3. Total compressibility is dominated by gas compressibility, i.e.,

$$c_t = S_g c_g \tag{10}$$

4. Pseudopressure at the constant flowing pressure is negligible compared to that at the initial pressure. In other words,

$$p_{pi} - p_{pwf} \approx p_{pi} \tag{11}$$

5. The intercept of inverse gas rate versus square root of time plot is ignored. In other words, the rate can be calculated using the following equation during linear flow period:

$$q = \frac{1}{m\sqrt{t}} \tag{12}$$

Using Eq. (12), the cumulative production at the end of linear flow (i.e., $t = t_{elf}$) is:

$$Q_{elf} = \int_0^{t_{elf}} qdt = \int_0^{t_{elf}} \frac{1}{m\sqrt{t}}dt = \frac{2}{m}\sqrt{t_{elf}} \tag{13}$$

Combining Eqs. (1), (8)–(11) and (13) and using the definition of gas formation volume

factor $B_{gi} = \frac{0.0282 Z_i T}{p_i}$ with Z_i=1 (ideal gas assumption),

$$Q_{elf} = 0.282 OGIP \tag{14}$$

where OGIP is the original gas-in-place in Mscf. This means that under assumptions mentioned above, 28% of the total gas in the reservoir geometry shown in Fig. 1 is produced during linear flow.

The relationship between cumulative production and time for hyperbolic decline is as follows:

$$Q = \frac{q_i}{(1-b)D_i}\left[1-\left(1+bD_i t\right)^{1-\frac{1}{b}}\right] \tag{15}$$

where q_i is the production rate at the start of the hyperbolic forecast period, b is the hyperbolic decline exponent, D_i is decline rate corresponding to q_i and t is time since the start of the hyperbolic forecast. Since hyperbolic forecast starts after the end of linear flow, we will use the hyperbolic decline equation in the form shown in Eq. (16), which is obtained from Eq. (15) by re-initializing the time at $t = t_{elf}$:

$$\Delta Q = \frac{q_{elf}}{(1-b)D_{elf}}\left[1-\left(1+bD_{elf}\left(t-t_{elf}\right)\right)^{1-\frac{1}{b}}\right] \tag{16}$$

In this equation, ΔQ is the volume produced during boundary-dominated flow using hyperbolic decline. Using q_{elf} and D_{elf} from Eq. (2) and Eq. (3) respectively (with b' = 0), the volume produced between $t = t_{elf}$ and $t = 6t_{elf}$ (i.e., when the decline exponent starts to deviate from b = 0.5) using b = 0.5 becomes:

$$\Delta Q\ (b = 0.5) = \frac{2.22\sqrt{t_{elf}}}{m} \tag{17}$$

Combining Eqs. (17) and (B-4),

$$\Delta Q\ (b = 0.5) = 0.313 OGIP \tag{18}$$

This shows that 31% of the original gas-in-place is produced between $t = t_{elf}$ and $t = 6t_{elf}$ using hyperbolic decline with b = 0.5. In other words, almost 60% of the total gas will be produced by the time the decline exponent starts to deviate from b = 0.5.

As shown in Appendix B, 25% of the total gas will be recovered after $t = 6t_{elf}$ using b = 0.5 to forecast for infinite time, whereas 12% of the total gas will be produced after $t = 6t_{elf}$ using exponential decline. Therefore, the volume of gas produced after $t = 6t_{elf}$ is between 12% and 25% of the original gas-in-place, as there is a transition from b = 0.5 to b = 0. This shows that for all practical purposes, we can ignore the change in decline exponent with time for $t \geq 6t_{elf}$.

Notes:

- Although the calculations presented above and in Appendix B are based on ideal gas assumption (Z = 1), they are valid for cases where Z is not changing drastically with pressure.
- The cumulative productions at different times presented above and in Appendix B are obtained based on the duration of linear flow from Eq. (1). Although it is reported in the literature that Eq. (1) is an approximation for the duration of linear flow[16–18], it is used for simplicity in this study.

3. SENSITIVITY OF FORECAST TO *b*-VALUE

As mentioned in the previous section, after the fractures start to interfere in a multi-fractured horizontal well, the decline exponent can vary between 0.5 and 2 due to different fracture lengths and/or unequal fracture spacing along the horizontal well (heterogeneous completions). The simplified forecasting procedure can be used to investigate the sensitivity of EUR to decline exponent, b, which is being used for forecasting during boundary-dominated flow.

3.1 EUR Based upon Time

Eq. (16) shows the volume produced after the end of linear flow according to a hyperbolic decline forecast. To obtain the expected ultimate recovery (EUR) at the end of the forecast (when $t > t_{elf}$), the volume produced using Eq. (16) can be added to the cumulative production at the end of linear flow calculated from Eq. (13). Combining Eqs. (2), (3), (13) and (16):

$$EUR = \frac{2\sqrt{t_{elf}}}{m}\left[1+\frac{1}{1-b}\left[1-\left(1+\frac{b}{2}\left(\frac{t}{t_{elf}}-1\right)\right)^{1-\frac{1}{b}}\right]\right] \tag{19}$$

Here, t is the economic life of the well. Using Eq. (19), it can be shown that the ratio between EUR values obtained for two different values of decline exponent depends on the value of $\frac{t}{t_{elf}}$, given that the two decline exponents are specified.

$\frac{EUR(b=1.3)}{EUR(b=0.5)}$ and $\frac{EUR(b=0.8)}{EUR(b=0.5)}$ versus $\frac{t}{t_{elf}}$ are shown in Fig. 5 and Fig. 6, respectively. These plots can be used to study the sensitivity of forecast to the value of decline exponent. For example, it can be seen from Fig. 6 that for $t = 30t_{elf}$, EUR for b = 0.8 is almost 20% higher than EUR for b = 0.5. It should be noted that b = 0.5 is for homogeneous completion, b = 0.8 is for slightly heterogeneous completion and b = 1.3 is for very heterogeneous completion[11].

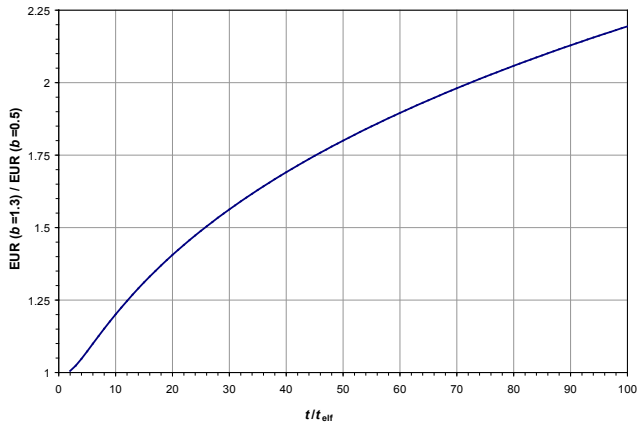

Figure 5
Plot of $\frac{EUR(b=1.3)}{EUR(b=0.5)}$ Versus $\frac{t}{t_{elf}}$

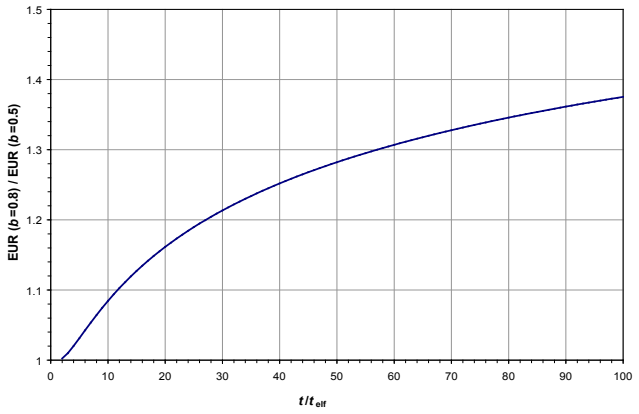

Figure 6
Plot of $\frac{EUR(b=0.8)}{EUR(b=0.5)}$ Versus $\frac{t}{t_{elf}}$

3.2 EUR Based upon Economic Limit

When economic limit, q_f, is known, the volume produced using hyperbolic decline is calculated using the following equation:

$$Q = \frac{q_i^b}{(1-b)D_i}\left[q_i^{1-b} - q_f^{1-b}\right] \quad (20)$$

Therefore, the volume produced during boundary-dominated flow ΔQ for hyperbolic decline is:

$$\Delta Q = \frac{q_{elf}^b}{(1-b)D_{elf}}\left[q_{elf}^{1-b} - q_f^{1-b}\right] \quad (21)$$

Using q_{elf} and D_{elf} from Eq. (2) and Eq. (3) respectively (with $b' = 0$) and assuming n is the ratio of the rate at the end of linear flow to the economic rate limit (i.e., $q_{elf} = nq_f$ with $n \geq 1$), the EUR for hyperbolic decline becomes:

$$EUR = \frac{2\sqrt{t_{elf}}}{m}\left[1 + \frac{1}{1-b}(1 - n^{b-1})\right] \quad (22)$$

Using Eq. (22), it can be shown that the ratio between EUR values obtained for two different values of decline exponent depends on the value of n, given that the two decline exponents are specified. When EUR is being calculated based upon economic limit, Eq. (22) can be used to investigate the sensitivity of EUR to decline exponent.

CONCLUSIONS

This paper applied the simplified forecasting method of Nobakht et al.[1] to study the sensitivity of expected ultimate recovery (EUR) to decline exponent used after the end of linear flow. This is important for reserve evaluation because of uncertainty in decline exponent due to factors like desorption and heterogeneity in completion. It was shown that for gas production under constant flowing pressure in a volumetric reservoir, at some point during depletion the decline exponent starts to deviate from 0.5. The time at which this deviation happens is almost $t = 6t_{elf}$ for the reservoir geometry shown in Fig. 1, where t_{elf} is the duration of linear flow. Using some assumptions, it was shown that ignoring the gradual decrease in b-value after $t = 6t_{elf}$ will not practically affect the EUR. Finally, the sensitivity of EUR to b-value is studied for both time-based and economic limit-based forecasts. It is found that for two different specified values of decline exponent, the ratio between their EURs depends on the ratio of economic life of the well to the duration of linear flow for time-based forecast and the ratio of the rate at the end of linear flow to the economic rate limit for economic limit-based forecast.

ACKNOWLEDGEMENTS

The authors would like to thank ConocoPhillips for their support of this research. Chris Clarkson would like to acknowledge Encana for support of his Chair position in Unconventional Gas at the University of Calgary, Department of Geoscience. Finally, both authors would like to thank Fekete Associates Inc., particularly Louis Mattar, for fruitful discussions on the subject of rate-transient analysis.

REFERENCES

[1] Nobakht, M., Mattar, L., Moghadam, S., & Anderson, D. M. (2010). Simplified Yet Rigorous Forecasting of Tight/Shale Gas Production in Linear Flow. *Paper SPE 133615 presented at the SPE Western Regional Meeting, Anaheim, California, 27–29 May*. DOI: 10.2118/133615-MS.

[2] Cipolla, C. L., Williams, M. J., Weng, X., & Maxwell, S. (2010). Hydraulic Fracture Monitoring to Reservoir Simulation: Maximizing Value. *Paper SPE 133877 presented at the SPE Annual Technical Conference and Exhibition, Florence, Italy, 19–22 September*. DOI:

10.2118/133877-MS.

[3] Arps, J. J. (1945). Analysis of Decline Curves. *Trans., AIME*, *160*, 228–247.

[4] Stright, D. H., & Gordon, J. I. (1983). Decline Curve Analysis in fractured Low Permeability Gas Wells in the Piceance Basin. *Paper SPE 11640 presented at the SPE/DOE Low Permeability Gas Reservoirs Symposium, Denver, Colorado, 14–16 March*. DOI: 10.2118/11640-MS.

[5] Maley, S. (1985). The Use of Conventional Decline Curve Analysis in Tight Gas Well Applications. *Paper SPE 13898 presented at the SPE/DOE Low Permeability Gas Reservoirs Symposium, Denver, Colorado, 19–22 March*. DOI: 10.2118/13898-MS.

[6] Hale, B. W. (1986). Analysis of Tight Gas Well Production Histories in the Rocky Mountains. *SPE Production Engineering*, *1*(4), 310–322. SPE-11639-PA. DOI: 10.2118/11639-PA.

[7] Wattenbarger, R. A., El-Banbi, A. H., Villegas, M. E., & Maggard, J. B. (1998). Production Analysis of Linear Flow into Fractured Tight Gas Wells. *Paper SPE 39931 presented at SPE Rocky Mountain Regional/Low Permeability Reservoirs Symposium and Exhibition, Denver, Colorado, 5–8 April*. DOI: 10.2118/39931-MS.

[8] Kupchenko, C. L., Gault, B. W., & Mattar, L. (2009). Tight Gas Production Performance Using Decline Curves. *Paper SPE 114991 presented at the CIPC/SPE Gas Technology Symposium, Calgary, Alberta, 16–19 June*. DOI: 10.2118/114991-MS.

[9] Ilk, D., Rushing, J. A., Perego, A. D., & Blasingame, T. A. (2008). Exponential vs. Hyperbolic Decline in Tight Gas Sands — Understanding the Origin and Implications for Reserve Estimates Using Arps' Decline Curves. *Paper SPE 116731, presented at the Annual Technical Conference and Exhibition, Denver, Colorado, 21–24 September*. DOI: 10.2118/116731-MS.

[10] Valkó, P. P. (2009). Assigning Value to Stimulation in the Barnett Shale: A Simultaneous Analysis of 7000 Plus Production Histories and Well Completion Records. *Paper SPE 119369 presented at SPE Hydraulic Fracturing Technology Conference, The Woodlands, Texas, 19–21 January*. DOI: 10.2118/119369-MS.

[11] Ambrose, R. J., Clarkson, C. R., Youngblood, J., Adams, R., Nguyen, P., Nobakht, M., & Biseda, B. (2011). Life-Cycle Decline Curve Estimation for Tight/Shale Gas Reservoirs. *Paper SPE 140519 presented at the SPE Hydraulic Fracturing Technology Conference and Exhibition, The Woodlands, Texas, 24–26 January*. DOI: 10.2118/140519-MS.

[12] Nobakht, M., Ambrose, R. J., & Clarkson, C. R. (2011). Effect of Heterogeneity in a Horizontal Well With Multiple Fractures on the Long-Term Forecast in Shale Gas Reservoirs. *Paper CSUG/SPE 149400 presented at the Canadian Unconventional Resources Conference, Calgary, Alberta, Canada, 15–17 November*. DOI: 10.2118/149400-MS.

[13] Okuszko, K. E., Gault, B. W., & Mattar, L. (2007). Production Decline Performance of CBM Wells. *Paper CIPC 2007-78, presented at Canadian International Petroleum Conference, Calgary, Alberta, 12–14 June*. DOI: 10.2118/2007-78.

[14] Nobakht, M., & Clarkson, C. R. (2011). A New Analytical Method for Analyzing Production Data from Shale Gas Reservoirs Exhibiting Linear Flow: Constant Pressure Production. *Paper SPE 143989 presented at the North American Unconventional Gas Conference, The Woodlands, Texas, 12–16 June*. DOI: 10.2118/143989-MS.

[15] Nobakht, M., & Clarkson, C. R. (2011). A New Analytical Method for Analyzing Production Data from Shale Gas Reservoirs Exhibiting Linear Flow: Constant Rate Production. *Paper SPE 143990 presented at the North American Unconventional Gas Conference, The Woodlands, Texas, 12–16 June*. DOI: 10.2118/143990-MS.

[16] Ibrahim, M., & Wattenbarger R. A. (2005). Rate Dependence of Transient Linear Flow in Tight Gas Wells. *Paper CIPC 2005-057 presented at Canadian International Petroleum Conference, Calgary, Alberta, 7–9 June*. DOI: 10.2118/2005-057.

[17] Ibrahim, M., & Wattenbarger R. A. (2006). Analysis of Rate Dependence in Transient Linear Flow in Tight Gas Wells. *Paper SPE 100836 presented at the Abu Dhabi International Petroleum Exhibition and Conference, Abu Dhabi, UAE, 5–8 November*. DOI: 10.2118/100836-MS.

[18] Nobakht, M., & Clarkson, C. R. (2011). Estimation of Contacted and Original Gas-in-Place for Low Permeability Reservoirs Exhibiting Linear Flow. *Paper CSUG/SPE 149398 presented at the the Canadian Unconventional Resources Conference, Calgary, Alberta, Canada, 15–17 November*. DOI: 10.2118/149398-MS.

APPENDIX A: Duration of Linear Flow and Development of Figure 4

When the well is producing under constant flowing pressure in the reservoir geometry shown in Fig. 1, the distance of investigation, y, can be obtained from the following equation during the linear flow period[7]:

$$y = 0.159\sqrt{\frac{kt}{(\phi\mu_g c_t)_i}} \tag{A-1}$$

According to this equation, the end of linear flow is given by:

$$\frac{y_e}{2} = 0.159\sqrt{\frac{kt_{elf}}{(\phi\mu_g c_t)_i}}, \tag{A-2}$$

where y_e is reservoir length and t_{elf} is the duration of linear flow. Eq. (A-2) can be rewritten as follows:

$$t_{elf} = \left(\frac{y_e\sqrt{(\phi\mu_g c_t)_i}}{2\times 0.159\sqrt{k}}\right)^2 \tag{A-3}$$

Using t_{elf} calculated from Eq. (A-3) in Eq. (7), t_{Dye} at the end of linear, $(t_{Dye})_{elf}$, becomes:

$$(t_{Dye})_{elf} = \frac{0.00633kt_{elf}}{\phi\mu c_t y_e^2} = 0.0625 \tag{A-4}$$

In other words, $t_{Dye} = 0.0625$ at the end of linear flow. Note that this value is different from t_{Dye}=0.25 Wattenbarger et al.[7] derived simply because in their work y_e was half of reservoir length, whereas in this study y_e is the reservoir length.

To generate the type curve shown in Fig. 4 for the reservoir geometry in Fig. 1, we used the following equation, which is linear flow solution for constant flowing pressure, for $t_{Dye} \le 0.0625$ (i.e., duration of linear flow).

$$\frac{1}{q_{Dd}} = \pi\sqrt{\pi t_{Dye}} \tag{A-5}$$

For $t_{Dye} \ge 0.0625$ (i.e., boundary-dominated flow), we used the following equation (with $b = 0.5$), which is the extension of Nobakht et al.[1] method in dimensionless form:

$$q_{Dd} = \frac{(q_{Dd})_{elf}}{\left[1 + bD_{elf}(t_{Dye} - (t_{Dye})_{elf})\right]^{1/b}} \tag{A-6}$$

Here, $(q_{Dd})_{elf}$ is value of q_{Dd} at $t_{Dye} = (t_{Dye})_{elf} = 0.0625$ ($(q_{Dd})_{elf} \approx 0.718$) and D_{elf} is as follows:

$$D_{elf} = \frac{1}{2(t_{Dye})_{elf}} = 8 \tag{A-7}$$

APPENDIX B: Calculation of Volume Produced During Different Time Intervals

For the reservoir geometry shown in Fig. 1, the end of linear flow, t_{elf}, is[1,7] :

$$t_{elf} = \left[\frac{Ah(\phi\mu_g c_t)_i m\ (p_{pi} - p_{pwf})}{200.6T}\right]^2 \tag{B-1}$$

Combining Eqs. (B-1), (8)–(11) results in:

$$\sqrt{t_{elf}} = \frac{Ah\phi\mu_{gi}}{200.6T}\frac{Sg}{p_i}m\frac{p_i^2}{\mu_{gi}} = \frac{Ah\phi S_g}{200.6}\frac{p_i}{T}m \tag{B-2}$$

Using the definition of gas formation volume factor $B_{gi} = \frac{0.0282Z_iT}{p_i}$ with $Z_i = 1$ (ideal gas assumption),

$$\frac{p_i}{T} = \frac{0.0282}{B_{gi}} \tag{B-3}$$

Combining Eqs. (B-2) and (B-3) and using the definition of $OGIP = 0.001\frac{Ah\phi S_g}{B_{gi}}$ ($OGIP$ is in Mscf),

$$\frac{\sqrt{t_{elf}}}{m} == \frac{Ah\phi S_g}{200.6}\frac{0.0282}{B_{gi}} = 0.141OGIP \tag{B-4}$$

Using the value of $\frac{\sqrt{t_{elf}}}{m}$ from Eq. (B-4) into Eq. (13),

$$Q_{elf} = 0.282OGIP \tag{B-5}$$

The rate at $t = 6t_{elf}$, can be calculated by combing Eqs. (3) and (5) (with $b' = 0$, i.e., zero intercept on inverse gas rate versus square root of time plot):

$$q_{6elf} = 0.198q_{elf} \tag{B-6}$$

Using hyperbolic decline with $b = 0.5$ between $t = t_{elf}$ and $t = 6t_{elf}$, the decline rate at $t = 6t_{elf}$ can be calculated using:

$$\frac{D_{6elf}}{D_{elf}} = \left(\frac{q_{6elf}}{q_{elf}}\right)^{0.5} \tag{B-7}$$

Combining Eqs. (B-6) and (B-7),

$$D_{6elf} = 0.444D_{elf} \tag{B-8}$$

The volume produced after $t = 6t_{elf}$ using hyperbolic decline with $b = 0.5$ and exponential decline can be calculated using Eqs. (B-9) and (B-10), respectively:

$$\Delta Q = \frac{q_{6elf}^b}{(1-b)D_{6elf}}\left(q_{6elf}^{1-b} - q_f^{1-b}\right) \tag{B-9}$$

$$\Delta Q = \frac{q_{6elf} - q_f}{D_{6elf}} \tag{B-10}$$

Using $q_f = 0$, Eqs. (B-9) and (B-10) will change to:

$$\Delta Q = \frac{2q_{6elf}}{D_{6elf}} = \frac{1.784q_{elf}}{D_{elf}} \tag{B-11}$$

$$\Delta Q = \frac{q_{6elf}}{D_{6elf}} = \frac{0.892q_{elf}}{D_{elf}} \tag{B-12}$$

Using Eqs. (2), (3) and (B-4),

$$\Delta Q = 0.246 OGIP \quad \text{(B-13)}$$

$$\Delta Q = 0.123 OGIP \quad \text{(B-14)}$$

It can be concluded from Eqs. (B-13) and (B-14) that 25% of the total original gas-in-place is produced after $t = 6t_{elf}$ using hyperbolic decline with $b = 0.5$, whereas 12% of the total original gas-in-place is produced after $t = 6t_{elf}$ using exponential decline.

CSCanada
Advances in Petroleum Exploration and Development
Vol. 3, No. 1, 2012, pp. 11-17
DOI:10.3968/j.aped.1925543820120301.153

ISSN 1925-542X [Print]
ISSN 1925-5438 [Online]
www.cscanada.net
www.cscanada.org

The Performance of Polymer Solution Added with Viscosity Stabilizer and the Evaluation of Its Oil Displacement Efficiency in Daqing Oilfield

WEI Jianguang[1]; ZHANG Qingjie[2,*]; JIANG Zhenhai[1,2]; ZHANG Haijun[2]; NI Xiangcai[2]; SHAO Hongyan[2]; WANG Zhonghui[2]

[1] Northeast Petroleum University, China.
[2] Daqing Oil Field Company Ltd., China.
[*] Corresponding author.

Received 7 February 2012; accepted 5 March 2012

Abstract

Aiming at the low viscosity of polymer solution, which is compounded with fresh water but diluted with produced water, and at the problems concerning oil displacement efficiency, an onsite test on polymer solution with viscosity stabilizer (PSVS) is carried out. As a result, it has great and guiding significance to the application and popularization of viscosity stabilizer by studying the performance of polymer solution with viscosity stabilizer and its influence on oil displacement efficiency. In this paper, aiming at two different kinds of polymer solutions among which one is compounded with fresh water but diluted with fresh produced water and the other with aerated produced water, two laboratory evaluative tests concerning viscosity stabilization, anti-shear stability, fluidity, and absorbability of polymer solution as well as its oil displacement efficiency are done. The results of onsite application of PSVS are traced and analyzed.

The viscosity stabilization of the polymer solution adding with viscosity stabilizer becomes much better than that of the normal polymer solution. The resistance and the residual resistance factors, the static oil sand adsorption rate and the dynamic core adsorption rate of the solution are all increased markedly. The working viscosity and oil displacement efficiency are improved markedly as well. In comparison with the polymer solution diluted with fresh produced water, the polymer solution diluted with aerated produced water is much better in terms of viscosity stabilization. Comparing with the normal polymer solution with viscosity stabilizer before sheared, the polymer solution which is sheared before adding with viscosity stabilizer performs obviously better in terms of viscosity stability. In contrast to the adjacent block injected with normal polymer solution, the block under onsite flooding test with injection of PSVS features that the average injection pressure increases slightly but keeps steady, the recovery speed of the average monthly water cut of production wells slows down, the thickness of the absorptive layers increases, and the periodic recovery rate improves as well.

Key words: Polymer solution; Viscosity stabilizer; Daqing oilfield

Wei, J. G., Zhang, Q. J., Jiang, Z. H., Zhang, H. J., Ni, X. C., Shao, H. Y., & Wang, Z. H. (2012). The Performance of Polymer Solution Added with Viscosity Stabilizer and the Evaluation of Its Oil Displacement Efficiency in Daqing Oilfield. *Advances in Petroleum Exploration and Development*, *3*(1), 11-17. Available from: URL: http://www.cscanada.net/index.php/aped/article/view/j.aped.1925543820120301.153
DOI: http://dx.doi.org/10.3968/j.aped.1925543820120301.153

INTRODUCTION

At present in Daqing Oilfield, the method of oil displacement usually adopts polymer solution of produced water diluted with fresh water. To solve the problem of low viscosity of polymer solution diluted with produced water, which affects the oil displacement efficiency, Daqing Oilfield carried out onsite experiments by adding viscosity stabilizer to polymer solution in September, 2006. The viscosity stabilizer is capable of restraining the polymer's degradation and stabilizing the viscosity of polymer solution, hence proving favorable to enhancing the oil displacement efficiency of polymer solution with produced water[1,2]. Therefore, the tracking and the analysis of numerous indoor research and onsite experiments, inquiring into the performance of polymer solution with viscosity stabilizer (PSVS) and its effects on oil displacement, is both theoretically and practically significant for applying and popularizing the technology of adding viscosity stabilizer to polymer solution. For

the time being, the PSVS technology is still at the stage of indoor and onsite experimentation[3,4]. To compare the two kinds of polymer solutions, one diluted with fresh water, the other diluted with aerated water, this paper evaluates the performance of PSVS and the indoor oil displacement experiment on drill core, thus it tracks and analyzes the onsite effects of PSVS application. This paper compares and analyzes the viscosity stability, anti-shear stability, fluidity, absorbability and oil displacement efficiency of PSVS and the normal polymer solution. It also calibrates the average injection pressure of the wells in the experiment block applied with viscosity stabilizer. The recovery speed of the average monthly water cut of production wells, the working viscosity, the laws of the fluctuating oil layer absorption profiles and periodic recovery rate are provided as well. Thus it sets a firm theoretical foundation of applying and popularizing the PSVS technology.

1. THE MECHANISM OF VISCOSITY STABILITY OF POLYMER SOLUTION

1.1 Oxide Sterilization[5]

In the water produced from oil well, there are a large amount of sulfate-reducing bacteria (SRB), iron bacteria (IB), total growth bacteria (TGB) among many other kinds of bacteria. Those bacteria, reproducing themselves voluminously, corrode the casing, the tubing, the pumps and other surface equipments. The SRB in particular is infamous for its severe damage on the molecular chain of polymer, which deteriorates the stability of polymer solution's viscosity. Oxygen can restrain the protein compounding within the bacteria, reducing their growth and even sterilize them, in a way to safeguard the molecular chain of polymer from being damaged. Accordingly, the polymer solution diluted with aerated water features increased oxygen content which, in sterilizing the bacteria, enhances the stability of polymer solution.

1.2 The Effect of Carbon Free Radical[6]

The polymer in the solution, under condition of 45℃, is partially disintegrated to generate carbon-centered free radicals. They have enough survival duration both in the aerated water and the fresh produced water, causing deterioration such as molecular bond break and reducing the polymer viscosity. The viscosity stabilizer, when added, can reduce the growth of carbon free radicals and thus prevent molecular bond break induced by carbon free radicals, realizing the function of stabilizing the polymer solution viscosity.

1.3 The Association of Chemical Bond[7]

The polymer molecule group is usually found in chain structure. However, it coils up when the negative electric charges at its surface are neutralized by the positive electric charges in highly mineralized water in the polymer solution. With stabilizer added, the association its stabilizing ingredient exerts together with the amide group's hydrogen bond and the hydrophobic group within the polymer itself leads to increased hydrodynamic scope of the molecular bond and strengthened inter-chain twisting and internal friction. Thus, the viscosity and the stability will be enhanced for the polymer solution of the produced water.

1.4 Performance Evaluation of Viscosity Stabilizer in Polymer Solution

The polymers applied in the experiment are those of high, middle and low molecular weight manufactured by Daqing Chemistry and Refinery Company. Their specifications are shown in Table 1 while the qualities of fresh water and used water for the experiment are illustrated in Table 2.

Table 1
Specifications of the Polymers for the Experiment

Type	Solid content (%)	MW (10,000)	Hydrolysis (%)	Viscosity (mPa·s)	Filtering factor	Insoluble (%)	Granularity rate(%)	
							≤0.2mm	≥1.0mm
HMW	89.54	3060	24.5	46.5	1.2	0.10	1.1	2.6
MMW	89.53	1550	23.9	42.9	1.5	0.004	0.4	0.9
LMW	89.77	330	25.1	10.7	1.2	0.01	0.0	1.9

Table 2
Water Quality Calibration

Type	PH value	Ca^{2+} (mg/L)	Mg^{2+} (mg/L)	Mineralization (mg/L)	Floating solid (mg/L)	Oil content (mg/L)	Polymer concentration (mg/L)
Used water	7.41	20.04	4.86	4985.70	7.0	2.9	316
Fresh water	8.28	20.04	9.74	357.27	0.4	/	/

1.4.1 Stability

The 5000mg/L polymer solutions compounded with fresh water are to be diluted to the level of 1200mg/L with fresh produced water and aerated water respectively, the content of viscosity stabilizer being 120mg/L. They are calibrated in terms of viscosity change by time before and after the addition of viscosity stabilizer into the polymer solutions.

Fig.1A and Fig.1B show the data of viscosity stability of viscosity stabilizer/ polymer solutions with aerated water and fresh water. Both the Tables illustrate that the polymer solutions, no matter that of fresh produced water or that of aerated water, when added with viscosity stabilizer, feature slight rise in the initial viscosity of different molecular weights and better long-term stability. For the polymer solutions compounded with fresh water and added with viscosity stabilizer, the viscosity retention rates of high, middle and low molecular weight on the thirtieth day are 56.0%, 49.0% and 30.2% respectively, increasing by 22.3%, 26.1% and 12.3% respectively over those without viscosity stabilizer; for the polymer solutions compounded with aerated water and added with viscosity stabilizer, the viscosity retention rates of high, middle and low molecular weight on the thirtieth day are 68.9%, 64.1% and 48.9% respectively, increasing by 27.9%, 31.5% and 24.3% respectively over those without viscosity stabilizer.

Table 3A and Table 3B also show that the polymer solution compounded with aerated water enjoys a slightly higher viscosity in the initial stage and better long-term stability than that compounded with fresh water. On the thirtieth day, the polymer solutions, with viscosity stabilizer added, of high, middle and low molecular weight have viscosity retention rates at 68.9%, 64.1% and 48.9% respectively, higher by 12.9%, 18.1% and 18.7% than those of the polymer solutions compounded with fresh produced water.

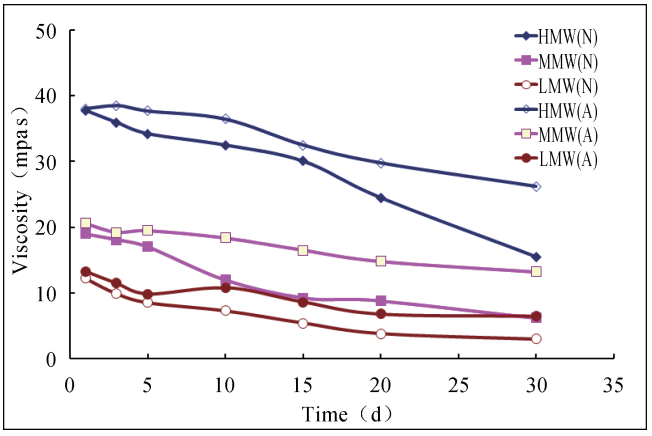

Figure 1A
The Stability Data of Viscosity Stabilizer/ Polymer Solution (Aerated Water)

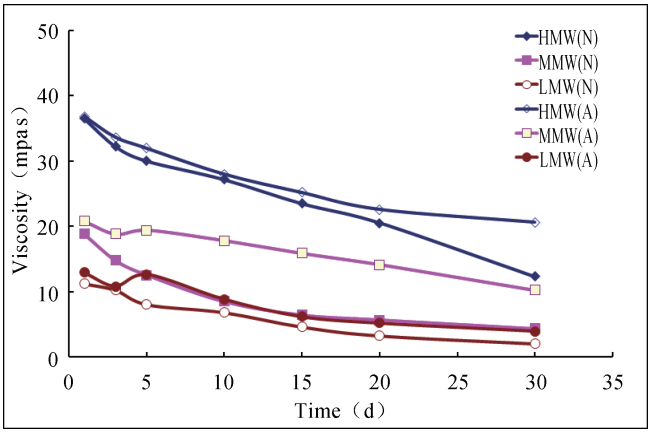

Figure 1B
The Stability Data of Viscosity Stabilizer/ Polymer Solution (Fresh Produced Water)

1.4.2 Anti-Shear Performance

The 5000mg/L polymer solutions compounded with fresh water are to be diluted to the level of 1200mg/L with fresh produced water and aerated water respectively, the content of viscosity stabilizer being 120mg/L either before or after the shear. They are calibrated in terms of viscosity change by time before and after the addition of viscosity stabilizer into the polymer solutions.

Table 4 shows the data of viscosity stability of polymer solutions compounded with aerated water and fresh water, with viscosity stabilizer added either before or after the shear. It can be found from Table 4 that the polymer solutions, no matter compounded with fresh or aerated water, have better viscosity if sheared before added with viscosity stabilizer than the case when added with viscosity stabilizer before sheared. On the sixtieth day, the retention rates stand at 75% and 76% for the polymer solutions compounded with fresh produced water and aerated water respectively, as sheared first and then added with viscosity stabilizer, higher by 8% and 28% respectively than those

added with viscosity stabilizer first and then sheared. For this reason, the location of viscosity stabilizer for onsite addition should be close behind the shearing equipment. Also it can found that the viscosity on the sixtieth day is higher than that on the thirtieth day, so to say, along with the addition of viscosity stabilizer, the viscosity stability of polymer solution is on the rise.

Table 4
The Viscosity Stability Data of Polymer Solutions Before and After the Addition of Viscosity Stabilizer

Polymer solution type		Polymer solution viscosity(mPa.s)						Retention rate (%)
		0d	3d	7d	15d	30d	60d	60d
Fresh	33% shear before adding stabilizer	36.7	32.6	27.2	26.7	23.4	27.7	75
	Adding stabilizer before 33% shear	36.4	32.5	25.7	21.3	23.0	24.7	68
Aerated	20% shear before adding stabilizer	43.2	37.0	36.3	34.1	30.5	33.0	76
	Adding stabilizer before 20% shear	43.4	30.6	27.9	26.7	22.1	20.7	48

1.4.3 Fluidity

The physical specifications of drill core are shown in Table 5 below. First the drill core is cleared of saturated strata water before injected with produced water by 4PV~5PV, the pressured recorded; then it is injected with polymer solution by 4PV~5PV; finally injected with fresh water by 4PV~5PV, also the pressured recorded. For the experiment, the injection speed is 0.3mL/ min, pressure recording interval 20min, the concentration of viscosity stabilizer 120mg/L, and the polymer solution is 5000mg/ L mother liquid compounded with fresh water, which is diluted to the level of 1000mg/L.

Table 6 shows the calibration results of resistance (The mobility ratio of injected water to polymer solution during the polymer flooding) and residual resistance factors (The mobility ratio of injected water before to after the polymer solution seeping through the rock) of polymer solutions, of both middle and high molecular weight, with the addition of viscosity stabilizer. According to Table 6, the viscosity stabilizer bears markedly on the fluidity characteristics of polymer solution, which, when added, gives rise to evident enhancement of resistance and residual resistance factors of the polymer solutions. The resistance and residual resistance factors of HMW polymer solution are respectively 15.0 and 5.3; those of MMW polymer solution are 8.4 and 5.1. Comparing with the polymer solution without viscosity stabilizer, the former factors increase by 3.7 and 4.0 while the latter ones increases by 3.0 and 4.0 respectively.

Table 5
Physical Factors of Drill Core

No.	Length (cm)	Diameter (cm)	Dry wt (g)	Wet wt (g)	Geometric bulk (cm^3)	Pore volume (cm^3)	Porosity (%)	Air permeability ($10^{-3}\mu m^2$)
4-4	9.33	2.54	76.6	90.1	47.3	13.5	28.6	275 3
4-7	9.20	2.54	76.5	90.1	46.6	13.6	29.2	2716
5-3	9.93	2.54	80.0	94.0	50.3	14.0	27.8	2813
5-4	9.94	2.54	79.8	93.8	50.4	14.0	27.8	2640

Table 6
Resistance and Residual Resistance Factors

No.	Permeability ($10^{-3}\mu m^2$)	Sample	Pressure/ (0.1MPa)			Resistance factor	Residual resistance factor
			Water flooding	Polymer flooding	Later water flooding		
4-4	2753	MMW normal	0.0102	0.055	0.011	5.4	1.1
4-7	2716	HMW normal	0.0096	0.108	0.012	11.3	1.3
5-3	2813	MMW + stabilizer	0.0103	0.087	0.053	8.4	5.1
5-4	2640	HMW + stabilizer	0.0105	0.157	0.056	15.0	5.3

1.4.4 Absorbability

The 1000mg/L polymer solution of MMW and HMW, prepared in proportion of 20:1, (the 5000mg/L mother liquid compounded with fresh water is diluted with aerated water to the level of 1000mg/L), is put into a plugged flask together with oil sand from Daqing Oilfield, evenly mingled then, and placed in 45℃ water of constant temperature to be surged for 24 hours before sent for centrifugal separation. The upper clear liquid is tested in terms of polymer concentration and then come under calculation of static absorption of polymer on the oil sand in accordance with the difference between initial and balanced concentration, the equation being as follows:

$$\text{static absorption (mg/g)}=\frac{\text{polymer mass before absorption(mg)-that after absorption(mg)}}{\text{oil sand mass(g)}}$$

Table 7 shows the calibration results of static absorption experiment on MMW and HMW polymer solutions before and after the addition of viscosity stabilizer. According to Table 7, the viscosity stabilizer affects evidently the static absorption of polymer on oil sand, which increases after the addition of viscosity stabilizer, standing at 1.2mg/g and 4.6mg/g for MMW and HMW polymer solutions respectively, higher by 0.5mg/g and 2.94mg/g than those without viscosity stabilizer.

Table 7
Test Result of Polymer Static Absorption

Sample	Oil sand mass (g)	Polymer concentration (mg/L)		Static absorption (mg/g)
		Before absorption	After absorption	
MMW normal	10	1000	965	0.70
MMW+ stabilizer	10	1000	940	1.20
HMW normal	10	1000	917	1.66
HMW+ stabilizer	10	1000	770	4.60

The dynamic absorption and fluidity experiments, conducted simultaneously, aim at calibrating the difference between the injection and outflow amounts of polymer mass and the drill core mass and calculating the dynamic absorption amount.

$$\text{dynamic absorption (mg/g)}=\frac{\text{Injection polymer mass (mg)-outflow polymer mass (mg)}}{\text{Drill core mass(g)}}$$

Table 8 shows the calibration results of the dynamic absorption experiment on MMW and HMW polymer solutions both before and after the addition of viscosity stabilizer. According to Table 8, the viscosity stabilizer affects evidently the dynamic absorption of polymer on drill core, which increases after the addition of viscosity stabilizer, standing at 0.31mg/g and 0.42mg/g for MMW and HMW polymer solutions respectively, higher by 0.12mg/g and 0.13mg/g than those without viscosity stabilizer.

Table 8
Test Result of Polymer Dynamic Absorption

Sample	Air permeability rate of drill core ($10^{-3}\mu m^2$)	Polymer concentration (mg/L)		Core mass (g)	Dynamic absorption (mg/g)
		Injection	Outflow		
MMW normal	2813	1000	388	79.99	0.19
MMW+ stabilizer	2454	1000	325	75.63	0.31
HMW normal	2640	1000	340	79.79	0.28
HMW+ stabilizer	2753	1000	263	76.56	0.41

2. OIL DISPLACEMENT EVALUATION OF VISCOSITY STABILIZER/ POLYMER SOLUTION

The model by size of 4.5cm×4.5cm×30cm, a man-made drill core made of epoxy quartz sand, is divided vertically into three layers of the top, the middle and the bottom, of 1.5cm in thickness for each layer, the permeability at 1000mD, 350mD and 150mD respectively. The experiment oil is compounded with the crude oil in Daqing Oilfield and kerosene, the viscosity at about 10mPa.s in temperature of 45°C. The polymers are those of MMW and HMW manufactured by Daqing Chemistry and Refinery Company, and their specifications are shown in Table 1. The water for the experiment are fresh water and the produced water from the Water Injection Station in Daqing Oilfield, their qualities shown in Table 2.

Table 9 shows oil displacement experiment on MMW and HMW polymer solutions in purpose of enhancing recovery rate both before and after the addition of viscosity stabilizer. According to Table 9, the viscosity stabilizer affects evidently the oil displacement effects of polymer; with the addition of viscosity stabilizer, the working viscosity and recovery rate are enhanced markedly. Those of HMW polymer solution through water and then polymer flooding are 26.5mPa.s and 24.4% respectively; those of MMW polymer solution are 13.5mPa.s and 17.2%. Comparing with data of solutions without viscosity stabilizer, the working viscosity and recovery rate of HMW polymer solution through water and then polymer flooding enhance by 10.7mPa.s and 8.5% respectively; those of MMW polymer solution through water and then polymer flooding by 7.5mPa.s and 7.5% respectively.

Table 9
Data of Oil Displacement Experiment on Polymer Solutions Before and After the Addition of Viscosity Stabilizer

No.	Content	Working viscosity (mPa·s)	Oil saturation (%)	Recovery rate (%)		Enhanced recovery rate (%)
				Water flooding	Polymer flooding	
1	Water flooding to 92% + 0.57PV polymer flooding (MMW)+ later water flooding to 98%	6.0	70.8	38.8	54.2	9.7
2	Water flooding to 92% + 0.57PV polymer flooding (MMW + viscosity stabilizer)+ later water flooding to 98%	13.5	71.5	38.1	61.7	17.2
3	Water flooding to 92% + 0.57PV polymer flooding (HMW)+ later water flooding to 98%	15.8	71.3	38.7	60.4	15.9
4	Water flooding to 92% + 0.57PV polymer flooding (HMW + viscosity stabilizer)+ later water flooding to 98%	26.5	71.6	38.4	68.9	24.4

3. ANALYSIS OF ONSITE APPLICATION OF VISCOSITY STABILIZER

From September 2006, Daqing Oilfield conducted the experiment of injecting viscosity stabilizer in the target block, covering 27 injection wells and 16 central production wells. The specific effects are shown as follows:

3.1 Stable Injection Pressure

From the average injection pressure in the experiment block, it slightly increases and keeps stable after the addition of viscosity stabilizer. Of the 27 wells, the average injection pressure stands at 12.55MPa before the addition of viscosity stabilizer and at 12.88MPa half a year after, a level evenly kept ever since. Thus that is a rise of 0.33MPa.

3.2 Decreased Recover Speed of the Average Water Cut

Comparing with the adjacent blocks without the injection of viscosity stabilizer, the experiment block after the injection, witnesses decreased recover speed of the average monthly water cut of the central production wells. Within one year after the injection of viscosity stabilizer, the recover speed of the average monthly water cut of the central production wells enhances by 0.16%. The adjacent block without the injection, the same speed enhances by 0.27%.

3.3 Slight Increase in the Viscosity of Liquid from Production Wells

Of the central production wells in the experiment block, the viscosity slightly increases after the injection of viscosity stabilizer. In the initial stage after the injection of viscosity stabilizer in the experiment block, the viscosity of the central production wells stands at 2.58mPa.s and rises to 2.74mPa.s in seven month and keeps stable at 2.8mPa.s, an increase of 0.22mPa.s.

3.4 Slight Increase in Periodic Recovery Rate and Absorption Thickness

Comparing with the adjacent blocks without the injection of viscosity stabilizer, the experiment block after the injection witnesses a slight increase of recovery rate and absorption of the oil layers in the central production wells. The periodic recovery rate of the experiment stands at 1.32%, an increase of 0.14%, and the absorption thickness covers three extra layers.

CONCLUSIONS

(1) The polymer solution with viscosity stabilizer added obviously performs better in terms of viscosity stability than that without. The same is true of the polymer solution diluted with aerated water, comparing with that diluted with fresh produced water. So is the case with solution sheared before the addition of viscosity stabilizer, comparing with that added with viscosity stabilizer before being sheared.

(2) Comparing with the normal polymer solution without viscosity stabilizer, that with the stabilizer features marked increase in resistance and residual resistance factors, static absorption of the oil sand and dynamic absorption of the drill core.

(3) As evident in the oil displacement experiment, the polymer solution with the addition of viscosity stabilizer after water flooding performs better than the normal polymer solution, with recovery rate increased by about 8.0%.

(4) Comparing with the adjacent blocks without the injection of viscosity stabilizer into the normal polymer solution, the experiment block after the injection witnesses first slightly increased and then stabled injection pressure in the injection wells, and decreased recover speed of the average monthly water cut, higher viscosity, larger thickness of the oil layers and increased periodic recovery rate of the central production wells in the experiment block.

(5) When the molecule weight of the polymer solution is compatible with the pore structure of the reservoir and formation plugging does not occur, the greater the polymer solution concentration and viscosity, the better the polymer flooding effects. But an optimum concentration value exists to make the oil production enhanced by per ton polymer solution the highest. Under our research condition, the optimum concentration value of polymer solution ranges between 1500 and 2000 mg/L.

REFERENCES

[1] He, N. Z., Zheng, W. L., & Pan, J. B. et al. (2003). Study of a Novel Polymer Solution as Viscosity Stabilizer. *Advances in Fine Petrochemicals*, *4*(7), 38-40.

[2] Han, Y. G. (2008). Discussion on the Issue of Viscosity of Polymer Solution Prepared by Oilfield Sewage. *Petroleum Geology and Recovery Efficiency*, *15*(6), 68-70.

[3] Sun, L., Pu, W. F., & Yang, H. J. (2007). Study on Viscosity Stabilizer for Alkali/Polymer Flooding. *Drilling & Production Technology*, *30*(2), 127-129.

[4] Zhang, J. G. (2005). Analysis of the Main Factors Affecting the Viscidity of the Solution of Polymer. *Fault-Block Oil & gas Field*, *12*(1), 57-59.

[5] Jiang, W. D., Zhang, K., & Xu, X. X. et al. (2007). Viscosity Differences and Mechanism Analysis of the Wasted Water-Polymer Solution in Aerobic and Anaerobic Environments. *Petroleum Geology and Recovery Efficiency*, *14*(6), 69-72.

[6] Fan, J., Wei, L., & Luo, W. L. et al (2011). Influencing Factors of the Viscosity Decrease on Polymer Sewage Solution. *Oilfield Chemistry*, *28*(3), 250-253.

[7] Su, Y. C. et al (2003). Research on Produced Water Mixing Polymer Solution. *Petroleum Geology & Oilfield Development in Daqing*, *22*(6), 44-47.

CSCanada
Advances in Petroleum Exploration and Development
Vol. 3, No. 1, 2012, pp. 18-32
DOI:10.3968/j.aped.1925543820120301.160

ISSN 1925-542X [Print]
ISSN 1925-5438 [Online]
www.cscanada.net
www.cscanada.org

An Analysis of Reservoir Production Strategies in Miscible and Immiscible Gas Injection Projects

Iman Farzad[1]; Mahmood Amani[2,*]

[1] National Iranian Oil Company
[2] Texas A&M University at Qatar
[*] Corresponding author.

Received 12 February 2012; accepted 16 March 2012

Abstract

Successful design and implementation of a miscible gas injection project depends upon the minimum miscibility pressure (MMP) and other factors such as reservoir and fluid characterization. The experimental methods available for determining MMP are both costly and time consuming. Therefore, the use of correlations that prove to be reliable for a wide range of fluid types would likely be considered acceptable for preliminary screening studies. This work includes a comparative evaluation of MMP correlations and thermodynamic models using an equation of state by PVTsim software (Schlumberger, 2001a). We observed that none of the evaluated MMP correlations studied in this investigation is sufficiently reliable. EOS-based analytical methods seemed to be more conservative in predicting MMP values.

Following an acceptable estimate of MMP, several compositional simulation runs were conducted to determine the sensitivity of the oil recovery to variations in injection pressure (at pressures above, equal to and below the estimated MMP), stratification and mobility ratio parameters in miscible and immiscible gas injection projects. Simulation results indicated that injection pressure was a key parameter that affects oil recovery to a high degree. MMP determined to be the optimum injection pressure. Stratification and mobility ratio could also affect the recovery efficiency of the reservoir in a variety of ways.

Key words: Reservoir production; Miscible gas injection; Immiscible gas; Minimum miscibility pressure

Farzad, I., & Amani, M. (2012). An Analysis of Reservoir Production Strategies in Miscible and Immiscible Gas Injection Projects. *Advances in Petroleum Exploration and Development*, *3*(1), 18-32. Available from: URL: http://www.cscanada.net/index.php/aped/article/view/j.aped.1925543820120301.160
DOI: http://dx.doi.org/10.3968/j.aped.1925543820120301.160

NOMENCLATURE

API= American Petroleum Institute
CGD= Condensing Gas Drive
OOIP= Originally Oil in Place, STB
MMP= Minimum Miscibility Pressure, psi
T= Temperature, °F
T_{pr}= pseudo reduced temperature of the reservoir Fluid
T_{pc}= pseudo critical temperature of the reservoir fluid,° R
P_{pc}= pseudo critical pressure of the reservoir fluid, psi
P_{pr}= pseudo reduced pressure of the reservoir fluid
x_{int}= mole percent of intermediate components (C_2 through C_5)in the reservoir fluid
y_{C2+} = mole fraction of the ethane plus fraction in the reservoir fluid

INTRODUCTION

Through the past decades, miscible displacement processes have been developed as a successful oil recovery method in many reservoirs. The successful design and implementation of a gas injection project depends on the favorable fluid and rock properties. The case studies using Eclipse compositional simulator considered the effect of key parameters, such as injection pressure, stratification and mobility ratio on the performance recovery in miscible and immiscible flooding of the reservoir (Schlumberger, 2001b). However,

accurate estimation of the minimum miscibility pressure is important in conducting numerous simulation runs. MMP is the minimum miscibility pressure which defines whether the displacement mechanism in the reservoir is miscible or immiscible. Thermodynamic models using an equation of state and appropriate MMP correlations were used in determining the MMP.

Compositional simulation runs determined the sensitivity of the oil recovery to the variations in above mentioned parameters. Significant increase in oil recovery was observed when interfacial tension dependent relative permeability curves were used. These relative permeability curves provide an additional accounting for miscibility by using a weighted average between fully miscible and immiscible relative permeability curves. The local interfacial tension determines the interpolation factor which is used in obtaining a weighted average of immiscible and miscible (straight line) relative permeabilities.

Simulation runs were performed at pressures below, equal to, and greater than estimated MMP for reservoir fluid/ injection gas system. Oil recovery was greatest when miscibility achieved. To investigate the effect of stratification on the performance recovery of the reservoir, the base relative permeability of two layers changed. Location of the high permeable layer (up or bottom layer) in the stratified reservoir greatly influenced the efficiency of the reservoir.

Understanding the effect of interfacial tension and adverse mobility ratio on the efficiency of the gas injection project was the last case study. Injection gas and reservoir fluid compositions differed in such a way to have interfacial tension and mobility dominated mechanism. To investigate the effect of interfacial tension water was considered as a fluid with much higher surface tension values with the oil. Lower surface tension values between rich gas and reservoir fluid (interfacial tension dominated) made gas injection project a more competitive recovery method than waterflooding. In mobility dominated displacement mechanism (lean gas/reservoir fluid system) the viscous instabilities were more important than the interfacial tension effect. For this case, waterflooding with favorable mobility ratio resulted in higher oil recoveries.

1. BACKGROUND

1.1 Classification of Miscible Displacements

Miscible displacement processes in the oil reservoirs are usually divided into two classes.

1.1.1 First Contact Miscible Processes (FCMP)

Displacements in which the injection fluid and the in-situ reservoir fluid form a single phase mixture for all mixing proportions. Pressure/composition (P-X) diagram is a useful method to illustrate the phase behavior of these mixtures. Pressure/composition diagrams for reservoir fluids are obtained by adding solvent (recycling gas produced in this case) into the reservoir oil and measuring the saturation pressure of the resultant mixture. Initially, as injection gas is added, mixtures will exhibit bubble points as the saturation pressure but as the concentration of the injection gas in the mixture increases, the mixtures formed will exhibit dewpoints. Single-phase mixture exists at pressures above the bubblepoint or dewpoint curves. The highest pressure at which two phases coexist in equilibrium is called the cricondenbar and is equal to FCMP.

1.1.2 Multi-Contact Miscible Processes

Processes in which the injected fluid and the reservoir oil are not miscible in the first contact but miscibility could develop after multiple contacts (dynamic miscibility). These processes are categorized into vaporizing, condensing, and combined vaporizing-condensing drive mechanisms.

The vaporizing-gas drive miscibility is one of the three alternative methods to obtain miscibility at pressures lower than FCM. In vaporizing-gas drive process or high- pressure gas process, lean injection gas vaporizes the intermediate components of the reservoir fluid and creates a miscible transition zone. In this displacement mechanism, miscibility is related to the gas front in the reservoir. As gas moves throughout the reservoir it comes into contact with original reservoir oil and thereby is enriched in intermediate components.

In condensing drive mechanism, injection gas containing low molecular weight hydrocarbon components (C_2-C_6), condenses in the oil to generate a critical mixture at the displacing front. It is reported that for some reservoir fluids, phase behavior in condensing-gas drives departs substantially from traditional three-component fluid concepts (Zick, 1986; Stalkup, 1987). Experimental observations and equation-of-state analysis indicate existence of combined condensing-vaporizing drive mechanism rather than condensing drive mechanism in the reservoir.

1.2 Minimum Miscibility Pressure Correlations

Multiple contact miscible floods have proven to be one of the most effective enhanced oil recovery methods currently available. The available displacement experimental (slim-tube and rising-bubble apparatus) procedures for determining the optimal flood pressure, defined as the minimum miscibility pressure, are both costly and time consuming (Metcalfe et al., 1972). Therefore, use of reliable correlations that were developed from reliable experimental data would be of great interest. The results of these correlations however would only be for the preliminary screening studies that would be conducted over a wide range of conditions. In this study a review of the literature of several MMP correlations of vaporizing gas drive (VGD) and condensing gas drive (CGD) mechanisms is investigated. An early correlation

was presented by Benham et al. (1960) where the required gas enrichment for condensing drive mechanism was correlated as a function of temperature, pressure, gas intermediate and heavy fractions of the oil molecular weights.

Glasø (1985) proposed a correlation which was the extension of Benham et al. (1960) study, and gives the MMP for VGD, CGD, CO_2, and N_2 systems. The input parameters for this correlation are temperature, mole percent of the methane in the injection gas, molecular weight of C_2-C_6 intermediates in the injection gas and the molecular weight of heptane-plus fraction of the oil. A new parameter called, paraffinicity characterization factor (K), was defined to account for oil composition effect on MMP.

A correlation developed by Sebastian et al. (1985) gives the MMP for CO_2-rich gas injection. This study takes into account the effects of impurities (up to 55% mole percent) in the injection gas. The new correlating parameter of this correlation is the pseudocritical molar average temperature of the injection gas. Alston et al. (1985) had investigated the effect of CO_2 impurities on MMP with a similar correlation with weight average critical temperature as a correlating parameter.

Firoozabadi and Aziz (1986) modeled the VGD with the Peng-Robinson equation of state and a compositional simulator. They proposed a simple correlation for the estimation of MMP of Nitrogen and lean-gas systems. The MMP was correlated as a function of molecular weights of heavy fractions of the oil, temperature and the molar concentration of intermediates in the oil.

Eakin and Mitch (1988) produced a general equation using 102 rising bubble apparatus (RBA) experiment data. The input parameters are heptane plus fraction, molecular weight, solvent composition and the pseudoreduced temperatures.

Many available MMP correlations in the literature are developed for CO_2 or impure CO_2 flooding. The evaluated MMP correlations in this study are suitable for hydrocarbon flooding. The reliability of each individual correlation was evaluated by determining, how close the predictive MMPs are to the equation-of-state based results. A comparative evaluation of MMP correlations is one of the objectives of this investigation. The following MMP correlations will be evaluated in the present study.

1.3 Glasø Correlation

Glasø (1980) proposed a correlation for predicting minimum miscibility pressure of multicontact miscible displacement of reservoir fluid by hydrocarbon gases, N_2 and CO_2. These equations are the equation form of the Benham[6] et al. correlation. These equations give the MMP as a function of reservoir temperature, molecular weight of C_{7+}, mole percent ethane in the injection gas and the molecular weight of the intermediates (C_2 through C_6) in the gas.

The proposed equations by Glasø (1980) are as follows:

$$(MMP)_{x=34} = 6{,}329 - 25.410\times y - (46.475 - 0.185\times y)\times z + (1.127\times 10^{-12}\times y^{5.258}\times e^{319.8zy^{-1.703}})\times T. \quad (1)$$

$$(MMP)_{x=34} = 6{,}329 - 25.410\times y - (46.475 - 0.185\times y)\times z + (1.127\times 10^{-12}\times y^{5.258}\times e^{319.8zy^{-1.703}})\times T. \quad (1)$$

$$(MMP)_{x=44} = 5{,}503 - 19.238\times y - (80.913 - 0.273\times y)\times z + (1.7\times 10^{-9}\times y^{3.730}\times e^{13.567zy^{-1.508}})\times T. \quad (2)$$

Where,

x= is the molecular weight of C_2 through C_6 components in injection gas, in lbm/mol,

y= is corrected molecular weight of C_{7+} in the stock-tank oil in lbm/mole and is equal to:

$$y = \left(\frac{2.622}{\gamma_{C_{7+}}^{-0.846}}\right)^{6.558}$$

γ_{C7+}=specific gravity of heptane-plus fraction, and

z = mole percent methane in injection gas

Prediction of the MMP for x values other than those specified by the mentioned equations should be obtained by interpolation. The accuracy of the MMP predicted from the three mentioned equations is related to the accuracy of the mole percent methane in the injection gas and the molecular weight of C_{7+} in the stock tank oil. The corrected molecular weight of the stock tank oil (y) indicates the paraffinicity of the oil which affects the MMP. The paraffinicity of the oil influences the solubility of hydrocarbon gas in the oil (Cook et al., 1969). Oil with paraffinicity characterization factor less than 11.95 represents oil with a relatively high content of aromatic components and consequently has corresponding higher MMPs.

1.4 Firoozabadi et al. Correlation

A simple correlation proposed by Firoozabadi et al. (1986) predicts MMP of reservoir fluids using lean natural gas or N_2 for injection. Three parameters account the effect of multiple-contact miscibility of a reservoir fluid under N_2 or lean gas flooding: The concentration of intermediates, the volatility, and the temperature.

The correlating parameter includes the ratio of the intermediates (mole percent) divided by molecular weight of the C_{7+} fraction. Intermediates contents of a reservoir fluid are usually attributed to the presence of C_2 through C_6, CO_2, and H_2S.

Firoozabadi et al. (1986) observed that exclusion of C_6 from intermediates improves the correlation of the MMP. Therefore, intermediates in this study are defined by C_2 through C_5 and CO_2 components. The heptane plus molecular weight provides an indication of the oil volatility. The equation is as follow:

$$MMP = 9{,}433 - 188\times10^{3}\times\left(\frac{x_{\text{int}}}{M_{C7+}T^{0.25}}\right) + 1430\times10^{3}\times\left(\frac{x_{\text{int}}}{M_{C7+}T^{0.25}}\right)^{2} \quad (4)$$

Where: MMP=Minimum Miscibility pressure, psi $x_{\text{int}} = x_{co_2} + \sum_{i=2}^{i=5} x_i$ =mole percent intermediates in the oil, and, M_{C7+} = molecular weight of heptane plus.

It should be noted that Peng-Robinson Equation-of-State (PR-EOS) based correlation proposed in this method is primary for estimating MMPs of VGD mechanisms by N_2 or lean hydrocarbon gases. The dependency of MMP on reservoir temperature is not well presented in this equation. More data are required to improve this temperature dependency (Firoozabadi et al. 1986).

1.5 Eakin and Mitch Correlation

The MMP data of combinations of oils, temperatures and solvents observed by Rising Bubble Apparatus (RBA) were represented by Eakin and Mitch (1988) correlation. Input variables for this equation are solvent composition, C_{7+} molecular weight, and the pseudoreduced temperature of the reservoir fluid. The base solvents used in their study were nitrogen, flue gas, carbon dioxide, and rich and lean natural gases. RBA is an alternative and much quicker apparatus for determining MMP but the obtained MMP is usually higher than the measured MMP by a slim-tube apparatus.

Kay's rules were used to calculate pseudocritical temperature, Tpc, and pseudocritical pressure, Ppc, of the oil (Kay, 1936).The general proposed correlation by Eakin and Mitch is:

$$\ln p_{pr} = \ln(MMP/p_{pc}) = (0.1697 - 0.06912/T_{pr})\times y_{c_1}\times M_{C7+}^{0.5} + (2.3865 - 0.005955\frac{M_{C7+}}{T_{pr}})\times y_{C2+} + (0.01221M_{C7+} - 0.0005899\frac{M_{C7+}^{1.5}}{T_{pr}})\times y_{CO_2} \quad (5)$$

This correlation has a standard deviation factor of 4.8% from the measured MMP values. The measured MMPs are only for two recombined sample of reservoir fluids with API gravities of 36.8 and 25.4, at 180 and 240°F.

1.6 Thermodynamic Method

In this method, selected EOS is calibrated to experimental PVT data including swelling and slim-tube measurements. Using of reliable experimental data in tuning EOS makes EOS (thermodynamic) methods the most reliable prediction methods.

In this method minimum miscibility pressure is explained traditionally by ternary diagrams. The limiting tie line is the extension of the tie line passing through the composition of the original oil and the tie line which passes through the critical point of the ternary diagram is called critical tie line. Monroe et al. (1987) showed three key tie lines which control displacement behavior in the reservoir: The tie lines that extend through injection gas composition, the tie line passing through the oil composition, and the third tie line called "the crossover tie line". Multi contact miscibility occurs if any of these tie lines correspond to the critical tie line. In vaporizing gas drive mechanisms miscibility is controlled only by the limiting tie line passing through the oil composition and is not dependent on injection gas composition. The gas phase composition varies along the dew-point phase boundary expressed at constant pressure and temperature in a pseudoternary diagrams towards the critical point composition. In condensing drive mechanisms the key tie line passing through the injection gas composition controls the development of miscibility. In this displacement mechanism miscibility is obtained at the site of injection. The intermediate components are condensed from the injection gas to the reservoir oil and miscibility develops as the tie line passing through the injection gas composition becomes the critical tie line expressed in ternary diagram model. Orr et al. (1987) and Johns et al. (1993) showed that crossover tie line controls the development of miscibility in combined vaporizing-condensing mechanisms.

1.7 Comparative Investigation of MMP Correlations

Multiple contact miscibility achieved by injection of lean hydrocarbon or flue gas into the reservoir is one of the most widely used oil recovery methods in the oil industry. The economic success of gas injection project can be improved by operating at pressures close to MMP. However, this requires accurate experimental measurements of MMP. The current proposed MMP correlations may be good substitute for both costly and time consuming experimental measurements.

Unfortunately, most of the MMP correlations are not flexible to represent a variety of solvent/oil combinations and care must be taken when selecting one of them. Reliable MMP correlations should be used for preliminary screening or feasibility studies, but should not be relied upon. The first part of this study provides an evaluation of the existing lean hydrocarbon or impure CO_2-stream MMP correlations published in the literature.

1.8 Reservoir Fluid Composition

To investigate the effect of oil composition on estimated minimum miscibility pressure, two different oil samples (reported by Core Laboratories, INC.) with API gravities of 20.8 and 44.5 have been considered. Table 1 provides composition data of these reservoir fluids. Mole percent of heptanes plus fraction (greater than 20%) and high critical point temperature compare to typical reservoir temperature, are indicative of black oil system. The reported simulation results in this chapter are the results of using PVTsim in modeling phase behavior of both reservoir fluids (Schlumberger, 2001).

Table 1
Reservoir Oil Compositions at First Part of the Study (Reported by Core Laboratories, INC.)

Component	Oil A, mole%	Oil B, mole%
N_2	0.03	1.85
CO_2	0.05	0.26
C_1	28.24	38.85
C_2	0.6	10.85
C_3	1.23	7.28
iC_4	0.47	2.81
nC_4	1.38	3.44
iC_5	0.86	2.33
nC_5	1.06	1.52
C_6	1.39	3.29
C_{7+}	64.69	27.52
C_{7+} Properties:		
Molecular Weight	308	175
Oil gravity, °API	20.8	44.5

Table 2
Injection Gas Composition

Component/Gas	A1	A2	A3	B1	B2	B3
N_2	0.289	0.216	0.188	7.401	5.366	4.1
CO_2	0.079	0.101	0.115	0.307	0.35	0.355
C_1	98.038	96.482	94.211	77.582	71.203	63.337
C_2	0.556	0.779	0.938	8.763	11.163	12.321
C_3	0.457	0.805	1.131	3.128	4.99	6.43
iC_4	0.096	0.195	0.301	0.802	1.471	2.096
nC_4	0.21	0.458	0.748	0.798	1.577	2.368
iC_5	0.069	0.176	0.321	0.349	0.803	1.347
nC_5	0.069	0.187	0.355	0.196	0.478	0.834
C_6	0.041	0.136	0.296	0.248	0.731	1.462
C_7	0.049	0.199	0.507	0.188	0.66	1.493
C_8	0.027	0.125	0.351	0.11	0.443	1.106
C_9	0.013	0.071	0.226	0.059	0.281	0.792
C_{10+}	0.007	0.07	0.312	0.069	0.484	1.959
C_{10+} Properties:						
Molecular Weight	162.71	164.74	168.43	150.16	157.29	167.66
Density,lb/ft^3	51.48	51.71	52.14	50.67	51.46	52.65
Injection Gas Properties:						
Gas A1:Flash of oil A @ T=100 °F & P=1,200 psi						
Gas A2:Flash of oil A @ T=200 °F & P=1,500 psi						
Gas A3:Flash of oil A @ T=300 °F & P=1,800 psi						
Gas B1:Flash of oil B @ T=100 °F & P=1,900 psi						
Gas B2:Flash of oil B @ T=200 °F & P=2,400 psi						
Gas B3:Flash of oil B @ T=300 °F & P=2,800 psi						

1.9 Injection Gas Composition

It is most economical to re-inject all or part of the produced dry gas back into the reservoir. Produced gas of the reservoir is an alternative source for gas injection and pressure maintenance processes. To achieve this purpose, the compositions of the injection gases are close to the equilibrium gas with the reservoir fluid. For each reservoir fluid (oil A and oil B), flash calculations at different temperatures (100, 200 and 300 °F) and at pressures, below the corresponding bubble point pressure of the oil at that temperature (Table 2), were made and the separator gas as a result of flash process, has been considered as the injection gas. The higher the temperature of the flash condition, the richer the gas is in intermediate components.

1.10 Correlation Results

There are only a few correlations applicable for this investigation. Most of the proposed MMP correlations are presented for CO_2 flooding rather than hydrocarbon flooding which is a general case. Among the MMP correlations mentioned above, Firoozabadi et al. (1986) are correlations that are not dependent on injection gas composition. Eakin and Mitch (1988) and Glasø (1985) correlations consider effects of gas and oil compositions in predicting MMPs.

Two different oil samples along with three injection gas compositions for each specific oil gravity cause various combination of gas flooding processes. Tables 3 through Table 5 indicate the predicted MMPs using the three correlations described above. As we know the heavier the reservoir fluid, the higher MMP is required to achieve miscibility. Reservoir fluid with API gravity of 20.8 (oil A) requires the highest MMPs. The injection gas with higher percentage of intermediate components provides lower MMPs for a specified oil reservoir. Therefore, the required MMP to achieve dynamic miscibility for oil A (lower API), is highest for injection gas A1 (leanest) and lowest for injection gas A3 (richest). As mentioned before, the injection gases used in this study are the separator gases which are the result of flash calculations. The separator gas with higher flash temperature contains more intermediate components and is most desirable in gas injection processes.

Table 3
Predicted MMPs Using Eakin and Mitch[11] Correlation

Reservoir Temperature, °F	MMP of Oil A (psia)			MMP of Oil B (psia)		
	Gas A1	Gas A2	Gas A3	Gas B1	Gas B2	Gas B3
100	6,067	5,856	5,532	3,511	3,263	2,936
200	6,808	6,594	6,265	3,840	3,610	3,295
300	7,411	7,197	6,866	4,102	3,889	3,587

Table 3 represents the predicted results using Eakin and Mitch (1988) correlation. Estimated MMP results are provided at reservoir temperatures of 100, 200 and 300 °F. The MMP for oil A and injection gases A1, A2 and A3 is trend consistent.

Table 4
Predicted MMPs by Firoozabadi[10] et al. Correlation (This Correlation like Majority of Lean Gas MMP Correlations Ignores the Effect of Injection Gas Composition)

Reservoir Temperature, °F	MMP of Oil A (psia)	MMP of Oil B (psia)
	Injection gases:A1, A2, A3	Injection gases:B1, B2, B3
100	8,399	3,564
200	8,557	4,000
300	8,639	4,294

The only parameters in Firoozabadi et al. (1986) correlation for vaporizing-drive mechanism are the concentration of intermediates, the oil volatility, and reservoir temperature. This correlation doesn't account for varying injection gas compositions and the estimated MMPs for light oil is relatively not dependent on injection gas composition. Predicted MMP results for reservoir fluids A and B are presented in Table 4.

Table 5
Predicted MMPs Using Glasø[7] Correlation. This Correlation Predicts Unreliable MMPs for Oil A and very Low Values for Injection Gas B2

Reservoir Temperature, °F	MMP of Oil A (psia)		MMP of Oil B (psia)	
	Gas A1	Gas A2	Gas B1	Gas B2
100	3,640	8,716	1,682	540
200	6,966	18,025	3,204	1,077
300	10,313	27,334	4,726	1,612

Table 5 indicates the correlation results using Glasø (1985) correlation. Unlike the previous correlation this correlation estimates the MMP of fluid with API gravity of 20.8 much higher than the other reservoir fluid but the effect of injection gas composition seems to be negligible. Gas A1 should provide the highest MMPs due to low concentrations of its intermediate components compared to A2 but the results are anomalous. Low estimated MMP values for injection gas B2 seem to be abnormal.

The discrepancy among these correlations makes the selection impossible unless there is evidence that correlation was adequate for an oil/solvent with similar characteristics.

1.11 Comparison of Simulation and Correlation Results

Since the reservoir fluid A is heavy the required MMP to achieve miscibility with injection gases A1, A2, and A3 are too high. Therefore, only reservoir fluid B with higher API gravity is appropriate for investigating multi-contact (VGD) miscibility pressures. Table 6 indicates the comparison of estimated MMPs (correlations) and simulation (Schlumberger, 2001b) results for oil B/Gas B1 system in VGD mechanism. Among these correlations Glasø[7] et al. correlation is strongly dependent on reservoir temperature. It can be clearly seen in this correlations that MMP values increase rapidly as temperature increases. Other correlations except for Glasø[7] approach, seems to represent parallel slopes and closer MMP values to each other.

Table 6
Comparison of Simulation[1] (Peng-Robinson EOS-Based Model) and Correlation Results for Fluid B/ Injection Gas B1 System (Vaporizing-Gas Drive Mechanism)

T, °F	Simulation	Eakin	Glasø	Firoozabadi
100	4,354	3,511	1,682	3,564
200	4,372	3,840	3,204	4,000
300	3,964	4,102	4,726	4,294

Evaluation of the accuracy of each MMP correlation illustrates that Firoozabadi et al. (1986) and Eakin and Mitch (1988) methods are found to be the most reliable correlations among the other ones. These correlations are EOS and statistic based models and the good agreement with simulation results could be attributed to this concept. As was mentioned before, simulation approach in calculating MMPs for different injection gas/oil systems is based on equation of state (EOS) model. It should be added that MMP data or other types of PVT data must be used to calibrate the EOS. The advantage of using EOS is that it is a self consistent method and can be easily tuned to available experimental data.

The large discrepancy of the Glasø (1985) correlation in predicting the vaporizing-gas drive MMPs is related to the limited slim tube experiments. This correlation was mostly developed from experimental slim tube MMP data of North Sea gas/oil system and special care should be paid to predict MMPs of other reservoir fluids.

As a general case, the evaluated MMP correlations in this study are not reliable and they should be applied with great care in particular situations even for preliminary MMP calculations and screening processes.

2. EVALUATION OF PARAMETERS ON MISCIBLE AND IMMISCIBLE GAS-INJECTION PROCESSES

Injection of cost-effective lean hydrocarbon gas or flue gases could be employed in reservoirs where a favorable combination of pressure, reservoir characteristics and fluid properties make the gas injection project a competitive process compare to other secondary oil recovery methods. However, for a gas injection project, to be competitive several conditions should be satisfied. The incremental oil recovery is largely dependent on injection pressure, reservoir characteristics and fluid properties such as heterogeneity, relative permeability, viscous fingering, fluid mobility, gravity segregation, etc.

In this section, following a reliable estimate of the MMP (based on both simulation and experimental results) a parametric study is done, using a 3D, compositional simulator to analyze the effect of such important parameters in miscible or immiscible performance recovery from the reservoir.

2.1 Field Description

The first constructed reservoir grid model is a two-layer homogenous model (9×9×2) with constant porosity (0.13), permeability, and thickness (40 ft). PVT data of the reservoir fluid including the injection gas composition are provided in Table 7.

Table 7
Reservoir Fluid and Injection Gas Composition

Component	Reservoir Fluid, mole %	Injection Gas, mole %
N_2	0.92	0
CO_2	0.32	0.877
C_1	41.25	87.526
C_2	8.68	6.36
C_3	7.27	3.906
C_4	4.9	1.331
C_5	2.89	0
C_6	4.29	0
C_{7+}	29.48	0
Heptanes Plus Properties:		
Molecular Weight		202
Specific Gravity		0.86

Reservoir fluid is initially undersaturated. The initial reservoir pressure is 4,300 psi and the saturation pressure of the reservoir fluid at 217 °F is 2,931 psi. Low water viscosity in the reservoir, 0.3 cp, giving rise to the low gas to oil mobility ratio. Setting the initial condition for the location of water/oil contact to 8,500 ft (80 ft below the oil zone), and setting the oil/water capillary pressure to zero could eliminate the transition zone between oil and water phases. The very small compressibility and volume of the water; however, makes water rather insignificant in this problem. Initial oil and water saturations are 0.78 and 0.22.

Injection well is perforated in the first layer whereas the production well is completed in the second layer and produced on deliverability against a 1,000 psi flowing bottomhole pressure. Lean gas with similar composition of the vapor phase in equilibrium with the reservoir fluid at reservoir temperature and at pressure slightly below the bubble point, is injected continuously into the first layer of the reservoir with average thickness of 40 ft. Constant injection pressure (4,800 psia) for the injection well is the only constraint applied to the injection well.

2.2 Relative Permeability Effect

The term miscible recovery is defined as any oil recovery displacement mechanism, where the phase boundary or interfacial tension between the displaced and displacing fluids is negligible. In this situation the capillary number becomes infinite and the residual oil saturation can be reduced to the lowest possible value because there is no interfacial tension (IFT) between the fluids. Setting the reference surface tension defines the interpolation factor as:

$$F = \left(\frac{\sigma}{\sigma_0}\right)^N$$

Consequently the appropriate relative permeability curve dependent on dominant flow will be used by the following equation:

$$K_{ro} = FK_{ro}^{imm} + (1-F)K_{ro}^{mis} \quad (6)$$

In this section, miscibility option is imposed by setting an arbitary high reference surface tension (σ_0). The immiscibility factor approaches to zero for gridblocks containing two phases become fully miscible ($\sigma \approx 0$) and form a single phase. Simulation runs conducted at injection pressure of 4,800 psi (This is the estimated MMP value determined for injection gas/reservoir fluid system at reservoir temperature of 217 °F) for two cases of miscible (straight line k_r) and immiscible (input saturation data) option.

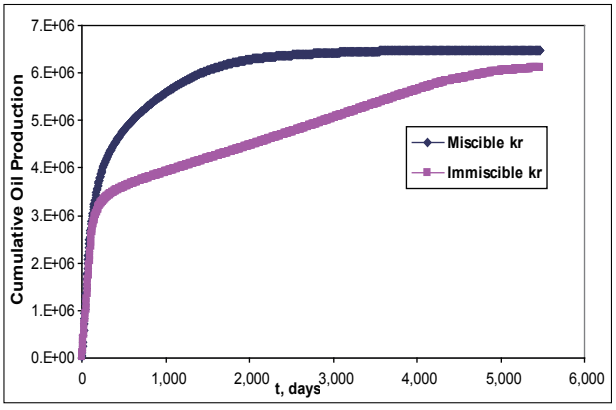

Figure 1
Comparison of Cumulative Oil Production for Miscible and Immiscible Relative Permeabilities (Injection Pressure of 4,800 psi)

Cumulative oil production and predicted recovery vs. pore volume of injection gas is provided in Fig. 1. Distinct recovery trends are estimated for different miscible and immiscible relative permeabilities. The calculated oil recoveries at 1.2 pore volume of injected gas for miscible k_r and immiscible k_r are 73.5% and 55.4% of OOIP. In other word, 18.1% OOIP is the incremental oil recovery using miscible k_r for the same injection pressure and pore volumes of injection gas as those of immiscible ones. Moreover, the revenue from additional oil recovery is concentrated in the early life of the project and the rate of return of investment using miscible k_r is higher compare with that of immiscible k_r. Considerable amount of recoverable oil is produces up to nearly seven years of gas injection for miscible k_r. Therefore it is most beneficial to stop flooding at this time, since only a maximum of 0.1% OOIP incremental oil recovery is predicted at the end of the project which is at 15 years of injection.

It should be noted that for highly undersaturated reservoirs with high-gravity crude oils, which is this case study, recovery increases significantly by initiating gas injection project at the highest pressure possible, even though miscibility is not developed. The improvement in recovery efficiency is mainly the result of reduction in oil

viscosity, oil swelling, and vaporization of the residual oil. Recovery in miscible displacement is strongly sensitive to changes in fluid properties and reduction in interfacial tension, resulting in variation of the relative permeability endpoints.

2.3 Injection Pressure Effect

In this part of the study, the effect of injection pressure on the oil recovery from the entire symmetrical grid model has been investigated. Injection and production wells are completed in the first and second layer, respectively. Estimated MMP based on equation of state analytical method is approximately 4,800 psi. Simulation runs have been conducted at pressures below, equal to and greater than this pressure (4400, 5000, 5600 and 6200 psi). Since in vaporizing drive mechanisms, the pressure at miscible front should be greater than the predicted miscible pressure, injection of gas at 5,000 psi will raise the average reservoir pressure from initial pressure to the miscibility pressure of 4,800 psi. Therefore, the injection pressure of 5,000 psi seems to be the best candidate for representing MMP in simulation model. Estimated recoveries at 1.2 pore volume of injected gas are about 50.9, 75.2, 79.6, and 82.6% OOIP which are attainable after 677, 537, 486, and 444 days of continuous gas injection, respectively.

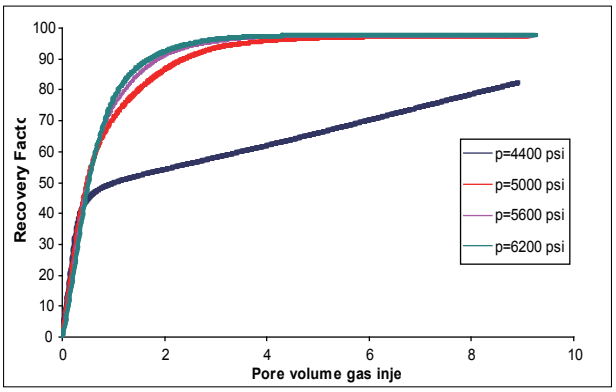

Figure 2
Incremental Oil Recovery After Around 4 Pore Volume of Injected Gas is Marginal at Pressures Above MMP

It is clearly seen in Fig. 2 that incremental oil recovery due to miscible injection is paramount; however the marginal increase in oil recovery as the result of injection at pressures higher than MMP may not compensate for additional equipment and operating costs at greater pressures. Oil recoveries are usually greatest when the gas injection process is operated under miscible conditions. Miscibility can be achieved by managing the reservoir pressure. Under appropriate condition of achieving miscibility, MMP will be the optimum injection pressure.

Table 8
Reservoir Grid Data (Stratified Reservoir) and Water Properties

Reservoir Grid Data				
NX=NY=9, NZ=2				
DX=DY=293.3 ft				
Porosity				0.13
Datum (subsurface), ft				8,420
Oil/water contact, ft				8,500
Capillary pressure at contact, psi				0
Initial pressure, psi				4,300
Reservoir temperature, °F				217
Layer	Horizontal permeability	Vertical Permeability	Thickness, ft	Depth to top (ft)
1	90 (3)	9 (0.3)	40	8,340
2	3 (90)	0.3 (9)	40	8,380
Water properties				
Compressibility, psi^{-1}				3×10^{-6}
Density, lbm/ft^3				63
Rock compressibility, psi^{-1}				4×10^{-6}
Viscosity, cp				0.3

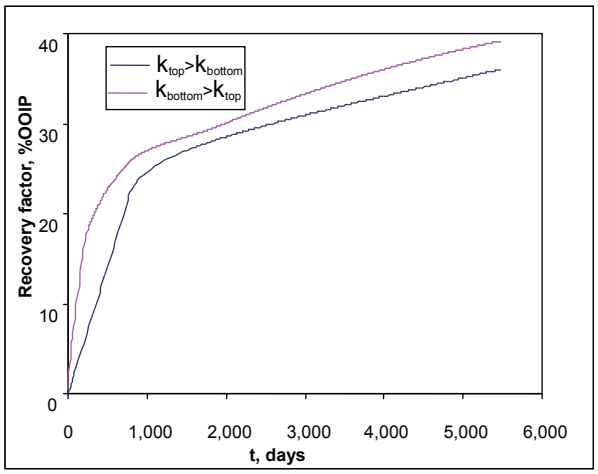

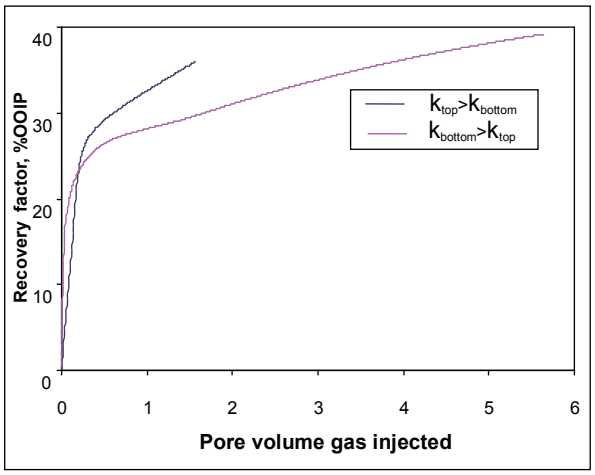

a) Estimated Oil Recovery at Injection Pressure of 4,400 psi

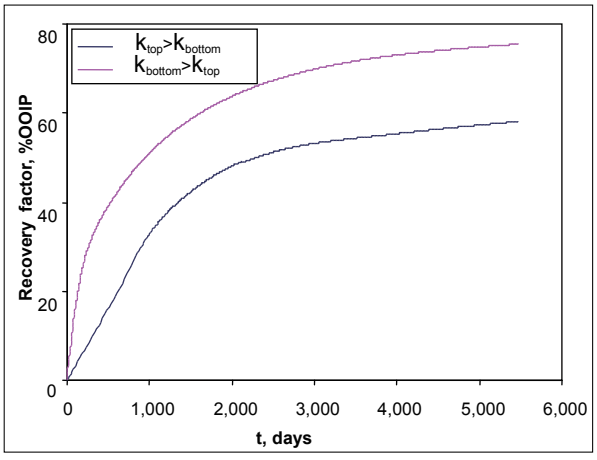

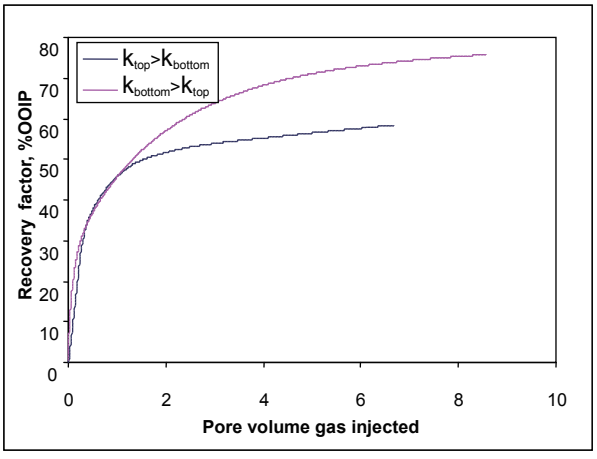

b) Estimated Oil Recovery at Minimum Miscibility Pressure of 5,000 psi

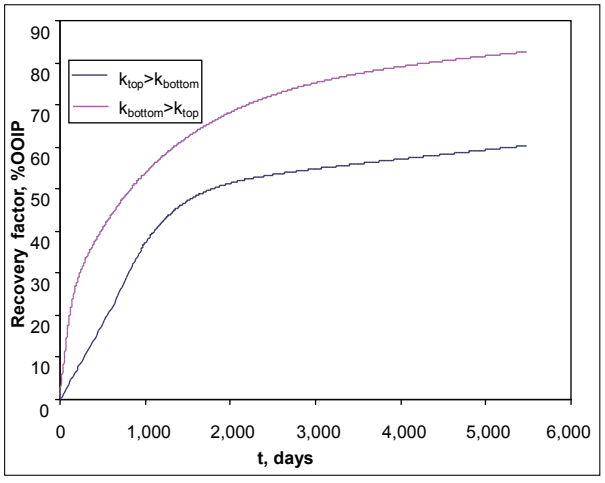

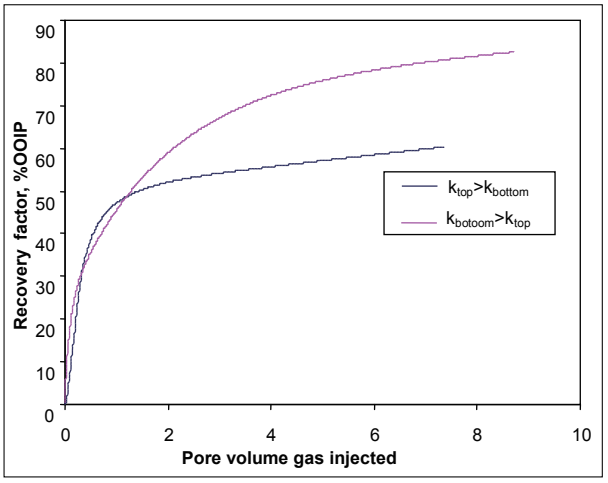

c) Estimated Oil Recovery at Injection Pressure of 5,600 psi

Figure 3
Stratification Effect on Oil Recovery at Different Injection Pressures

2.4 Stratification Effect

Conformance efficiency is one of the determinant factors that control maximum oil recovery from a reservoir. Conformance efficiency is defined as the fraction of the total pore volume within the pattern area that is contacted by the displacing fluid. The dominating factors that control conformance area are the gross sand heterogeneity and size distribution of the rock interstices, which usually are defined in terms of permeability variation or stratification.

Two new stratified reservoir models were constructed to ascertain the effect of stratification on the miscible and immiscible oil recovery processes. The new constructed model (Table 8) is a two-layer stratified reservoir. The layers have horizontal permeability values of 90 and 3 mD, and vertical permeabilities of 9 and 0.3 mD, respectively. The ratio of horizontal to vertical permeabilities of each layer is 10. In all of the simulation models the injection and production wells are completed in the first and second layers of the reservoir, respectively (one reservoir has k_{top}= 90, k_{bottom}=3 mD and anther one has k_{top}= 3, k_{bottom}=90 mD).

Table 9
Comparison of Oil Recovery at 1.2 Pore Volume of Injected Gas (Injection is Always in the Top Layer and Production from the Bottom of the Reservoir)

Injection Pressure, psi	Predicted Oil Recovery and GOR at 1.2 Pore Volume of Injected Gas			
	$k_{top} > k_{bottom}$ (k_{top} =90 mD ; k_{bottom} =3 mD)		$k_{bottom} > k_{top}$ (k_{top} =3 mD ; k_{bottom} =90 mD)	
	t, days	Rec., %OOIP	t, days	Rec., %OOIP
4,400	4,378	33.8	1,546	28.6
5,000	1,955	47.7	854	48.4
5,600	1,633	48.7	784	48.8

Table 9 summarizes the simulation results regarding recovery performance of the stratified reservoir under miscible and immiscible gas injection. The calculated oil recoveries are provided at 1.2 pore volume of gas injected and for the cases where the higher permeable layer is located in the upper or lower part of the reservoir. The injection and production wells are completed in the first and second layers of the reservoir, respectively. Recovery performance of the stratified reservoir during 15 years of miscible or immiscible gas injection of the reservoir is presented in Fig. 3. The predicted recoveries are presented as function of time and volume of injected gas at the same time. Comparison of the simulation results leads to the following conclusions:

(1) Significant increase in oil recovery is observed for a miscible displacement mechanism. Incremental oil recovery between injection pressures of 5,000 and 5,600 psi indicates minimum miscibility pressure (5,000 psi) as the optimum injection pressure from economic point of view.

(2) Comparison of the estimated recovery values for two different cases, $k_{top} > k_{bottom}$ (k_{top} =90 mD and k_{bottom} =3 mD) and $k_{bottom} > k_{top}$ (k_{top} =3 mD and k_{bottom} =90 mD), indicate the key factor that determines the effect of layering on oil recovery at a particular injection pressure, is the vertical location of the high-permeability streak in the stratified reservoir. If the high permeability layer is located in the lower half of the reservoir ($k_{bottom} > k_{top}$), the oil recovery improves since the combination of the stratification and gravity effects retard the segregation of the gas into the top portion of the reservoir cross-section. This effect is more evident in miscible displacement mechanism where the gas is injected at pressures equal to or above MMP value. It should be noted that in making this comparison, the determinant time factor in evaluating the incremental oil recovery or project economics should be taken into account. Reported recovery values for the second case, where the more permeable layer is located on the lower half of the reservoir ($k_{bottom} > k_{top}$), are in earlier times of project life compare with those of the first case.

(3) High potential of gas injectivity (smaller times required to inject 1.2 pore volume of gas) when $k_{bottom} > k_{top}$ makes this case advantageous in comparison for the other case where $k_{top} > k_{bottom}$.

2.5 Interface Tension and Mobility Ratio Effects

Oil recovery by miscible flooding has not been applicable as widely as waterflooding. Unlike the case for miscible flooding, waterflooding can be employed successfully from both technical and economic point of view in most oil recovery projects. In this part of the study, appropriate questions, when evaluating a gas injection design are discussed with more details.

The benefit of gas injection is mostly because of the fact that it exhibits better surface tension effect than water. High cost includes operating and equipment costs, solvent availability, and pressure/composition requirements for miscibility are the major limiting factors in miscible flooding. Nevertheless, the interfacial tension benefit can often outweigh the extra expense.

The benefit of gas injection can be easily concluded from the relation of capillary pressure as a function of interfacial tension and pore throat radius. Capillary pressure is proportional to the interfacial tension and inversely proportional to the pore throat radius. This indicates that as long as the water-oil interfacial tension is greater than the gas-oil interfacial tension, gas injection, no matter how immiscible, would be of benefit since the smaller pore throats will be accessed during gas injection. However, adverse mobility ratio which originates from large oil/gas viscosity ratio (range of oil viscosity, 0.23-0.31 cp), associated in most gas injection projects makes this recovery method risky. Therefore, understanding the interaction between interfacial tension and adverse mobility ratio is subject of great importance for a gas injection project. Next section is the simulation approach that is followed to investigate the effect of mobility ratio and interfacial tension on the recovery of the reservoir.

An 18×18×3 cross-section model is used in this simulation to make a quarter of a five-spot pattern (Table 10). The three layers of the reservoir are homogeneous with constant porosity, permeability and thickness values. It should be noted that miscible gas recoveries are not sensitive to the shape of the relative permeability curves. As miscibility develops, the saturation curve approaches to the straight line with different endpoints relative permeabilities.

Table 10
Reservoir Data and Water Properties

Reservoir Grid Data				
NX=NY=18,				
NZ=3				
DX=DY=293.3 ft, DZ=27 ft				
Porosity				0.13
Datum (subsurface), ft				8,421
Oil/water contact, ft				8,600
Capillary pressure at contact, psi				0
Initial pressure, psi				4,300
Water Properties				
Compressibility, psi^{-1}				3×10^{-6}
Density, lbm/ft^3				63
Rock compressibility, psi^{-1}				$4*10^{-6}$
Layer	Horizontal Permeability	Vertical Permeability	Thickness, ft	Depth to Top (ft)
1	90	0.9	27	8,340
2	90	0.9	27	8,367
3	90	0.9	27	8,394

The average water viscosity 0.31 cp, which is close to the reservoir oil viscosity, gives rise to an exceptionally low and favorable mobility ratio for water-oil displacement. The varied fluid composition and injection gases are provided in Table 11.

The first dry injection gas A is intended to represent a dominated mobility ratio displacement, whereas the rich injection gas B represents an interfacial tension dominated factor occurring in the reservoir. The initial reservoir pressure is 4,300 psi and the saturation pressure of the reservoir fluid with API gravity of 33 is 2,255 psi.

Injection and production wells are located on the corners of the grid model to make a five-spot pattern. Gas injection well is perforated in the first and second layers of the reservoir, whereas, water injection and production wells are completed in the second and third layers. Constant injection pressure and reservoir volume water injection rate are the injection well constrains. The water injection rate is determined in such a way that same order of injected water and injected gas pore volumes at the end of the project would be injected. Minimum flowing bottomhole pressure of 1,000 psi is the production-well constrain especially at the early times of production where pressure declines dramatically.

The injection gas composition varies in such a case to have interfacial tension and mobility ratio dominated

Table 11
Reservoir Fluid and Injection Gas Compositions

Gas Component	Reservoir Fluid	Injection Gas A	Injection Gas B
N_2	0.139	0.461	0.67
CO_2	0.049	0.266	5.03
C_1	34.279	78.923	60.95
C_2	4.364	18.34	23.76
C_3	3.486	2.01	9.59
iC_4	2.633	0	0
iC_5	4.875	0	0
C_6	3.771	0	0
C_{7+}	46.464	0	0
Heptanes plus properties:			
Molecular weight: 202			
Specific gravity: 0.86			
Oil viscosity: 0.31 cp			
Injection-gas A viscosity:0.02 cp			
Injection-gas B viscosity:0.04 cp			

displacement mechanisms of the particular reservoir fluid. Mobility ratio of the lean injection-gas A (viscosity of 0.02 cp) and the reservoir fluid is around 15.6, whereas the calculated mobility ratio of the oil and the intermediate injection-gas B equals 7.8.

Recovery comparison is based on the differences between the estimated recovery for the gas and water injection projects. Unit mobility ratio is employed in simulating waterflooding project. Figs. 4 and 5 provide the oil recovery comparison results in mobility and interfacial surface tension dominated displacement mechanisms. The calculated recoveries at 1.2 pore volume of gas or water injection are 41.98 and 49.95 % OOIP for mobility dominated mechanism, and 75.46 and 50.32 % OOIP for interfacial tension dominated mechanism, respectively. As results indicate, for a mobility dominated displacement mechanism the viscous instabilities are more important than the interfacial tension effect and the injection gas composition is less important from an interfacial surface tension point of view. In these cases waterflooding with favorable mobility ratio yields higher oil recovery values (Fig. 4).

Absence of unfavorable mobility ratio in miscible flooding results in significant oil recovery due to the low interfacial tension between the injection gas and reservoir fluid (Fig. 5).

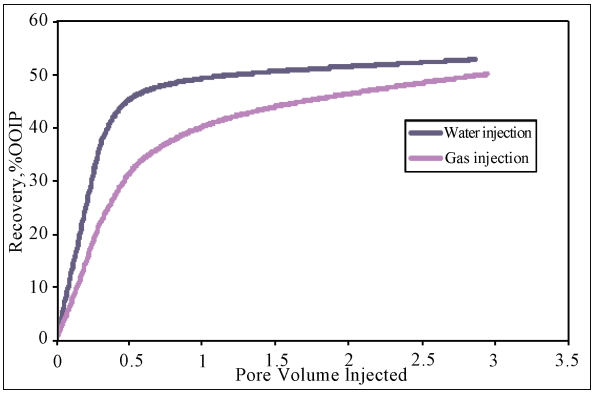

Figure 4
High Mobility Ratio in Gas Injection Project Decreases the Oil Recovery from the Reservoir (Njection with Lean Gas A, Mobility Ratio=15.6)

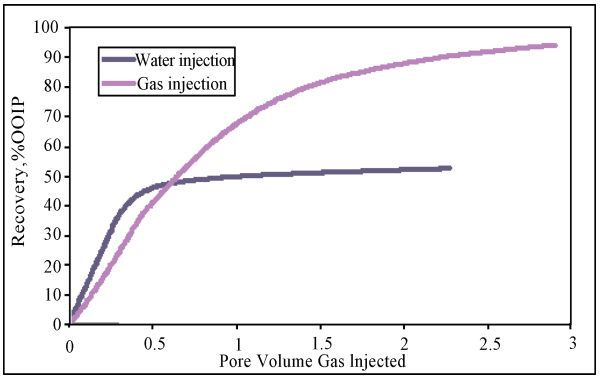

Figure 5
Absence of Unfavorable Mobility Ratio in Miscible Flooding Improves the Oil Recovery to a High Degree (Injection with Rich Gas B, Mobility Ratio=7.8)

CONCLUSIONS

The first part of this study presented an evaluation of the existing MMP correlations published in the literature for lean hydrocarbon gases. The reliability of individual correlations was evaluated by determining, on average, how close the appropriate MMPs and EOS-based analytical calculations are. As a general observation, the evaluated MMP correlations studied in this investigation were not sufficient for preliminary MMP-calculation purposes. Many of these correlations have proven not to honor the effect of fluid composition properly. The methods of Firoozabadi[10] et al. and Eakin and Mitch were found to be the most reliable of the correlations tested. In most cases EOS-based analytical methods seemed to be more conservative in predicting MMP values. Hence, experimental MMP measurements would also be required for the design of gas-injection projects and calibration of fluid model.

Following a reliable estimate of MMP, numerous compositional simulation models were used to investigate the effect of key parameters in miscible or immiscible recovery performance of the reservoir. Distinct recovery trends were observed using different miscible and immiscible relative permeabilities. For the same injection pressure and pore volumes of injection gas as those of immiscible relative permeability curve, the incremental oil recovery using miscible k_r, was substantial.

Incremental oil recovery was determined by injection pressure. Pressure was the key parameter in determining whether or not the injection gas will be miscible with the in-situ oil. A multiple-contact miscible process was proven viable to increase the oil recovery to a high degree. Oil recoveries were usually greater when the gas-injection process was operated under miscible conditions. Miscibility can be achieved by injecting gas at pressures equal to or greater than MMP. At pressures higher than the MMP, the incremental recovery obtained was not substantial.

Comparison of estimated oil recoveries illustrated that stratification can affect oil recovery substantially. The major factor on the stratification effects was the vertical location of the higher-permeability layer. A high-permeability layer located in the lower half of the reservoir may improve the oil recovery potential. The maximization of oil recovery for this case may be the result of a combination of vertical displacement caused by gravity override and horizontal displacement of the oil by the high-permeability layer.

If a system is viscosity-dominated, the injection-gas composition may not be important from an interfacial tension perspective. In this situation, an alternative waterflooding recovery method may show more productivity improvement even with less investment. Therefore, understanding the effect of adverse mobility ratio and interfacial tension on the recovery of the reservoir is of great importance for a gas injection project to be implemented successfully.

REFERENCES

[1] Alston, R. B., Kokolis, G. P., & James, C. F. (1985). CO_2 Minimum Miscibility Pressure: A Correlation for Impure CO_2 Streams and Live Oil Systems. *SPE Journal*, *25*(2), 268-274.

[2] Benham, A.L., Dowden, W.E., & Kunzman, W.J. (1960). Miscible Fluid Displacement-Prediction of Fluid Miscibility. *Petroleum Transactions, AIME*, *219*, 229-237.

[3] Cook, A.B., Walter, C.J., & Spencer, G.C. (1969). Realistic K-Values of C_{7+} Hydrocarbons for Calculating Oil Vaporization During Gas Cycling at High Pressure. *JPT*, *21*(7), 901-915.

[4] Eakin, B.E., & Mitch, F.J. (1988). *Measurement and Correlation of Miscibility Pressure of Reservoir Oils.* SPE 18065, Presented at the Annual Technical Conference and Exhibition, 2-5 Oct, 1988, Houston, TX.

[5] Firoozabadi, A., & Aziz, K. (1986). Analysis and Correlation of Nitrogen and Lean-Gas Miscibility Pressure. *SPE J.*, *1*(6), 575–582.

[6] Glasø, Ø. (1980). Generalized Pressure-Volume-Temperature Correlations. *Journal of Petroleum Technology*, *32*(5), 785-795.

[7] Glasø, Ø. (1985). *Generalized Minimum Miscibility Pressure Correlation. SPE 12893.* Presented at the SPE Annual Technical Conference and Exhibition. Dec. 1985, San Antonio, TX.

[8] Johns, R. T., Dindoruk, B., & Orr, F. M., Jr. (1993). Analytical Theory of Combined Condensing/Vaporizing Gas Drives. *SPE Adv. Tech. Ser.*, *2*(3), 7-16.

[9] Kay, W. B. (1936). Density of Hydrocarbon Gases and Vapors at High Temperatures and Pressure. *Ind. Eng. Chem.*, *28*(9), 1014-1019.

[10] Metcalfe, R. S., Fussell, D. D., & Shelton, J. L. (1972). *A Multicell Equilibrium Separation Model for the Study of Multiple Contact Miscibility in Rich-gas Drives*. SPE 3995. Presented at the SPE Annual Technical Conference and Exhibition 8-11 Oct 1972, San Antonio, TX.

[11] Monroe, W. W., Silva, M. K., Larsen, L. L., & Orr Jr., F. M. (1990). Composition Paths in Four- Component Systems: Effect of Dissolved Methane on 1-D CO_2 Flood Performance. *SPE Res. Eng., 5*(3), 423-432.

[12] Orr Jr., F. M., & Silva, M.K. (1987). Effect of Oil Composition on Minimum Miscibility Pressure-Part 2-Correlation. *SPE Res. Eng.*, *2*(4), 479-487.

[13] Schlumberger. (2001a). *PVTsim, version 12 user's guide*: *Calsep Inc.* Houston, TX.

[14] Schlumberger. (2001b). *Eclipse, version 2001A user's guide*: *Calsep Inc.* Houston, TX.

[15] Sebastian, H.M., Wenger, R.S., & Renner, T.A. (1985). Correlation of Minimum Miscibility Pressure for Impure CO_2 Streams. Journal of Petroleum Technology, *37*(11),

2076-2082.

[16]Stalkup, F. I. (1987). *Displacement Behavior of the Condensing/Vaporizing Gas Drive Process*. SPE 16715. Presented at the SPE Annual Technical Conference and Exhibition. 27-29 Sep 1987, Dallas, TX.

[17]Zick, A.A. (1986). *A Combined Condensing-Vaporizing Mechanism in the Displacement of Oil by Enriched Gases*. SPE 15493. Presented at the SPE Annual Technical Conference and Exhibition. 5-8 Oct 1986, New Orleans, LA.

CSCanada
Advances in Petroleum Exploration and Development
Vol. 3, No. 1, 2012, pp. 33-37
DOI:10.3968/j.aped.1925543820120301.155

ISSN 1925-542X [Print]
ISSN 1925-5438 [Online]
www.cscanada.net
www.cscanada.org

Numerical Simulation of Fracture Width Influencing Law on Reservoir Permeability After Fracturing

YANG Ningning[1,*]

[1] Institute of Drilling Technology, Shengli Petroleum Administration Bureau, Dongying 257017, China.
[*]Corresponding author.

Received 9 January 2012; accepted 10 February 2012

Abstract
Based on the fluid-solid coupling theory in porous media, a finite element simulation model for dynamic fracture creation is established and the finite element simulation program is developed, and then relevant finite element simulation is conducted on the permeability distribution under the simultaneous influence of fracture creation and pressure-released production. Research results demonstrate that the permeability distribution law after fracturing is similar for fractures with different widths, and the permeability distribution shapes in ellipse. When the maximal fracture width is greater than or equal to 6mm, the influence region on the permeability increases apparently with the increment of fracture width, so does the influence in the vicinity of the wellbore. The fracture creation and pressure-released production alternately dominates the alteration of permeability in different regions. Dynamic fracture creation plays a more important role in permeability alteration within the region less than 5m away from the wellbore axis. The larger for the fracture width, the more sensitive for the permeability alteration gradient is observed in the region in the vicinity of the wellbore. In the region 20m away from the wellbore axis, the pressure-released production affect more apparently since dynamic fracture creation has a negligible effect in the region.

Key words: Fluid-solid coupling; Permeability; Fracture; Wellbore; Simulation

YANG, N. N. (2012). Numerical Simulation of Fracture Width Influencing Law on Reservoir Permeability After Fracturing. *Advances in Petroleum Exploration and Development*, *3*(1), 33-37. Available from: URL: http://www.cscanada.net/index.php/aped/article/view/j.aped.1925543820120301.155
DOI: http://dx.doi.org/10.3968/j.aped.1925543820120301.155

Nomenclature
κ = the reservoir permeability
μ= the oil phase viscosity
c_t = the total compressibility
ε_v= the volumetric strain
σ_{ij}= the effective stress component
f_i = the volumic force
α= the Biot's poroelastic constant
a = the fitting coefficient of experiment
b = the fitting coefficient of experiment
σ = the effective stress

INTRODUCTION
The low permeability reservoir commonly shows relatively stronger stress sensitivity, and the petrophysical parameters will change with the suffered effective stress for reservoir rock frame[1-5].The artificial fracture creation in hydraulic fracturing and the pressure-released production will impose specified additional stress on the reservoir rock, which result in the change of formation pore configuration and reservoir permeability. Based on the fluid-solid coupling theory in porous media, a finite element simulation on dynamic fracture creation and pressure-released production is conducted, and the distribution law of permeability is quantitatively studied under the influence of both fracture creation and pressure-released production, and the effect of the dynamic creation of fracture with different widths is analyzed.

1. BASIC EQUATIONS OF FLUID-SOLID COUPLING THEORY IN POROUS MEDIA
The fluid-solid coupling mathematical model basically consists of three parts, including the fluid-flow equation, stress-deformation equation and auxiliary equation [6-10]. The single phase flow equation is adopted in the seeping field, and a linear elastic constitutive equation is

introduced in the stress field.

The fluid-flow equation is:

$$\frac{K}{\mu C_t}\nabla^2 p - \frac{1}{C_t}\frac{\partial \varepsilon_v}{\partial t} = \frac{\partial P}{\partial t} \quad (1)$$

The balance equation of stress-deformation can be expressed as:

$$\frac{\partial \sigma_{ij}}{\partial x_j} + \alpha\frac{\partial P}{\partial x_i} + f_i = 0 \quad (2)$$

Liu Jianjun[5] have experimentally concluded that the permeability of low permeable reservoir is a function of effective stress (σ).

$$K = a \cdot e^{-b\sigma} \quad (3)$$

In addition to the above-mentioned basic equations, the boundary condition and initial condition of the seeping field and stress field are also required for the solution of the fluid-solid coupling model. With respect to the seeping field, the commonly used boundary condition is either the constant pressure or the constant flow rate. With respect to the stress field, the commonly used boundary condition is either the stress or the displace [9-10].

Based on the fluid-solid coupling theory, the relevant finite element program is developed with the software of FEPG (Finite Element Program Generator), and the finite element model of dynamic fracture creation is analyzed.

2. ESTABLISHMENT OF DYNAMIC FRACTURE CREATION MODEL

Two basic assumptions adopted in the model are as follows: (1) the assumption of plain strain is introduced, and (2) the double wing of the hydraulic vertical fracture is symmetrical. A quarter of the model is simulated and analyzed because of the structural symmetry of the model. The size of the model is 300m×300m, the basic parameters of finite element simulation are presented in Table 1.

Table 1
Basic Parameters of Finite Element Simulation

Radius of bore hole /m	Maximum horizontal in-situ stress /MPa	Minimal horizontal in-situ stress /MPa	Pore pressure /MPa	Young's modulus / MPa	Poisson ratio
0.15	45	32	20	2.5×10^4	0.25
Biot's poroelastic constant	Reservoir permeability /m^2	Oil phase viscosity /Pa • s	Total compressibility /Pa^{-1}	Coefficient of sensitivity(a) /mD	Coefficient of sensitivity(b)
0.8	20×10^{-15}	3×10^{-3}	3.0×10^{-10}	97.7	0.0675

The finite element model of dynamic fracture creation is shown in Fig.1, and the geometry of hydraulic fracture is wedge. The fracture length is 120m, and the fracture width at the fracture tip is 0mm.The dynamic creation of fractures with width of 3mm, 4mm, 6mm, 8mm and 10mm are simulated.

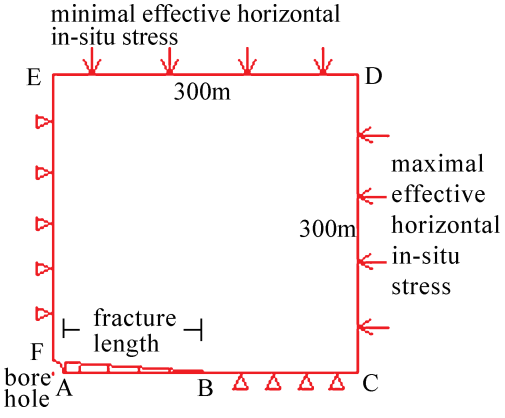

Figure 1
Schematic Diagram of the Dynamic Fracture Creation Model

The radius of borehole is very little compared with the size of the model, so the borehole can be simplified into a point in the simulation. And then the boundary condition and the initial condition are applied to the seeping field and the stress field.

The simulation without the dynamic fracture creation is also conducted. The edges of AB and BC are under the same boundary condition of displace constraint, the maximal effective horizontal stress is imposed on the edge of CD, and the minimal effective horizontal stress is imposed on the edge of DE. The flow conductivity of hydraulic fracture is assumed to be infinite, the flowing pressure of fracture surface is setup up to be 17MPa in the pressure-released production, and the initial value of pore pressure is setup to be 20MPa.

The formation time of fracture is assumed to be 30 minutes, the edge of AB is setup to be under the condition of dynamic displacement in the process of dynamic fracture creation, and the edge of AB is under the condition of displacement constraint after fracturing. With respect to the seeping field, the edge of AB is under the condition of dynamic flowing pressure. The value of flowing pressure of the edge of AB is setup to be 23MPa

during the dynamic fracture creation, and it will become into 17MPa (producing pressure) after fracturing.

The fluid-solid coupling model is solved by explicitly iterative calculation. After the calculation of the seeping field is completed, the increment of pore pressure is transferred to the stress field, the alteration of the effective stress induces change of the reservoir permeability, and then the updated permeability is used again in seeping field. Considering the simultaneous influence of fracture creation and pressure-released production, the boundary conditions of the coupling field and the dynamic parameters are regenerated at each time step.

3. DISTRIBUTION LAW OF RESERVOIR PERMEABILITY UNDER THE INFLUENCE OF FRACTURE CREATION

The simulation without the dynamic fracture creation is also conducted. Research results demonstrate that the value of permeability in the vicinity of the fracture surface declined from 20mD to 18mD, and the percent of permeability decrease is 10%. The permeability distribution under the simultaneous influence of fracture creation and pressure-released production is showed in Figs.2 through 6, and the unit of permeability is mD in this figures. The value of permeability near wellbore and fracture surface is obviously less than 18mD, and the further decrease of permeability originates from the dynamic fracture creation.

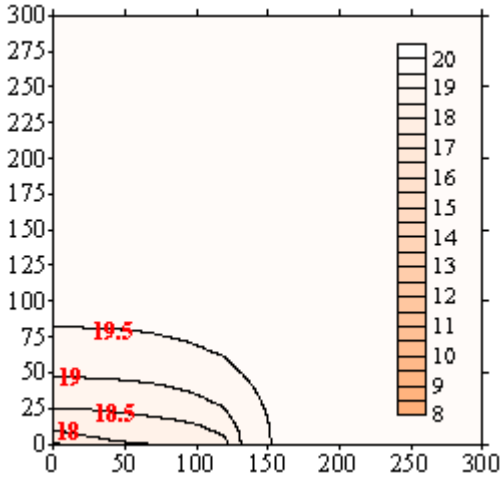

Figure 2
Permeability Distribution for Fracture with Maximal Width of 3mm

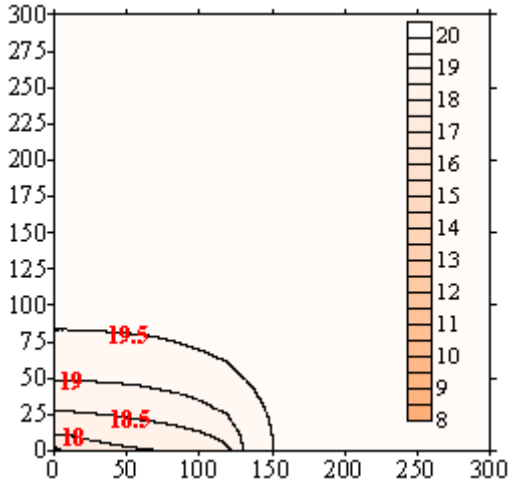

Figure 3
Permeability Distribution for Fracture with Maximal Width of 4mm

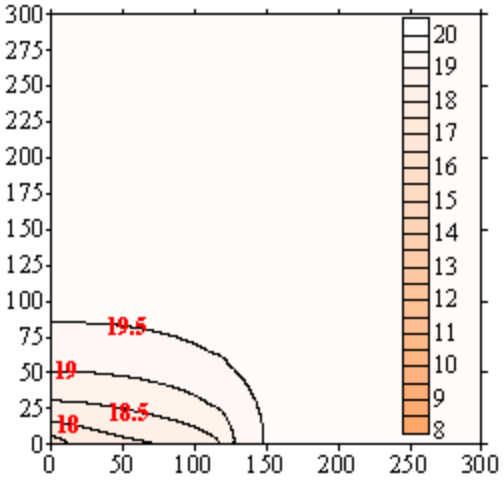

Figure 4
Permeability Distribution for Fracture with Maximal Width of 6mm

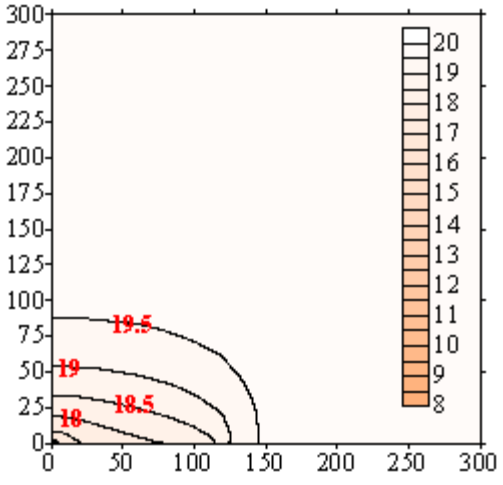

Figure 5
Permeability Distribution for Fracture with Maximal Width of 8mm

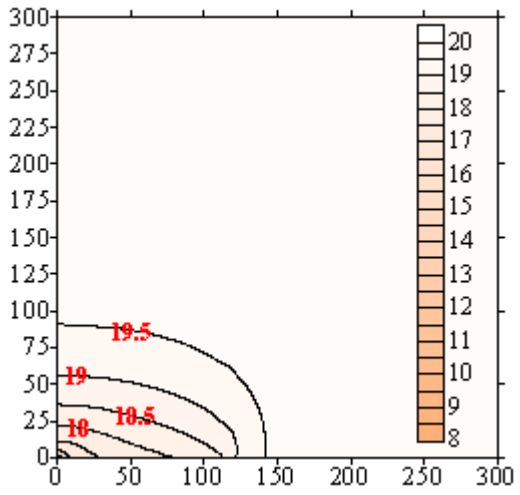

Figure 6
Permeability Distribution for Fracture

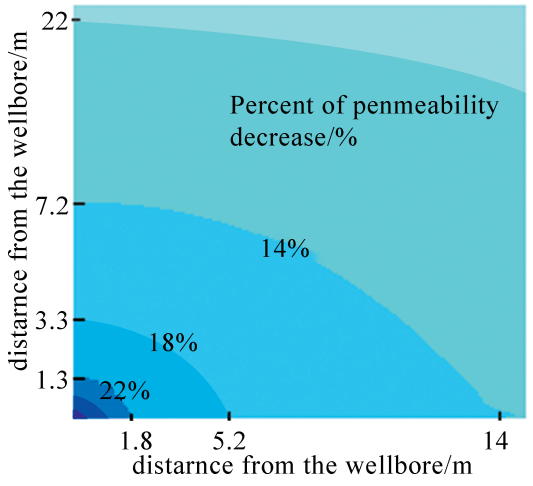

Figure 7
Effect on Permeability Around the Wellbore with Maximal Width of 10mm

Figs.2 to 6 show that the permeability distribution law is similar for wedge fractures with the same length and different widths, and the permeability distribution shapes in ellipse. The influence region along the fracture surface by fracture creation has a negligible increase with the increment of the fracture width. When the maximal fracture width is greater than or equal to 6mm, the influence region on the permeability increases apparently with the increment of fracture width, so does the influence in the vicinity of the wellbore.

When the maximal fracture width is greater than or equal to 6mm, an occurrence of the apparent influence region near wellbore is observed. An example of fracture with width of 10mm is used to demonstrate the permeability distribution near wellbore, and Fig. 7 shows the permeability distribution near wellbore. Fig. 7 shows that the permeability distribution also shapes in ellipse under the influence of dynamic fracture creation. Moreover, the more adjacent to the wellbore, the more sensitive for the permeability alteration is observed. The fracture creation has obvious influence on permeability in the region less than 4m away from the wellbore, and the percent of permeability decrease in this region is even about 50%.

Fig.8 shows the percent of permeability decrease along the boundary of fracture (the edge of AB in Fig.1), and Fig.9 shows the percent of permeability decrease along the vertical boundary of fracture model (the edge of EF in Fig.1).

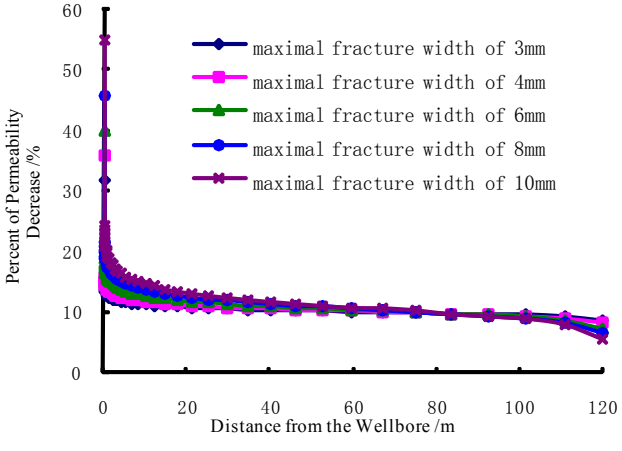

Figure 8
Effect on Permeability Along the Boundary of Fracture

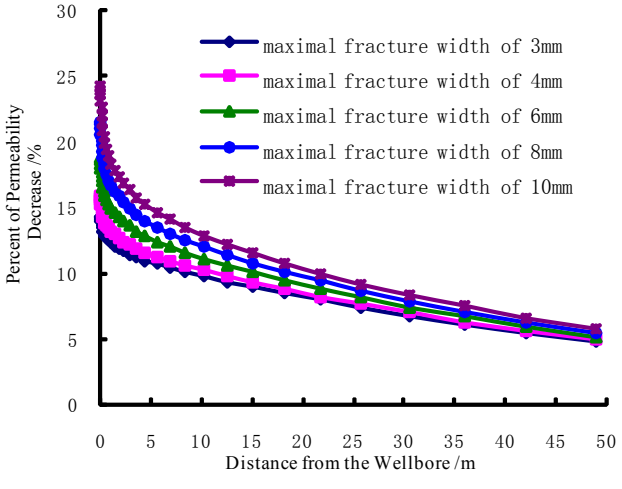

Figure 9
Effect on Permeability Along the Vertical Boundary of Fracture Model

Fig.8 and Fig.9 show the obvious decrease of reservoir permeability under the simultaneous influence of fracture creation and pressure-released production, and the fracture creation and pressure-released production alternately dominates the alteration of permeability in different regions. With respect to the fractures with different widths, the fracture creation apparently dominates the change of permeability in the region near the wellbore and the fracture surface. Moreover, the more adjacent to the wellbore, the more apparent for the effect of fracture creation is observed. Dynamic fracture creation plays a more important role in permeability alteration within the region less than 5m away from the wellbore. The larger for the fracture width, the more sensitive for the permeability alteration gradient is observed in the region near wellbore. In the region 5m away from the wellbore, the effect of fracture creation decreases sharply with the increment of the distance from the wellbore. In the region 20m away from the wellbore, the pressure-released production affect more apparently since dynamic fracture creation has a negligible effect in the region.

CONCLUSIONS

(1) Based on the fluid-solid coupling theory in porous media, a finite element simulation model for dynamic fracture creation is established, the relevant finite element program is developed with the software of FEPG.

(2) The permeability distribution after fracturing shapes in ellipse for fractures with different widths. When the maximal fracture width is greater than or equal to 6mm, the influence region on the permeability increases apparently with the increment of fracture width, so does the influence in the vicinity of the wellbore.

(3) The fracture creation and pressure-released production alternately dominates the alteration of permeability in different regions. Dynamic fracture creation plays a more important role in permeability alteration within the region less than 5m away from the wellbore. The larger for the fracture width, the more sensitive for the permeability alteration gradient is observed in the region in the vicinity of the wellbore. In the region 20m away from the wellbore axis, the pressure-released production affect more apparently since dynamic fracture creation has a negligible effect in the region.

REFERENCES

[1] Tran, D., Nghiem, L., & Buchanan, L. (2005). An Overview of Iterative Coupling Between Geomechanical Deformation and Reservoir Flow. *SPE97879*.

[2] Belhaj, H. A., Ryan, R. J., Nouri, A. M., et al (2004). A New Coupled Fluid Flow/Stress Model for Porous Media Behavior: Numerical Modeling and Experimental Investigation. *SPE90265*.

[3] Tran, D., Settari, A., & Nghiem, L. (2004). New Iterative Coupling Between a Reservoir Simulator and a Geomechanics Model. *SPE 88989*.

[4] Onaisi, A., Samier, P., & Koutsabeloulis, N., et al (2002). Management of Stress Sensitive Reservoirs Using Two Coupled Stress-Reservoir Simulation Tools: ECL2VIS and ATH2VIS. *SPE78512*.

[5] Liu, J. J., Liu X. G., & Hu, Y. R. (2002). Study of Fluid-Solid Coupling Flow in Low Permeablable Oil Reservoir. *Chinese Journal of Rock Mechanics and Engineering*, *21*(1), 88-92.

[6] Zhang, G. Q., Chen, M., & Jin, Y. (2005). Three-Dimensional Model and Procedures for Prediction of Sand Production in Gas Reservoirs. *Chinese Journal of Geotechnical Engineering*, *27*(2), 198-201.

[7] Xu, X.R., & Fan, X. P. (2002). Math Simulation on Coupled Fluid Flow and Geomechanics for Multiple Phases Reservoir. *Chinese Journal of Rock Mechanics and Engineering*, *21*(1), 93-97.

[8] Xue, S. F., Tong, X. H., & Yue, B. Q., et al (2000). Progress of Seepace-Rock Mass Coupling Theory and Its Application. *Journal of the University of Petroleum, China(Edition of Natural Science)*, *24*(2), 109-114.

[9] Liu J. J., & Feng, X. T. (2003). Advance of Studies on Thermo-Hydro-Mechanical Interaction in Oil Reservoir in China. *Rock and Soil Mechanics*, *24*(Sup), 645-650.

[10] Liang, B., Sun, K. M.,& Xue Q. (2001). The Research of Fluid-Solid Coupling in the Ground Engineering. *Journal of Liaoning Technical University (Natural Science)*, *20*(2), 129-134.

CSCanada
Advances in Petroleum Exploration and Development
Vol. 3, No. 1, 2012, pp. 38-43
DOI:10.3968/j.aped.1925543820120301.154

ISSN 1925-542X [Print]
ISSN 1925-5438 [Online]
www.cscanada.net
www.cscanada.org

A Study on Alkali Consumption Regularity in Minerals of Reservoirs During Alkali(NaOH)/Surfactant/Polymer Flooding in Daqing Oilfield

JIANG Zhenhai[1]; ZHANG Qingjie[1,*]; WEI Jianguang[2]; GAO Yunsong[1]

[1] Daqing Oil Field Company Ltd., China.
[2] Northeast Petroleum University, China.
[*] Corresponding author.

Received 7 February 2012; accepted 16 March 2012

Abstract

In the process of oil displacement of ASP (Alkali/Surfactant/Polymer) flooding , when Alkali interacts with the fluid and minerals of the reservoir, the alkali is subject to be consumed. The consumption regularity is the key factor affecting ASP ingredient, injection plan, scaling regularity for production wells and oil displacement effectiveness. Therefore to study the alkali consumption is of great significance in guiding ASP ingredient, injection project design, and the analysis for oil displacement mechanism. In this paper, aiming at the main components of minerals in the reservoir in Daqing Oilfield, the laboratory study on static alkali consumption for five kinds of minerals (kaolinite, grundite, chlorite, feldspar and quartz) in ASP system and single component NaOH solution are done respectively. The alkali consumption regularities for five kinds of minerals in ASP and single component NaOH solution are concluded.

The research indicates that the amount of alkali consumption for kaolinite, grundite, chlorite, feldspar and quartz is changing from larger to less accordingly, but is mainly caused by clay minerals; the average alkali consumption is 18.3% higher than that by matrix minerals. In single component NaOH solution, the alkali consumption styles of clay minerals and the matrix minerals take the chemical reaction as the lead, and the physical adsorption as the second. In ASP system solution, the alkali consumption style of clay minerals, takes the physical adsorption as the lead, and of matrix minerals takes the chemical reaction as the lead. In ASP solution, compared with single component solution, polymer and surfactant have the functions of restraint to alkali consumption in minerals of the reservoir, and the amount of alkali consumption decreases evidently.

Key words: Alkali; Surfactan; Polymer; ASPl; Oil displacement

Jiang, Z. H., Zhang, Q. J., Wei, J. G., & Gao, Y. S. (2012). A Study on Alkali Consumption Regularity in Minerals of Reservoirs During Alkali(NaOH)/Surfactant/Polymer Flooding in Daqing Oilfield. *Advances in Petroleum Exploration and Development*, *3*(1), 38-43. Available from: URL: http://www.cscanada.net/index.php/aped/article/view/j.aped.1925543820120301.154
DOI: http://dx.doi.org/10.3968/j.aped.1925543820120301.154

INTRODUCTION

In the process of oil displacement of ASP system, alkali in ASP system not only interacts with the fluids in the reservoir, but also interacts with the rock minerals definitely; therefore the consumption of Alkali is occurred. They are two kinds of consumption styles: One is chemical consumption when alkali interacts with the rock minerals. The other is alkali absorption on the surface of the rocks. The consumption regularity is the key factor affecting ASP ingredient, injection plan, scaling regularity for production wells and oil displacement effectiveness. Therefore to study the alkali consumption is of important significance in guiding ASP ingredient, injection project design, and the analysis for oil displacement mechanism. The initial report on ASP flooding was published in 1977[1], and from then on, a great number of researches have been performed by the scholars from different countries, and the researches involve ASP's chemical agent development, fluid rheology behavior, displacing mechanism, scaling mechanism and etc.[2-7]. But there are little systematic and profound reports concerning alkali consumption regularity and scale controlling measures in the process of strong Alkali (NaOH)/Surfactant/Polymer flooding [8-12]. In this paper, aiming at the main components of minerals in the reservoir in Daqing Oilfield, the

laboratory study on static alkali consumption for five kinds of minerals (kaolinite, grundite, chlorite, feldspar and quartz) in ASP and single component NaOH solution are done respectively. The alkali consumption regularities for five kinds of minerals in ASP and single component NaOH solution are concluded and the comparison analysis is done as well.

1. ALKALI CONSUMPTION MECHANISMS OF MINERALS

When ASP is injected into the reservoirs, some of the alkali interacts with organic acid in the crude oil. In this process, surfactant is created, which is conductive to driving oil. The other alkali interacts with rock minerals and water in the formation. Deposit is created in the same process, which resulted in a great amount of consumption of alkali. They are two kinds of consumption styles. One is chemical alkali consumption when alkali interacts with the rock minerals. The other is alkali absorption on the surface of the rocks.

1.1 Mechanism of Physical Absorption

Cation Na^+ in solution exchanges with H^+ and absorbs on the surface of the rocks, and alkali is consumed, the chemical equation is as follow:

$$M\text{-}H + Na^+ + OH^- \rightleftharpoons M\text{-}Na + H_2O$$

1.2 Mechanisms of Chemical Alkali Consumption

The minerals in the formation are composed of frame minerals and clay minerals. The frame minerals in Daqing oilfield are mainly quartz, feldspar and etc., and clay minerals are mainly grundite, kaolinite, chlorite, and etc. There are Ca^{2+} and Mg^{2+} in fluid in the formation, when the rock minerals interact with alkali, the main chemical reaction equations are as follows:

The chemical formula of the feldspar presents as $K[AlSi_3O_8]+Ca[Al_2Si_2O_8]$, and when the feldspar reacts with alkali, its chemical equation is:

$$K[AlSi_3O_8]+Ca[Al_2Si_2O_8]+9OH^- \rightleftharpoons Al(OH)_3\downarrow+K^++Ca^{2+}+SiO_3^{2-}$$

The chemical formula of the quartz is SiO_2, and the chemical equations between quartz and alkali are as the follows:

$$SiO_2+2OH^- \rightleftharpoons SiO_3^{2-}+H_2O$$

$$SiO_3^{2-}+H_2O \rightleftharpoons H_2SiO_4^{2-}$$

$$H_2SiO_4^{2-}+H_2O \rightleftharpoons SiO(OH)_3^- + OH^-$$

$$SiO(OH)_3^- + H_2O \rightleftharpoons SiO(OH)_4\downarrow + OH^-$$

$Al_2Si_2O_5(OH)_4$ is the chemical formula of kaolinite, and its chemical equations reacted with alkali are :

$$Al_2Si_2O_5(OH)_4 + 2OH^- + 4H_2O \rightleftharpoons 2Al(OH)_3\downarrow + 2H_3SiO_4^-$$

$$Al_2Si_2O_5(OH)_4 + 2OH^- + 2Na^+ + 4Si(OH)_4 \rightleftharpoons 2NaAlSi_3O_5 + 11H_2O$$

$$Al_2Si_2O_5(OH)_4 + 2OH^- + 2Na^+ + 2Si(OH)_4 \rightleftharpoons 2NaAlSi_2O_5\cdot H_2O + 5H_2O$$

The chemical formula of grundite, chlorite, and montmorillonite are similar presented as $Al_2[Si_4O_{10}](OH)_2$.Crystal strata may form differently. When reacted with alkali, the chemical equations are:

$$Al_2[Si_4O_{10}](OH)_2 + 10H_2O \rightleftharpoons 2Al(OH)_3\downarrow + 4Si(OH)_4\downarrow$$

$$Al_2[Si_4O_{10}](OH)_2 + 2Na^+ + 2OH^- + 2Si(OH)_4 \rightleftharpoons 2NaAlSi_3O_8 + 6H_2O$$

$$5Al_2[Si_4O_{10}](OH)_2 + 12Na^+ + 2Al(OH)_3 + 12OH^- + 10H_2O \rightleftharpoons 4Na_3Al_3Si_5O_{16}\cdot 6H_2O$$

The silicic acid is unstable, and under alkali conditions, intro-molecular aggregation arises and poly-silicic acid, polysilicate and trimer silicic acid are formed:

$$Si(OH)_4 + 2OH^- \rightleftharpoons [Si(OH)_6]^{2-}$$

$$2[Si(OH)_6]^{2-} \rightleftharpoons [Si_2(OH)_{10}]^{2-} + 2OH^-$$

$$[Si(OH)_6]^{2-} + [Si_2(OH)_{10}]^{2-} \rightleftharpoons [Si_3(OH)_{14}]^{2-} + 2OH^-$$

2. LABORATORY RESEARCH OF ALKALI CONSUMPTION OF MINERALS

2.1 Test Introduction

The water used to prepare ASP system is injection water from Daqing oil field, the salinity is 4826.7mg/L. The mass percentage of surfactant and NaOH in ASP is 0.3%, and 1.2% respectively. The concentration of partially hydrolysis polyarylamide is 2000 mg/L, the molecular weight is 25 millions. The degree of hydrolysis is 25%.

Minerals of formation are prepared as quartz, feldspar, grundite, kaolinite, and chlorite separately, the purity of them is more than 95%. Acid proof plastic bottle, AAS-475 atomic absorption spectrum instrument, THZ-82 temperature constant bath oscillator, JY33-TGL-16 hi-speed centrifuge, JKY/SJ-4A PH test paper. The detailed testing methods and procedures are as follows:

(1) Get quartz, feldspar, grundite, kaolinite grinded to less than 120 mesh, dried to be standby.

(2) According to the proportion of 5g: 20mL, mix the dried powder of quartz, feldspar, grundite, kaolinite with NaOH solution whose mess concentration is 1.2%, or with ready prepared ASP solution respectively, put the mixture into the plastic alkali proof container whose volume is 50 mL, and got it sealed, after oscillating violently, put it into a thermotank with constant temperature 45°C, and conduct static soak test.

(3) Get it oscillated once a day, sampling on different fixing days (1, 5, 16, 30, 40 day), put the sample into oscillating tube, got it oscillated at the speed of 8000rpm for 20mins, take the clear liquid in the top of the tube, measure the concentration of NaOH, silicon ion and aluminium ion.

(4) Take phenothalin and metryl orange whose mess concentration is 0.5% as indicator, to titrate with diluted hydrochloric acid (0.04948 mol/L), according to equivalent law, apply the following equation to calculate the concentration of NaOH after chemical reaction, then to attain the consumption amount of alkali：

$$A_i = \frac{C_0 - C_i}{C_0} \times 100\%$$

In the equation: A_i is the alkali consumption percentage of each kind of mineral, %；C_0 is the initial concentration of NaOH, mg/L; C_i is the final concentration of NaOH after chemical reaction with each kind of mineral, mg/L.

(5) To measure the concentration of silicon ion and aluminium ion using AAS-475 atomic absorption spectrum instrument.

2.2 Test Results Analysis

2.2.1 Alkali Consumption Test for NaOH Reacting with Sigle Mineral

Fig 1 is the relation curve between static alkali consumption and time when kaolinite, grundite, chlorite, feldspar and quartz reacts with NaOH solution respectively. From the fig we can see, the longer the reaction time is, the larger the alkali consumption is, and in the initial time, the alkali consumption speed is faster; In addition, for different kind of mineral, it has a different alkali consumption speed, in the initial time, for kaolinite, it has the alkali consumption of 16.0%, for grundite, it has 15.6%, for chlorite, it has 11.6%, for feldspar, it has 7.2% and for quartz, it has 4.7%; When the reacting time is 40 days, for kaolinite, it has the alkali consumption of 38.9%, for grundite, it has 29.8%, for chlorite, it has 22.2%, for feldspar, it has 13.1% and for quartz, it has 10.9%, thus it can be seen that the order of alkali consumption for the minerals are: kaolinite, grundite, chlorite, feldspar and quartz, and the alkali consumption amount for clay minerals is 18.3% larger in average than frame minerals, it's obvious that the alkali consumption in minerals is mainly caused by clay minerals.

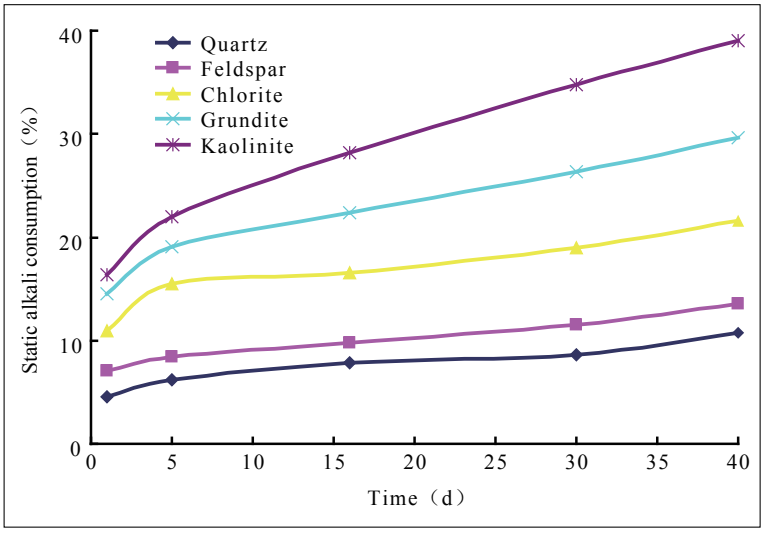

Figure 1
The Relation of Static Alkali Consumption Versus Time in NaOH Solution

The total amount of alkali consumed by minerals includes physical absorption and chemical reaction consumption. In order to make clear the alkali consumption proportion on the total for each of process mentioned above, the concentration of silicon ion and aluminum ion in the NaOH solution after reaction is traced and mea-

sured, the result is shown in Fig 2 and 3. From Fig 2 and 3 we can see that for each kind of mineral, the longer the reaction time with the NaOH solution is, the larger the concentration of silicon ion is increased gradually, and the increments are all large. The order of the concentration of silicon ion consumed from large to little is listed as: grundite, kaolinite, chlorite, feldspar and quartz; But only for grundite, the increment of concentration of aluminum ion is measured large, for other minerals, it's measured less. After reaction for minerals with NaOH solution, the order of the concentration of silicon ion consumed from large to little is listed as: grundite, kaolinite, chlorite, feldspar and quartz; The order of the concentration of aluminum ion consumed from large to little is listed as: grundite, kaolinite, chlorite, feldspar. The concentration of silicon ion and aluminum ion after reaction for frame minerals with NaOH solution is lower than that for clay minerals with NaOH solution. It is illustrated that the amount of alkali consumed by clay minerals is larger than frame minerals.

According to the concentration of silicon ion and aluminum ion after reaction for all kinds of minerals with NaOH solution, using the chemical reaction equation for AL_2O_3, SiO_2 reacting with NaOH respectively, the amount of alkali consumption and physical absorption for each kind of minerals reacting with NaOH can be calculated. In table 1, the total amount of alkali consumption, chemical reaction alkali consumption and physical absorption caused by all kinds of minerals reacting with NaOH solution are tabulated after 40 days reaction time. From table1 we can see that, after reactions for kaolinite with NaOH, the amount of chemical alkali consumption take the percentage of 79.5% of the total, for grundite, chlorite, feldspar and quartz, it is of 80.9%, 79.4% and 75.8% accordingly. It's given the fact that, after reaction for all kinds of minerals with NaOH solution, the chemical alkali consumption is the main style, the physical absorption take the second place.

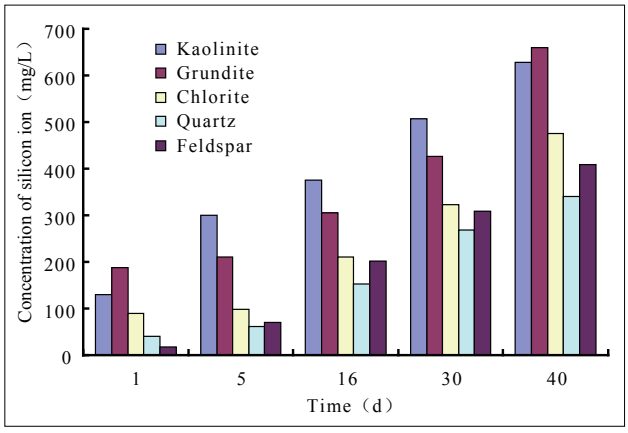

Figure 2
The Relation of the Concentration of Silicon Ion Versus Time in NaOH Solution

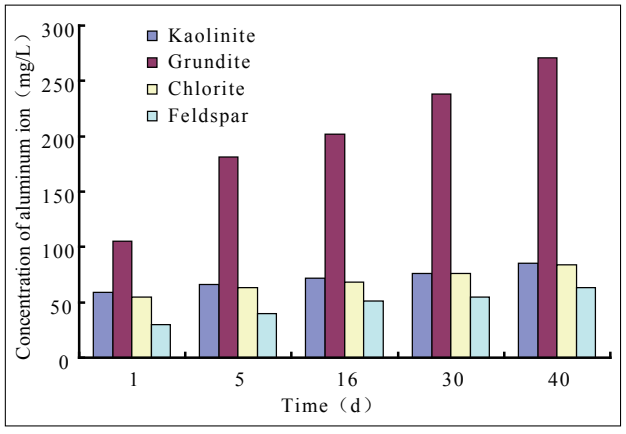

Figure 3
The Relation of the Concentration of Aluminum Ion Versus Time in NaOH Solution

Table 1
The Percentage of Chemical Alkali Consumption and Physical Absorption (in NaOH Solution)

Mineral Type	Total Amount Alkali Consumption（%）	The Percentage of Chemical Alkali Consumption in the Total（%）	The Percentage of Physical Absorption in the Total（%）
Kaolinite	38.9	79.5	20.5
Grundite	29.8	90.6	9.4
Chlorite	22.2	80.9	19.1
Feldspar	13.1	79.4	20.6
Quartz	10.9	75.8	24.2

2.2.2 The Alkali Consumption Test for ASP System Reacting with Single Mineral

Fig 4 is the relation curve between static alkali consumption versus time when kaolinite, grundite, chlorite, feldspar and quartz reacts with ASP system respectively. From the fig 4 we can see, the alkali consumption regularity for all kinds of mineral reacting with ASP system has the same trend basically with that when reacting with NaOH solution. That is the longer the reaction time is, the larger the alkali consumption is,

and in the initial time, the alkali consumption speed is faster, but by comparison with NaOH solution, the alkali consumption is lower, the alkali consumed from large to little by grundite, kaolinite, chlorite, feldspar and quartz is 26.9%, 22.5%, 19.4%, 6.8% and 9.0% respectively, dropped 30.8%, 24.5%, 12.6%, 48.1% and 17.4% respectively. This indicates that the alkali consumption has been restrained effectively by the presence of polymer and surfactant in ASP system. After reacted with ASP system, the order of alkali consumption caused by the minerals is: kaolinite, grundite, chlorite, quartz and feldspar. It's obvious that the alkali consumption in minerals is mainly caused by clay minerals, but for ASP system, the alkali consumed by quartz is larger than that by feldspar.

The variations of concentration of silicon ion and aluminum ion in ASP system after reaction are shown in Fig 5 and 6. From Fig 5 and 6 we can see that for each kind of mineral, by comparison with NaOH solution, both the concentration of silicon ion and aluminum ion in ASP system have been dropped,the dropping value of silicon ion is bigger than aluminum ion. This indicates that the chemical reaction alkali consumption has been restrained by the presence of polymer and surfactant in ASP system. After reacted with ASP system for each kind of minerals, the order of concentration of silicon ion in the ASP system from large to little is: kaolinite, grundite, feldspar, chlorite, and quartz, for the concentration of aluminum ion, the order from large to little is: grundite, chlorite, kaolinite and feldspar.

In table 2, the total amount of alkali consumption, chemical reaction alkali consumption and physical absorption caused by all kinds of minerals reacting with ASP system are tabulated after 40 days reaction time. From table 2 we can see that, after reaction for kaolinite with ASP system, the amount of chemical alkali consumption take the percentage of 32.5% of the total, for grundite, chlorite, feldspar and quartz, it is of 43.6%, 44.8%, 60.0% and 62.2% accordingly. By contrast with the reaction with NaOH, the alkali consumption dropped 59.1%, 51.9%, 44.6%, 24.4% and 17.9% respectively. It's given the fact that, to some extent, the chemical reaction alkali consumption has been dropped by the presence of polymer and surfactant in ASP system. But the dropping range of chemical reaction alkali consumption caused by clay minerals is larger than frame minerals, thereby, for clay minerals, the alkali absorption in ASP system is the main style. For matrix minerals, the chemical reaction alkali consumption in ASP system is the main style.

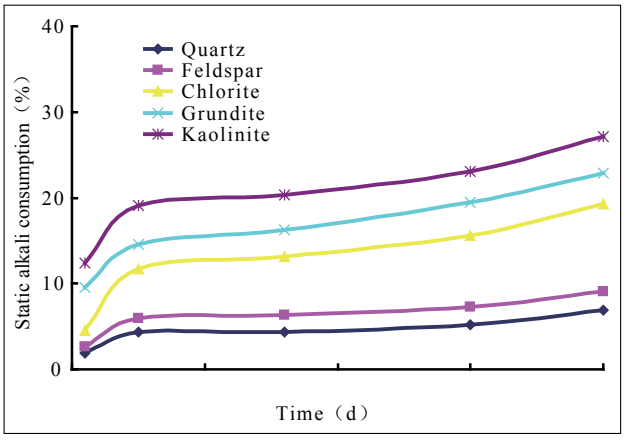

Figure 4
The Relation Curve Between Static Alkali Consumption Versus Time in ASP System

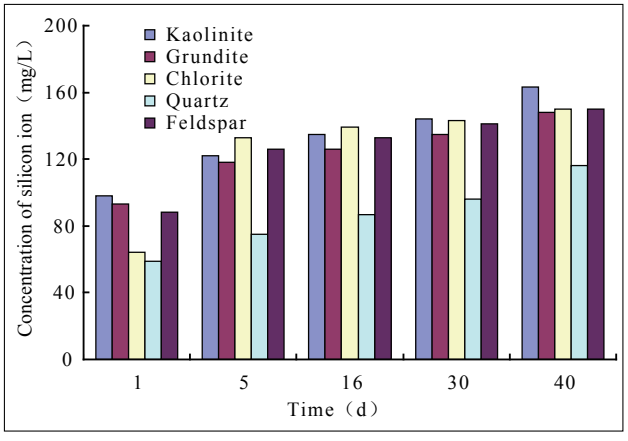

Figure 5
The Relation of the Concentration of Silicon Ion Versus Time in ASP System

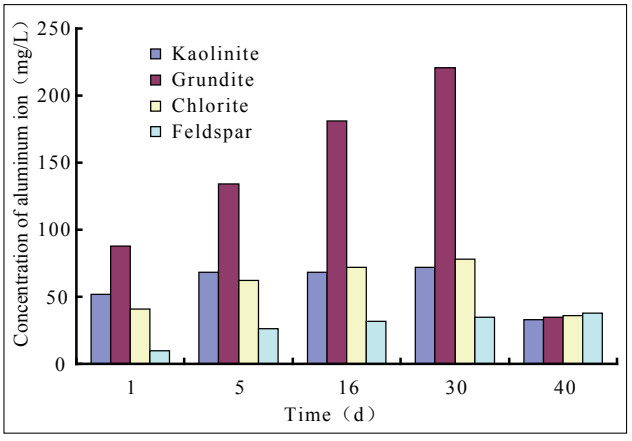

Figure 6
The Relation of the Concentration of Aluminum Ion Versus Time in ASP System

Table 2
The Percentage of Chemical Alkali Consumption and Physical Absorption (in ASP System)

Mineral Type	Total Amount Alkali Consumption（%）	The Percentage of Chemical Alkali Consumption in the Total（%）	The Percentage of Physical Absorption in the Total（%）
kaolinite	26.9	32.5	67.5
grundite	22.5	43.6	56.4
chlorite	19.4	44.8	55.2
feldspar	6.8	60.0	40.0
quartz	9.0	62.2	37.8

CONCLUSIONS

(1) The order of alkali consumption for 5 kinds of the minerals is: kaolinite, grundite, chlorite, feldspar and quartz, and the amount of alkali consumption is mainly caused by clay minerals, the alkali consumption amount for clay minerals is 18.3% larger in average than matrix minerals.

(2) When kaolinite, grundite, chlorite, feldspar and quartz reacts with NaOH solution respectively, the amount of chemical alkali consumption take the percentage of 79.5%, 90.6%, 80.9%, 79.4% and 75.8% of the total. It's given the fact that, after reaction for all kinds of minerals with NaOH solution, the chemical alkali consumption is the main style, the physical absorption take the second place.

(3) The alkali consumption regularity for all kinds of mineral reacting with ASP system, has the same trend basically with that of reacting with NaON solution, but the alkali consumption is lower, the alkali consumed from large to little by grundite, kaolinite, chlorite, feldspar and quartz is 26.9%, 22.5%, 19.4%, 6.8% and 9.0% respectively, this indicates that polymer and surfactant in ASP system have effective restrain functions to the alkali consumption.

(4) When kaolinite, grundite, chlorite, feldspar and quartz reacts with ASP system, the amount of chemical alkali consumption take the percentage are 32.5%, 43.6%, 44.8%, 60.0% and 62.2% of the total respectively, It's given the fact that for clay minerals, the main alkali consumption style in ASP system is the physical absorption; but for matrix minerals, the main alkali consumption style is the chemical reaction.

REFERENCES

[1] Holm, L. W., & Robertson, S. D. (1978). Improved Micellar-Polymer Flooding with High pH Chemicals. *Journal of Petroleum Technology*, *33*(1), 161-172.

[2] Wang, H. F., Wu, X. L., & Zhang, G. Y. (2004). Search Progress on the Surfactants for ASP Flooding in Daqing Oilfield. *Oil & Gas Recovery Technology*, *11*(5), 62-64.

[3] Hou, J. R., Liu, Z. C., & Xia, H. F. (2001). Influence of Viscoelastic Effect in Ternary Combination System on Oil Displacement Efficiency. *Oil & Gas Recovery Techinology*, *8*(3), 61-64.

[4] Chen, T. L., Dong, F., & Long, D. Q. (1998). Studies on the Rheological Behavior of ASP System. Journal of Southwest Petroleum Institute, 20(1), 53-55.

[5] Liu, J. J., Song, Y. M., & Pan, Y. S. (2003). Study on Microscopic Mechanism of Oil Displacement by Alkaline Surfactant-Polymer Flooding. *Journal of Liaoning Technical University*, *22*(3), 53-55.

[6] Li, P., Cheng, Z. F., & Wang, X. J. (2003). Forming Mechanism and Prediction Method of Silica Scaling in Oil Wells with Alkaline-Surfactant-Polymer Flooding. *Acta Petrolei Sinica*, *24*(5), 63-66.

[7] Xu, D. P., Xue, J. F., & Bao, Y. C. (2001). Mechanism of Oil Well Scale Formation During ASP Flooding. *Petroleum Geology & Oilfield Deuelopment in Daqing*, *20*(2), 98-100.

[8] Krumrine, P. H., Mayer, E.H., & Brock, G.F. (1985). Scale Formation During Alkaline Flooding. *Journal of Petroleum Technology*, *37*(8), 1466-1474.

[9] Jiang, M. Z., Zhun, J., & Li, J. L. (2003). Fouling Analysis of 3-Element Compound-Drive Oil Well and Research on Fouling Inhibitor. *Petrochemical Corrosion and Protection*, *20*(3), 25-27.

[10] Wang, Y. P., & Cheng, J. C. (2003). The Scaling Characteristics and Adaptability of Mechanical Recovery During ASP Flooding. *Journal of Daqing Petroleum Institute*, *27*(2), 20-22.

[11] Tang, H. M., Xiang, W. T., & Zhao, J. S. (2000). A Study on Consumption of Surfacetant by Reservoir Minerals. *Oilfield Chemistry*, *17*(3), 276-280.

[12] Chen, Z., Zhao, J. S., & Tang, H. M. (1999). Study on Co-Effect of Alkali Consumption Between Clay Minerals and Grain-Sized Minerals. *Mineral Petrol*, *19*(3), 61-64.

CSCanada
Advances in Petroleum Exploration and Development
Vol. 3, No. 1, 2012, pp. 44-48
DOI:10.3968/j.aped.1925543820120301.151

ISSN 1925-542X [Print]
ISSN 1925-5438 [Online]
www.cscanada.net
www.cscanada.org

New Method of High Quality and High Speed Drilling Based on Stratigraphic Naturally Whipstocking Law

WANG Guanglei[1,2,*]; CHENG Yuanfang[1]; JIA Jianghong[2]

[1] College of Petroleum Engineering, China University of Petroleum, Qingdao, Shandong Province, China.
[2] Shengli Drilling Technology Research Institute, Dongying, Shandong Province China.
[*]Corresponding author.

Received 9 January 2012; accepted 8 February 2012

Abstract
High steep dip formation is one of the important keys effecting well deviation and azimuth during drilling. According to space gridding data of formation,calculation method of angle and tendency and analysis model of offset of deviation and azimuth are derived considering formation anisotropy. Combined with the field experiment, calculation orbit is similar to true track, also increasing drilling speed. The result shows that using formation natural deflecting law to optimize well position and design well trajectory, to increase drill pressure in order to increase ROP while not effect reaching the target naturally are feasible. This indicates analysis method is correct and reasonable. It has important theoretical value and practical worth in engineering.

Key words: Formation anisotropy; Whipstocking law; Weight on bit; New drilling method

Wang, G. L., Cheng, Y. F., Jia, J. H. (2012). New Method of High Quality and High Speed Drilling Based on Stratigraphic Naturally Whipstocking Law. *Advances in Petroleum Exploration and Development*, *3*(1), 44-48. Available from: URL: http://www.cscanada.net/index.php/aped/article/view/j.aped. 1925543820120301.151
DOI: http://dx.doi.org/10.3968/j.aped.1925543820120301.151

INTRODUCTION
Demonstrated by drilling practice that stratigraphic naturally whipstocking characteristic is one of the main factors influencing well deviation and azimuthal change. Due to the obvious difference of geologic structure and formation lithology in different area[1], formation deflecting force is also changed. Although geologic factors are out of man force control, but the relationship between borehole deviation & azimuth change and attitude of stratum can be used to optimize well position and well track. By using this method, exploratory target can be realized and WOB (weight on bit) can be released. The final goal for drilling engineering, that is raising ROP(rate of penetration), can also be obtained. For that, researching on stratigraphic naturally whipstocking law is very useful for optimizing wellbore trajectory, raising ROP and wellbore quality. It has important theoretical and practical value.

1. CALCULATION OF INCLINATION ANGLE AND DIP DIRECTION IN HIGH STEEP DIP FORMATION
In order to calculating inclination angle and dip direction of arbitrary point in formation, space grid data of various stratigraphic horizon can be obtained from geologists, and then calculate followed by certain steps. The projection of various stratigraphic horizon grid on horizontal plane is by serial-arrangement and regular spread square grid. The grid point on horizontal plane and corresponding grid point of various stratigraphic horizon are at the same pedal line in spite of the different vertical depth. Fig. 1 shows horizontal projection schematic drawing of stratigraphic space grid. The horizontal projection of arbitrary point A(N,E,D) is located at square(a,b,c,d).

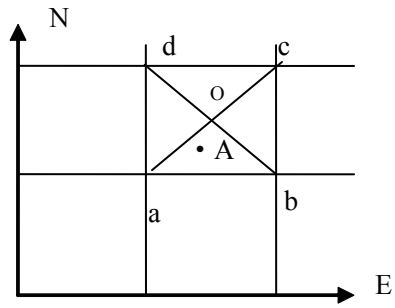

Figure 1
Horizontal Projection Schematic Drawing of Stratigraphic Space Grid

1.1 Locating Four Apexes Coordinates of the Square Point A Located on Horizontal Projection Plane

On the horizontal projection plane,because grid space is a fixed value - *grid_space*, so the coordinates (N, E) of various point on projection plane are integral multiple of the fixed value *grid_space*. Showed as figure 1, the coordinates (N,E) of point a are as follows:

$$N_a = \text{int}\left(\frac{N}{grid\_space}\right) \times grid\_space \tag{1}$$

$$E_a = \text{int}\left(\frac{E}{grid\_space}\right) \times grid\_space \tag{2}$$

So the coordinates(N,E) of point b, point c and point d showed as follows:

$$N_b = N_a \tag{3}$$

$$E_b = E_a + grid\_space \tag{4}$$

$$N_c = N_a + grid\_space \tag{5}$$

$$E_c = E_a + grid\_space \tag{6}$$

$$N_d = N_a + grid\_space \tag{7}$$

$$E_b = E_a \tag{8}$$

1.2 Locating Point A in the Square on Horizontal Projection Plane

On horizontal projection plane(Fig.1),the two diagonal lines of arbitrary square(e.g. square abcd) can divide it into four triangle pieces, that is: ⊿oab, ⊿obc, ⊿ocd& ⊿oda. The diagnosis that locates point A in which triangle piece can be made by following equations (9)~(12).

The condition that point A locates in ⊿oab is:

$$\begin{cases} N - N_a < E - E_a \\ N - N_b < E_b - E \end{cases} \tag{9}$$

The condition that point A locates in ⊿obc is:

$$\begin{cases} N - N_a < E - E_a \\ N - N_b > E_b - E \end{cases} \tag{10}$$

The condition that point A locates in ⊿ocd is:

$$\begin{cases} N - N_a > E - E_a \\ N - N_b > E_b - E \end{cases} \tag{11}$$

The condition that point A locates in ⊿oda is:

$$\begin{cases} N - N_a > E - E_a \\ N - N_b < E_b - E \end{cases} \tag{12}$$

1.3 Arbitrary Surface's Normal Component in the Prism Obtained by Vertically Extended Triangle Piece of Point A's Projection Located

Suppose that the four square space apexes(a,b,c,d) of point A's projection located correspond to four space apexes (i,j,k,l), so the normal component can be calculated by following equations (13)~(16).

When point A locates in ⊿oab:

$$\begin{aligned} \vec{n} = &\left[(H_a - H_d, N_a - Nd, E_a - E_d) \times (H_b - H_a, N_b - N_a, E_b - E_a)\right. \\ &\left. + (H_b - H_a, N_b - N_a, E_b - E_a) \times (H_c - H_b, N_c - N_b, E_c - E_b)\right]/2 \end{aligned} \tag{13}$$

When point A locates in ⊿obc:

$$\begin{aligned} \vec{n} = &\left[(H_b - H_a, N_b - N_a, E_b - E_a) \times (H_C - H_b, N_C - N_b, E_C - E_b)\right. \\ &\left. + (H_c - H_b, N_c - N_b, E_c - E_b) \times (H_d - H_c, N_d - N_c, E_d - E_c)\right]/2 \end{aligned} \tag{14}$$

When point A locates in ⊿ocd:

$$\begin{aligned} \vec{n} = &\left[(H_c - H_b, N_c - N_b, E_c - E_b) \times (H_d - H_c, N_d - N_c, E_d - E_c)\right. \\ &\left. + (H_d - H_c, N_d - N_c, E_d - E_c) \times (H_a - H_d, N_a - N_d, E_a - E_d)\right]/2 \end{aligned} \tag{15}$$

When point A locates in ⊿oda:

$$\begin{aligned} \vec{n} = &\left[(H_d - H_c, N_d - N_c, E_d - E_c) \times (H_a - H_d, N_a - N_d, E_a - E_d)\right. \\ &\left. + (H_a - H_d, N_a - N_d, E_a - E_d) \times (H_b - H_a, N_b - N_a, E_b - E_a)\right]/2 \end{aligned} \tag{16}$$

1.4 Calculation of Normal Component of Point

Using the range formula of point to plane, calculate the range from point A to corresponding triangle piece on various plane and find out the nearest two up and down triangle piece from point A. Then point A's normal component $\vec{n}_A(\vec{n}_A = H_A\vec{e}_H + N_A\vec{e}_N + E\vec{e}_E)$ is:

$$\vec{n_A} = \frac{d_{\min 1}}{d_{\min 1} + d_{\min 2}}\vec{n_2} + \frac{d_{\min 2}}{d_{\min 1} + d_{\min 2}}\vec{n_1} \tag{17}$$

where

d_{min1}—range from point A to the nearest up triangle piece,m;d_{min2}—range from point A to the nearest down triangle piece,m;

$\vec{n}_1$—normal component of the nearest up triangle piece; $\vec{n}_2$—normal component of the nearest down triangle piece.

1.5 Formation Inclination Angle Calculation of Point A Formation Inclination Angle

$$a_d = \arccos\frac{|H_A|}{|\vec{n}_A|}$$

formation azimuth

$$\varphi_d = \begin{cases} \arctan\dfrac{E_A}{N_A} & (N_A 0) \\ \arctan\dfrac{E_A}{N_A} + \pi & (N_A 0) \\ \dfrac{\pi}{2} & (N_A = 0, E_A \geq 0) \\ \dfrac{3\pi}{2} & (N_A = 0, E_A 0) \end{cases}$$

2. OFFSET DISTANCE CALCULATION OF WELL POSITION

During drilling design, if surface condition permitted, stratigraphic naturally whipstocking law can be used to reach geologic target by removing well ground position. It can also release WOB and enhance the ROP. Because the parameters of well deviation, azimuth and depth are already known and it was well known that the main reason leading to the offset of deviation and azimuth is formation anisotropy, so we should calculate based on the formation anisotropy[2], and then by using inverse method, calculate from bottom hole to wellhead. By this, we can obtain the off-set value from new well position to the in-situ one.

Based on the relationship between drilling bit acting force and ROP[3,4,5], the equation of formation anisotropy exponent h, formation deflecting coefficient K_α and azimuth drifting coefficient K_φ can be obtained.

$$h = \frac{F_x\tan\Delta\alpha - F_z}{(\tan\Delta\alpha\sin(\beta-\alpha) - \cos(\beta-\alpha))(F_x\sin(\beta-\alpha) + F_z\cos(\beta-\alpha))} \tag{18}$$

$$K_\alpha = \frac{h(\cos\alpha\cos\beta + \sin\alpha\sin\beta\cos(\varphi-\gamma))(\cos\alpha\sin\beta\cos(\varphi-\gamma) - \sin\alpha\sin\beta)}{hc + (1-h)} \tag{19}$$

$$K_\varphi = \frac{h(\cos\alpha\cos\beta + \sin\alpha\sin\beta\cos(\varphi-\gamma))\sin\beta\sin(\varphi-\gamma)}{hc + (1-h)} \tag{20}$$

$$c = g_2^2 + g_3^2 + g_1(g_2\tan\Delta\varphi + g_3\tan\Delta\alpha)$$

$$g_1 = \cos\alpha\cos\beta + \sin\alpha\sin\beta\cos(\varphi-\gamma)$$

$$g_2 = \sin\beta\sin(\varphi-\gamma)$$

$$g_3 = \cos\alpha\sin\beta\cos(\varphi-\gamma) + \sin\alpha\cos\beta$$

Inclination offset value $\Delta\alpha = \Delta L \cdot K_\alpha$

Azimuth offset value $\Delta\varphi = \Delta L \cdot K_\varphi$

then

$$\alpha_{i+1} = \alpha_0 + \Delta\alpha$$

$$\varphi_{i+1} = \varphi_0 + \Delta\varphi$$

where

F_x, F_z—bit acting force component on x and y axis in borehole axial line coordinate system, N;α—hole deviation angle, *rad;*

β—formation dip direction, *rad*;φ—azimuth angle, *rad*;γ—formation dip direction azimuth angle, *rad*; ΔL —length

between two trajectory nodes, *m;* α_0—bottom hole deviation angle, *rad;* φ_0—bottom hole azimuth angle, *rad*; *i*-node number.

3. CASE STUDY

The depth of well Y225 is 3150m. Based on the analysis of off-set well data, lower formation has certain natural deflecting ability. Calculating by the new method mentioned above, lower formation inclination is 15° and dip direction 185°. The predictive result is consistent with the actual result properly. It verifies the calculation method. Based on the design parameters of well targets and combining with formation anisotropy research, wellhead position is optimized. Demonstrated by calculation, wellhead position should be removed 98m at the direction of 180°, illustrated in figure 2 and figure 3. The true measured track is illustrated in figure 4.

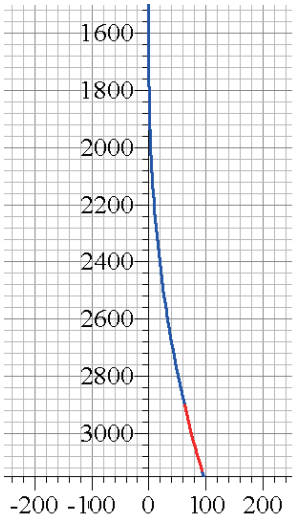

Figure 2
Vertical Projection Drawing (m)

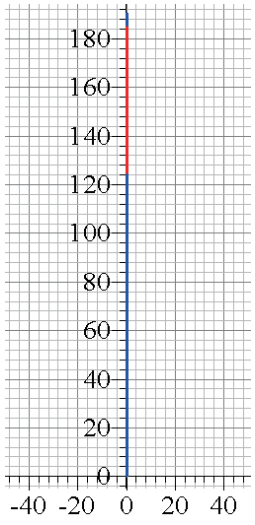

Figure 3
Horizontal Projection Drawing (m)

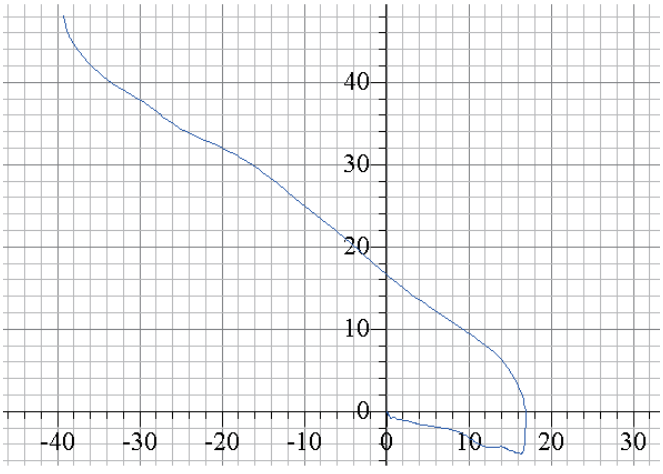

Figure 4
Actual Trajectory Horizontal Projection of Well Y225(m)

As illustrated in figure 4, calculation orbit is similar to true track in lower formation and it verifies the validity of the new drilling method. After releasing the WOB about one multiple amount, the ROP of rock roller bits enhanced by the percentage of 15%. The practice in well Y225 shows that the new drilling method of using formation natural deflecting law to optimize well position and design well trajectory, to increase drill pressure in order to increase ROP while not effect reaching the target naturally is feasible. This indicates the analysis method is correct and reasonable. It has important deployment worth.

CONCLUSION

(1) Based on the space grid data of various formation horizon, the calculation method of formation inclination angle and dip direction is built. It can help engineers confirming formation naturally whipstocking law with geologic data.

(2) Considering the characteristic of formation anisotropy, the calculation module of deviation and azimuth offset distance is deducted.

(3) The practical result shows that the new drilling method of using formation natural deflecting law to optimize well position and design well trajectory, to increase drill pressure in order to increase ROP while not effect reaching the target naturally is feasible and rational.

REFERENCES

[1] Zhu, B. C., Tang, S. H., Yan, Z. F., & Zhang, J. Z. (2009). Effects of Crustal Stresses and Natural Fractures on Fracture Pressure of Coal Reservoirs. *Journal of China Coal Society*, *34*, 1199-1202.

[2] He, S. M., & Xia, Y. W. (1998). A Study on Angle of Bedding Effect on Rock Drillability. *Drilling & Production Technology*, *21*, 11-15.

[3] Qi, L., Wang, X. Q., Liu, X. S., & Du, H. (1995). Analysis on Rock Drillability and Anisotropy Experiment. *Journal of Daqing Petroleum Institute*, *19*, 121-124.

[4] Dong, S. M., & Shi, T. H. (1995). Experiment Study of Tectonic Stress Influence on Wellbore Trajectory. *Oil Drilling & Production Technology*, *17*, 50-52.

[5] Luo, Y., Ai, C., Yan, T., Li, C. Z., & Hou, H. Z. (1995). Measurement Technology of Rock Anisotropy Index and Application. *Chinese Journal of Rock Mechanics and Engineering*, *14*, 69-73.

CSCanada
Advances in Petroleum Exploration and Development
Vol. 3, No. 1, 2012, pp. 49-54
DOI:10.3968/j.aped.1925543820120301.161

ISSN 1925-542X [Print]
ISSN 1925-5438 [Online]
www.cscanada.net
www.cscanada.org

Study on Matching Ability Between Cement Particle Size and Permeability in the Process of Oil Reservoir Plugging

ZHANG Qingjie[1,*]; WEI Jianguang[2]; SUN Guojun[1]; JIN Liyang[1]; GUAN Pengjun[1]

[1] Daqing Oil Field Company Ltd., China.
[2] Northeast Petroleum University, China.
[*] Corresponding author.

Received 12 February 2012; accepted 15 March 2012

Abstract

In order to satisfy the plugging demands of injecting the cement plugging agent into reservoirs with different radial depths, the technical studies of cement particle size optimization should be conducted. Through indoor experiment, the relationship between cement particle size and permeability was investigated by both macroscopic and microcosmic analysis. It is observed that the reservoirs which permeabilities are within 50~200mD are matching well with the cement agents which particle sizes are less than 5μm. And the permeabilities within 200~400mD are matching well with the cement agents which particle sizes are within 5~10μm, the permeabilities within 400~700mD are matching well with the cement agents which particle sizes are within 10~20μm, the permeabilities are above 700mD are matching well with the cement agents which particle sizes are more than 20μm. The plugging success rates of all the matching experiments are exceeding 90%. This research result is important to direct the plugging operation in the field.

Key words: Plugging off and channeling prevention; Cement particle size; Permeability; Matching relationship; Experimental study

Zhang, Q. J., Wei J. G., Sun, G. J., Jin, L. Y., & Guan, P. J. (2012). Study on Matching Ability Between Cement Particle Size and Permeability in the Process of Oil Reservoir Plugging. *Advances in Petroleum Exploration and Development*, *3*(1), 49-54. Available from: URL: http://www.cscanada.net/index.php/aped/article/view/j.aped.1925543820120301.161
DOI: http://dx.doi.org/10.3968/j.aped.1925543820120301.161

INTRODUCTION

In the world, about 95% of the conducted plugging operation is injected by cement agent, but the success rate is only about 30%. The main reason is the cement agent can not be injected into reservoir as the particle size of general standard cement is too large [1,2]. As is reported, there are about 20 operation companies conducted more than 100 experiments in 15 oil and gas fields during initial 9 months after the extra-fine cement accessing to markets [3]. Recently, in Daqing Oilfield, the work amount of old wells plugged back is increasing dramatically with the incessant modulation of injection and production system [4]. In the process, in order to keep channels to satisfy the demands of reservoir dynamic monitoring, cement plugging technique is widely used to plug the middle and (or) top layers of the reservoirs. However, for the cement plugging process, the cement particle size needs to be optimized, because the paramount clause of realizing the reservoir effectively plugging is ensuring the cement agent can be injected in. The optimal matching ability between the permeability of plugged reservoir and cement particle size has not been studied, so the plugging success rate is influenced. Therefore, to perfect the cement plugging process, enhance plugging success rate and reduce the cost effectively, the optimization research of cement plugging process is extraordinarily necessary to be conducted.

1. PREPARATION OF THE CEMENT PLUGGING AGENT

In laboratory, 4 grades samples of cement particle size are selected by cement screens. They are d_{50}≥20μm, d_{50}: 10~20μm, d_{50}: 5~10μm and d_{50}＜5μm respectively. And water cement ratio is 1:2, that is to say the weight of cement is twice as much as water. The amout of dispersing agent is 1.5% of cement weight, and the amout of retarder is 1 % of cement weight.

2. MATCHING RELATIONSHIP EXPERIMENT BETWEEN CEMENT PARTICLE SIZE AND PERMEABILITY

2.1 Flowrate Variation Characteristics

Fig. 1 and Fig. 2 are the flow performance of 4 grades particle size cements in different cores. The effective permeability of the two cores are 410mD and 240mD respectively.

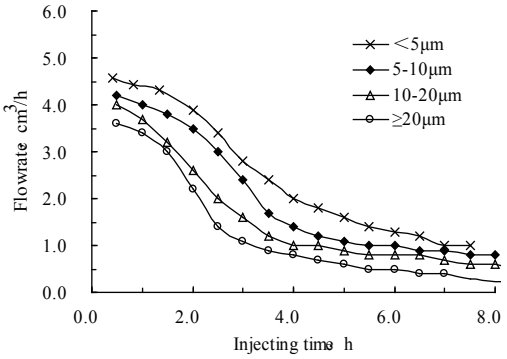

Figure 1
The Permeability is 410 mD

The precondition of matching ability between cement particle size and permeability is ensuring the cement agent can be injected in. It is known from the flowrate variation characteristic that, if analysed by injection ability alone, all the 4 grades cement particle sizes are matched well with the 410mD permeability. Except the grade of ≥20μm cement particle size, the other three grades are matched well with the 240mD permeability. In order to understand the matching ability generally, more further analyses combining the other properties are needed.

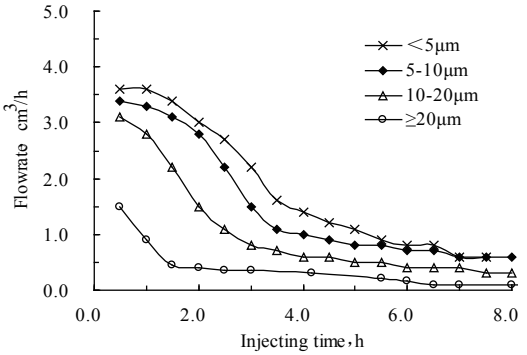

Figure 2
The Permeability is 240 mD

3. CORE EDGE POLLUTION AND LEADING ADVANCE

3.1 Cement Particle Size Grade

The cement particle size is less than 5μm (＜5μm).

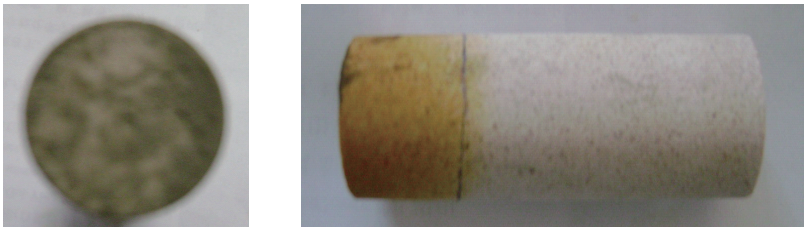

Figure 3
Condition of Core Edge Pollution and Leading Advance (Effective Permeability is 70mD)

Seen from Fig.3, the core edge is polluted, but there is no mud cake produced. And the length of water cement leading advanced is 30% of the core sample.

3.2 Cement Particle Size Grade

The cement particle size is among 5~10μm.

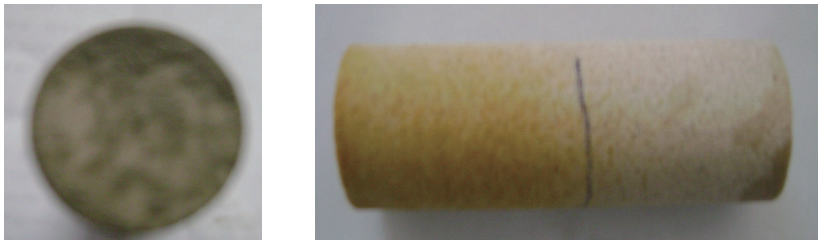

Figure 4
Condition of Core Edge Pollution and Leading Advance (Effective Permeability is 150mD)

Seen from Fig. 4, the core edge is polluted, but there is no mud cake produced. And the length of water cement leading advanced is more than 50% of the core sample.

3.3 Cement Particle Size Grade

The cement particle size is among 10~20μm (10~20μm).

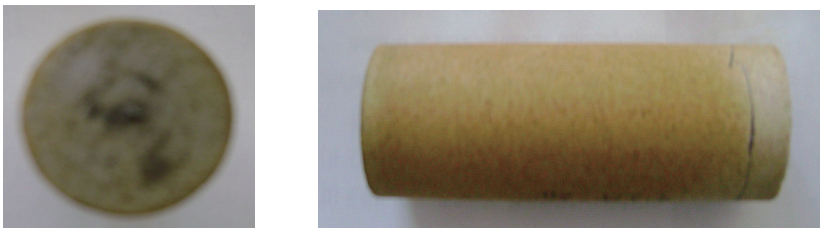

Figure 5
Condition of Core Edge Pollution and Leading Advance (Effective Permeability is 240mD)

Seen from Fig. 5, after injecting the cement grade of 10~20μm into the core of 240mD,the pollution of core edge is light, and there is a little mud cakes produced. And the length of water cement leading advanced is more than 80% of the core sample.

3.4 Cement Particle Size Grade

The cement particle size is more than 20μm (≥20μm).

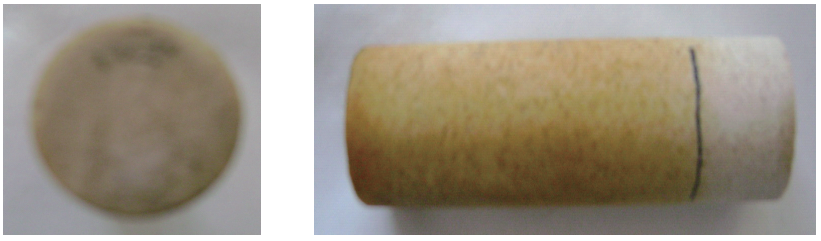

Figure 6
Condition of Core Edge Pollution and Leading Advance (Effective Permeability is 410mD)

Seen from Fig. 6, the pollution of core edge is light, and there is a little mud cakes produced and the cakes can be dusted off easily by water. And the length of water cement leading advanced is more than 70% of the core sample.

4. PERFORMANCE OF BREAK THROUGH AND PLUGGING

The evaluate results of cement plugging agent waiting to solidify, break through after solidifying and plugging ability indicate that the cement agent can be injected into core is not meaning the core channels can be blocked off completely. For example, according to the injection ability, the cement grade of 5~10μm is matching well with the permeability of above 100mD. But on the basis of plugging effect, the core permeability of 150mD can be breaked through after solidifying, the plugging success rate can not reach 100%. So it shows that the cement particle size is not completely matching with the pore throat characteristics of the cores with this permeability. May be it is caused by the cement agent which is not injected deep enough, or by the differential distribution difference of cement particle size. In addition, when selecting cement particle size to plug target reservoir, the particle size is not the smaller the better. For example, it also can be breaked through though taking the cement particle size of 5~10μm to plug 400mD core. It shows that on the condition of ensuring the injection ability, the larger of the cement median particle size, the better of the plugging effect. Because the permeability of the reservoir is not low, and the wider of particle size distribution, the better it can fit the nonhomogeneity. What's more, when injecting small particle size cement agent, the length of water cement leading advanced is long and the migration probability of cement in the target pore throat is bigger than remaining probability, caused low solidification intension and incomplete plugging.

5. MICROCOSMIC PORE STRUCTURE

The scanning electron microscope is used to observe the microcosmic pore structures of core slice. The core slices include before and after cement solidification under different plugging schemes. And the cut location is 2cm from the injecting side and the length of core sample is 10cm. In addition, the amplification factor of all the following pictures is 200.

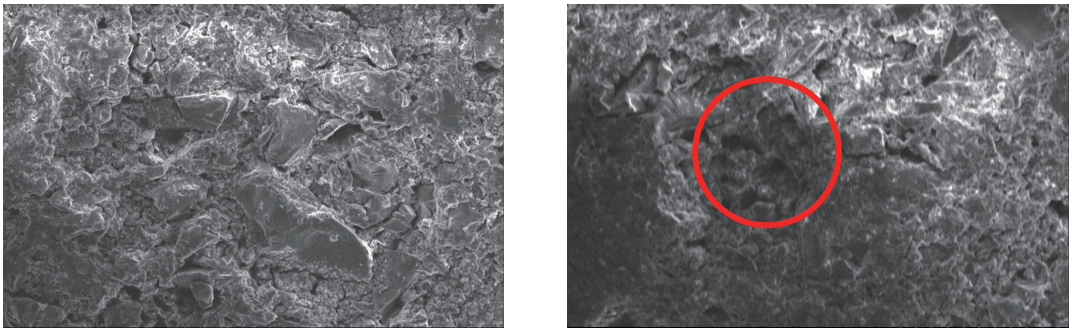

Figure 7
Pore Structure Variation of 422mD Core Before and After Plugging by < 5μm Cement Agent

Seen from Fig. 7 that the surface of rock mineral is sharp and the form is clear before plugging. The sharp degree of surface decrease, the mineral form becomes vague and the specific surface area increase after plugging. It shows that the cement agent is injected in successfully, then adsorbed and solidified in the pore channels. But at the same amplification factor, we can see that some pore channels are still interconnected after plugging. Which results in the incomplete plugging consequentially.

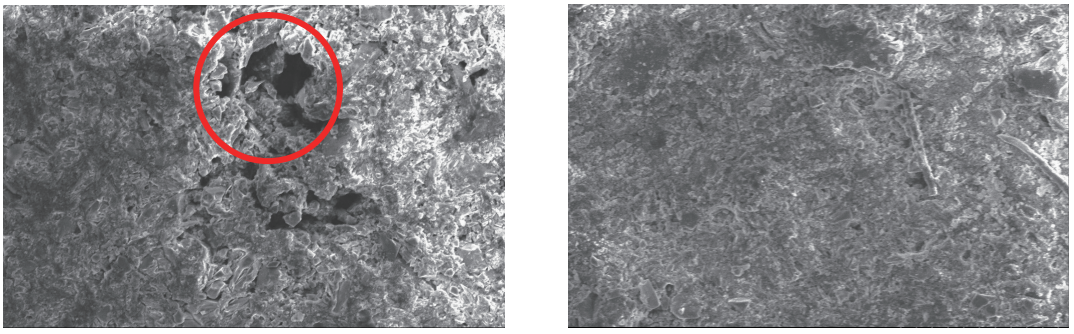

Figure 8
Pore Structure Variation of 145mD Core Before and After Plugging by < 5μm Cement Agent

Seen from Fig. 8, the permeability of this core is 145mD, the permeability is low, the arranging of particles is very close, and most particles are zyklopisch together, so the connectivity is bad. but there are some larger pore throats on the local area. After plugging pore throats by <5μm cement agent, the connectivity becomes worse and the mineral form becomes very vague. It shows that the cement can be injected in and the pore throats can be plugged completely.

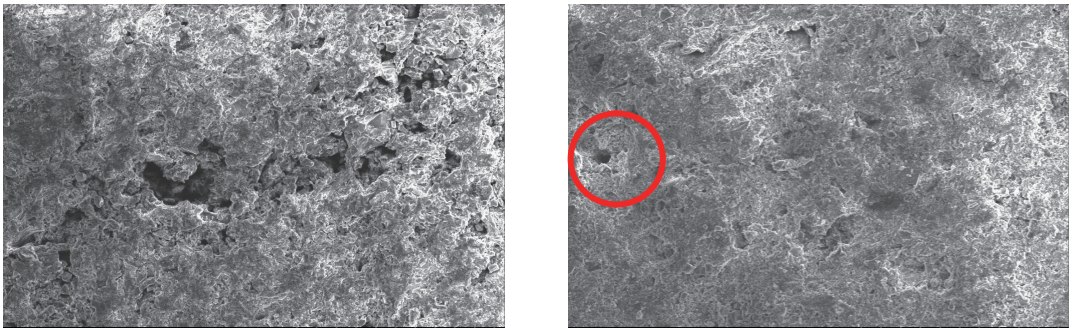

Figure 9
Pore Structure Variation of 153mD Core Before and After Plugging by 5~10μm Cement Agent

Seen from Fig. 9, after injecting 5~10μm cement agent to plug pore throats of 153mD core, the connectivity becomes bad markedly. But on account of the cement agent is not injected deeply, or differential distribution difference of cement particle size, the pore throats were not plugged completely. So it probably to be broken through in later stage. The effect of plugging is influenced.

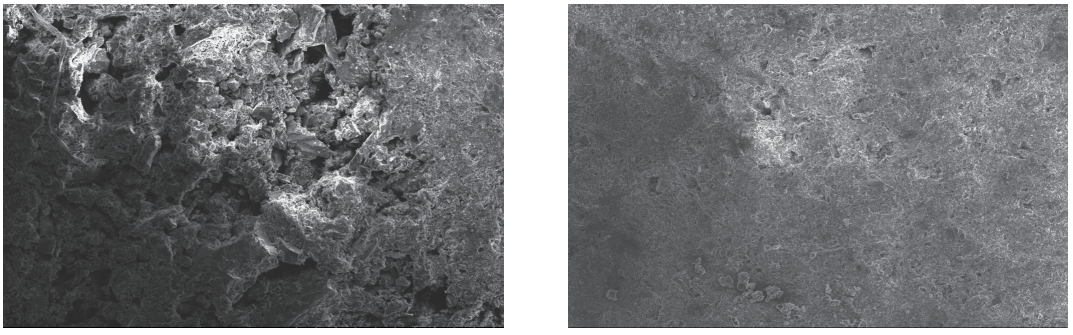

Figure 10
Pore Structure Variation of 416mD Core Before and After Plugging by 5~10μm Cement Agent

Seen from Fig. 10, 416mD core is plugged by the 5~10μm cement agent completely. The mineral form becomes very vague after plugging, and there is no interconnected channel.

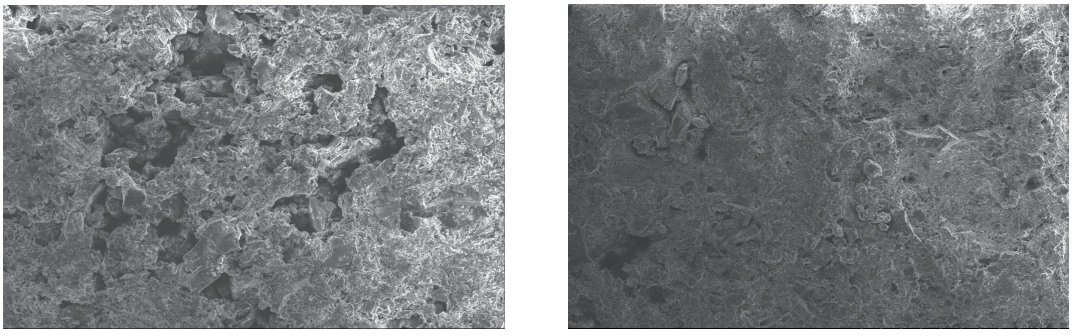

Figure 11
Pore Structure Variation of 738mD Core Before and After Plugging by 10~20μm Cement Agent

Seen from Fig. 11, the 10~20μm cement agent has a good plugging effect to the cores, which permeabilities are above 700mD. And the cement agent is injected enough depth in the core.

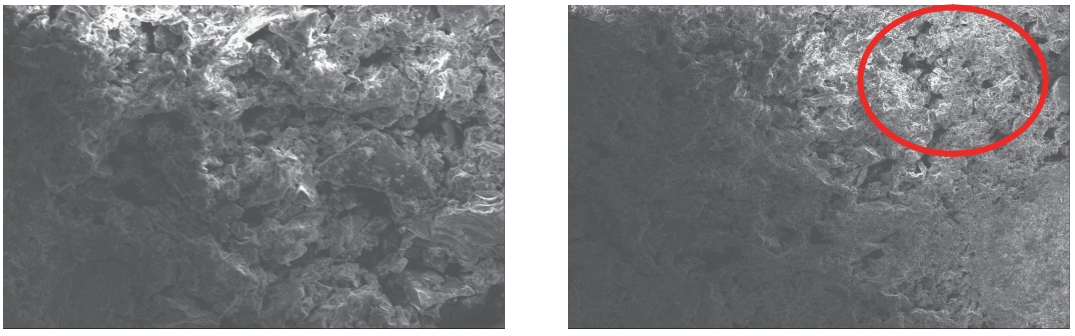

Figure 12
Pore Structure Variation of 411mD Core Before and After Plugging by ≥20μm Cement Agent

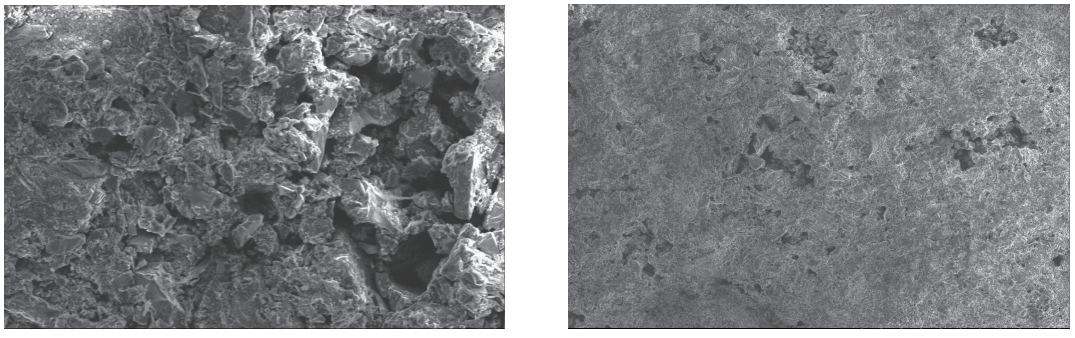

Figure 13
Pore Structure Variation of 1285mD Core Before and After Plugging by ≥20μm Cement Agent

Seen from Fig.12 and Fig.13, for the cement agent which particle size is not below 20μm, the matching ability to 400mD core is bad. And the cement agent is not injected enough depth in pore throats, so the solidification intension is low. Therefore, it is easy to be broken through and result in the incomplete plugging. While for the 1285mD core, the permeability is larger than the prior core and the pore throat ratio is decrease. So the cement agent is injected enough depth and the matching ability to the pores is very well. The effects of solidification intension and plugging are considerable perfect.

6. MATCHING LAW BETWEEN CEMENT PARTICLE SIZE AND PERMEABILITY

By comprehensive analysis the experimental results above, the matching relationship chart between cement particle size and permeability is established as Fig.14.

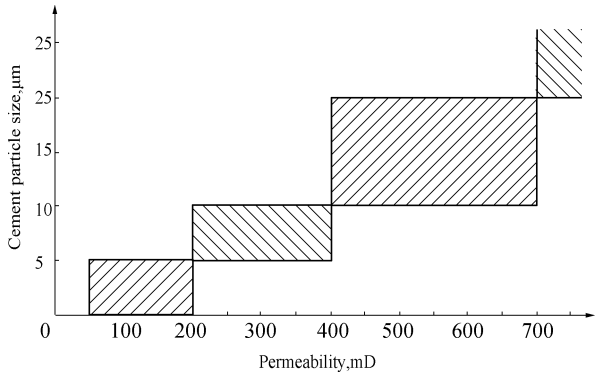

Figure 14
Matching Relationship Chart Between Cement Particle Size and Permeability

CONCLUSION

The matching between cement particle sizes and plugging reservoir should ensure the cement agent must be injected in and the plugging is complete.

To the reservoirs permeabilities distribution of 50~1500mD, the matching relationship of 4 grades cement particle sizes and oil reservoirs permeabilities are established by comprehensive analysis of injecting performance, plugging effect and microcosmic pore structure variation. And the 4 grades cement particle sizes are d_{50}≥20μm, d_{50}: 10~20μm, d_{50}:5~10μm and d_{50}<5μm respectively.

From the field test results of cement agents plugging target wells, the feasibility of this relationship is high, the plugging validity period is long, plugging success rate is high.Therefore, the matching relationship can be promoted and applied widely.

REFERENCES

[1] Dalrymple, E.D., Dahl, J.A., East, L.E., & McKown, K.W. (1992). *A Selective Water Control Process*. Casper, Wyoming: SPE Rocky Mountain Regional Meeting.

[2] David, K., & Prentice, C. (1992). Computer Simulation Improves Remedial Cementing Success. *World Oil*, *1*, 59-62.

[3] Bahramian, Y., Movahedinia, A., & Rasaei, M. R. (2007). *Prediction of Slurry Permeability, K, Using Static Gel Strength, SGS, Fluid Loss Value and Particle Size Distribution*. Oklahoma City, Oklahoma, U.S.A.: Production and Operations Symposium.

[4] Yang, W. H., Ge, H. J., & Liu, S. Q., et al. (2010). Experimental Study of the Matching Ability Between Inorganic Particles Plugging Agent and Formation Pore Constriction. *Oil Drilling & Production Technology*, *11*(6), 93-96.

CSCanada
Advances in Petroleum Exploration and Development
Vol. 3, No. 1, 2012, pp. 55-60
DOI:10.3968/j.aped.1925543820120301.166

ISSN 1925-542X [Print]
ISSN 1925-5438 [Online]
www.cscanada.net
www.cscanada.org

The Bench Test and Field Test of Rotary Steering Motor (RSM) System

DONG Guanghua[1]; LIU Xinhua[1]; FENG Guangtong[1]; JIA jianghong[1,*]

[1] Institute of Drilling Technology, Shengli Petroleum Administration Bureau, Dongying 257017, China.
[*]Corresponding author.

Received 9 January 2012; accepted 16 March 2012

Abstract
Rotary steering system may improve drilling speed, reduce downhole accidents and decrease drilling cost greatly when it is used to drill extended reach well and multilateral horizontal well. The feature and components of Rotary Steerable Motor (RSM)system are first briefly introduced in this paper : it consists of rotary steerable head, mud motor and flex sub and works in Push the Bit mode, steering or non-steering condition and each blade are controlled by using independent electromagnetic valves, mud motor provides power for bit and the hydraulic system by driving shaft; then the pre-test procedures, test set-up and procedures of bench test are described in detail: including blade sequence test, blade firing delay time test and acceptance test of RSM system, finally the note and analysis of the field tests of RSM system in ShengLi Oil Field are enumerated. The bench tests and field tests show that control method of this system is simply, reliable and easily realizable, with improvements this system will be used in practical application soon.

Key words: Rotary Steering Motor (RSM) System; Mud motor; Bench test; Field test; Steering blade

Dong, G. H., Liu, X. H., Feng, G. T., & Jia, J. H. (2012). The Bench Test and Field Test of Rotary Steering Motor (RSM) System. *Advances in Petroleum Exploration and Development*, *3*(1), 55-60. Available from: URL: http://www.cscanada.net/index.php/aped/article/view/j.aped.1925543820120301.166
DOI: http://dx.doi.org/10.3968/j.aped.1925543820120301.166

INTRODUCTION
Rotary steering system may improve drilling speed, reduce downhole accidents and decrease drilling cost greatly when it is used to drill extended reach well and multilateral horizontal well. By 2011, the big drilling services company such as Schlumberger, Baker Hughes, Halliburton, Weatherford all have their own Rotary steering system using in business. Rotary Steerable Motor(RSM) system is developed by APS technology Inc. and Institute of Drilling Technology Shengli Petroleum Administration Bureau, consists of rotary steerable head, mud motor and flex sub and works in Push the Bit mode, the bit is driven by both mud motor and rotary table. When it is used in downhole, can works in three modes: Vertical Steering Mode, Rotary Steerable Mode and Steering Disabled Mode, the modes can change to each other by downlink; well trajectory can be effectively controlled by adjusting steering blades. Steering or non-steering condition and each blade are controlled by using independent electromagnetic valves, which guarantees reliability and control accuracy of RSM, also simplifies the control method. Mud motor provides power for bit and the hydraulic system by drive shaft, alternator gets power from drive shaft and provides power to electronics system, also receives the downlink command from ground. The bench tests and field tests show that control method of this system is simply, reliable and easily realizable, with improvements this system will be used in practical application soon.

1. THE COMPONENT OF RSM
The RSM system consists of rotary steerable head(including Steering Blades, Hydraulic Pump &Control Manifold, Alternator &Regulator, Control Electronics , Sealed Bearing Pack, Drive Shaft, Flow Restrictor Module…), power section(mud motor) and

flex sub (Figure 1), Control Electronics keep track of position while rotating and control blade to work as Figure 2, each blade are controlled by using independent electromagnetic valves(Figure 3)and get power from Hydraulic Pump(Figure 4).

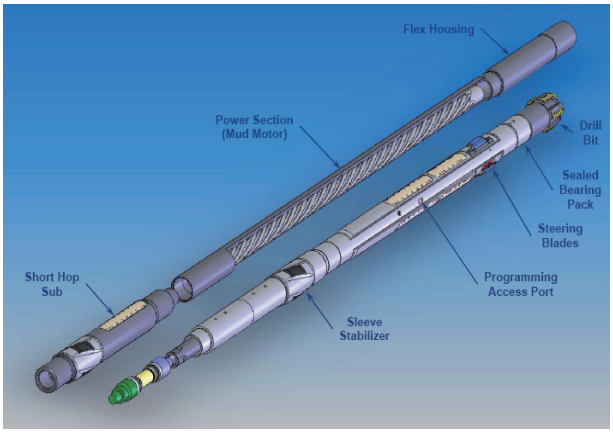

Figure 1
Component of RSM System

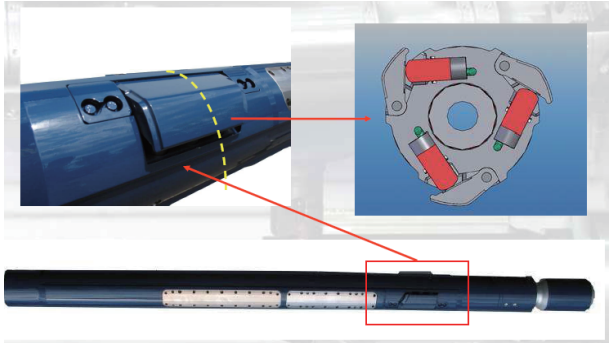

Figure 2
RSM Steering Blades Working

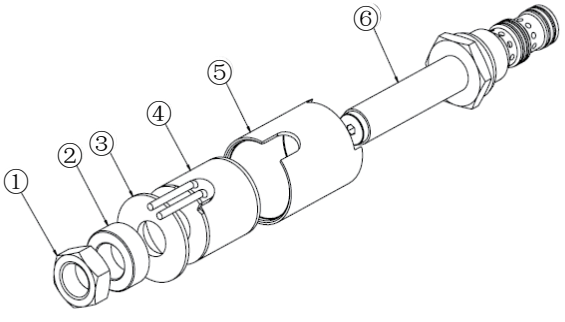

Figure 3
Electromagnetic Valve

①Nut ②Liner ③Spacer ④Coil ⑤Valve Shell ⑥Valve Rod

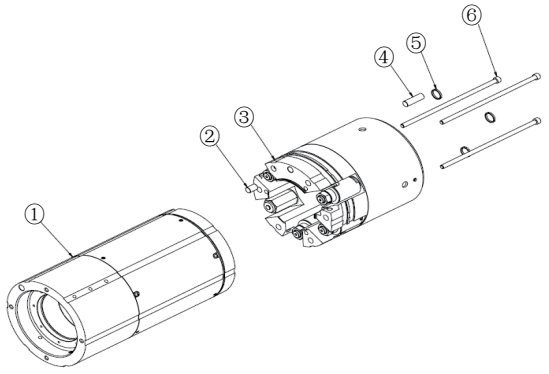

Figure 4
Pump and Control Manifold

①Pump ②Locating Pin ③Control Valves ④&⑥Fixed Screw ⑤High-Pressure Seal

2. THE BENCH TEST OF RSM

The RSM tool must be tested per field test, the final acceptance tests include functional testing of the assembled system and leak testing to ensure the integrity of all the oil to ambient seals.

2.1 Pre-Test Procedures

The RSM tool will be completely assembled per specification prior to conducting any final acceptance tests. The two seal compensation systems and the main compensation system will be de-aired and filled with Mobil 629 oil using a VacOil system. The software for the tool will be installed prior to conducting any testing per this procedure.

2.2 Test Set-up

A 20 HP electric motor and reducer gearbox provide the shaft rotation to the tool. The drill string is not rotated during the test. The tool is held in place by two V blocks that secure the housing to the test rig. A load ring is located over the actuating blades to monitor the force and displacement of each blade. The rotation simulator Hemholtz coil is located over the electronic hatch with the rotation sensor. No hydraulic plumbing is required as the completed tool is tested with its internal closed loop hydraulic circuit. A photograph of the completed setup is shown in figure 5.

Figure 5
RSM Tool in Test Stand with Load Ring and Rotation Sensor

Install a cooling loop by placing a hose into the ID of the drive shaft. The hose end should be located ¾ to full length of the drive shaft. Water flows out of the drive shaft and is captured by a reservoir and re-circulated via a submersible circulating pump.

Install a regulated air pressure line to the mud compensation cavity. The air pressure should be set at 20 psi +/- 5 psi. This supply induces a force on the compensator piston to provide a positive hydraulic supply pressure head to t he vane pump.

Install the Air / Hydraulic Load Fixture Assembly over the extending arm section. Lubricate between the pistons and the outer surface of the extending arms with lubricant. Tighten the clamp onto the sub ensuring that the forcing pistons are centered on the arms. Connect the hydraulic lines. Fill the oil chamber of the pressure unit with hydraulic oil (power steering fluid or jack oil is acceptable).Using a regulator, pressurize to approximately 5 psi and bleed the three cylinders at the hose connections. Loosen the fittings from top to bottom until most of the air has escaped. The pneumatic to hydraulic converter will need cycling by disconnecting the air supply and then re-connecting to stroke the piston. When the system is bled, adjust the air pressure up to 500 psi to load the RSM arms.

2.3 Blade Sequence Test

The blade sequence is checked as follows:

Rotate the drive shaft at 100 RPM.

Using the interface program, click on the “blade A” button on the interface screen and confirm that blade A has fired.

Next, click on “blade B” on the interface screen and confirm that blade B has fired.

Finally, click on “blade C” an the interface screen and confirm that blade C has fired.

If the blades do not fire in the proper sequence, the solenoid valves are not properly wired in the valve driver board. Connect the solenoid wires as required to the valve driver board to obtain the proper blade firing sequence.

2.4 Blade Firing Delay Time Test

The delay time that is measured is the time from detecting the encoder board signal to the actual movement of the “A” steering blade. The rotation sensor is installed in fixture tool for the blade timing calibration.

Install the rotation sensor in the sensor fixture with the motor drive of the fixture pointed downward but at a slight angle (greater than 2 degrees) from vertical. The sensor must be installed in the fixture with the dowel pin hole opposite the scribe line on the fixture.

Prior to conducting the blade timing test, there are several steps to ensure that any magnetic interference from the rotating drive shaft is accounted for by the tool firmware.

Run the tool at 100 +/- 5 RPM for a minimum of 30 seconds to allow the firmware to detect magnetic perturbations thresholds due to the rotating shaft.

Rotate the rotation sensor in fixture T-11103 at 30 to 40 RPM and observe on the interface screen that the tool has detected rotation.

Wait for the firmware to detect magnetometer peaks. This typically takes up to 70 seconds. Detection of the peaks will be indicated on the interface screen.

Turn off the rotation of the sensor. The tool is now

ready to accept down linking commands and conduct the blade timing test.

Downlink the tool to Rotary Steerable mode for this test. Set the initial pump speed to 120 RPM. Reduce the speed to 90 RPM for 20 +/- 5 seconds and return the pump speed to 120 RPM. Wait 120 seconds and reduce the speed to 90 RPM again for 20 +/- 5 seconds. Return the speed to 120 RPM.

After completing these dips in drive shaft speed, wait 20 seconds and begin rotation of the rotation sensor in fixture tool. The tool will begin firing blades A, B, and C in sequence. The output of the "A" blade control of the encoder board is connected to one channel of an oscilloscope. The output of the load ring is connected to the second channel of the oscilloscope. Record the time delay between these two signals at the simulated rotation speeds provided in a table 1, the table 1 is the data record of #2 RSM tool.

Table 1
Time Delay to Record

Drive Shaft Speed (RPM)	Simulated Rotation Speed (RPM)	Delay Time (seconds)
120	27.1	1600
120	31.6	1420
120	39.1	1130
120	50.1	930
120	59.8	830
120	69.5	720
120	79.9	650
120	89.0	600
120	98.1	560
120	111.3	500
120	121.0	480

Apply a best fit polynomial curve(y=ax2+bx+c, x= Simulated Rotation Speed, y= Delay Time) fit to the data taken in table 1,getting a=2.32775 、b=-3.42023E-2 、c=1.59865E-4 . Input the curve fit values of a, b, and c into the program to calibrate the Delay Time and test again, ensure the Delay Time less than 5ms.

2.5 Acceptance Test of Tool

Install the coil clamp assembly of the rotation simulator. The coils should be positioned over the rotation sensor just up hole of the load ring assembly. Connect the coil harness to the interface box using the harness provided. Connect the interface box to a computer with the rotation sensor software installed. The Center of the Rotation Simulator coil to be placed 2.5 inches is from the lower edge of the Hatch cover next to the steering Blades.

The functional test of the tool is completed by running the tool in the test stand and completing the necessary down-linking commands to ensure proper operation. Three modes of operation are checked during the test: rotary steerable mode, vertical drilling mode, and steering disabled mode. The rotation sensor should be removed from the fixture tool and installed in the sensor hatch pocket of the tool for the remaining tests. The hatch cover should be in place over the sensor for the tests.

Prior to conducting the down linking test, there are several steps to ensure that any magnetic interference from the rotating drive shaft is accounted for by the tool firmware.

Run the tool at 100 +/- 5 RPM for a minimum of 30 seconds to allow the firmware to detect magnetic perturbations thresholds due to the rotating shaft.

Turn on the rotation coil and observe on the interface screen that the tool has detected rotation.

Wait for the firmware to detect magnetometer peaks. This typically takes up to 70 seconds. Detection of the peaks will be indicated on the interface screen.

Turn off the rotation coil. The tool is now ready to accept down linking commands.

2.5.1 Vertical Steering Mode Test

Set the initial pump speed to 120 RPM. Reduce the speed to 90 RPM for 20 +/- 5 seconds and return the pump speed to 120 RPM. Wait 30 seconds and reduce the speed to 90 RPM again for 20 +/- 5 seconds. Return the speed to 120 RPM. Wait 30 seconds and reduce the speed to 90 RPM again for 20 +/-5 seconds. Return the speed to 120 RPM.

Turn on the rotation coil (which should be set at 40 RPM and 0.5 gauss).The blades should begin firing in sequence within 45 seconds of turning on the rotation coil.

2.5.2 Rotary Steerable Mode Test

Make sure the rotation coil is turned off before beginning the down linking sequence. Set the initial pump speed to 120 RPM. Reduce the speed to 90 RPM for 20 +/- 5 seconds and return the pump speed to 120 RPM. Wait 60 seconds and reduce the speed to 90 RPM again for 20 +/- 5seconds. Return the speed to 120 RPM. This will put the tool in 50 % steering mode.

Turn on the rotation coil (which should be set at 40 RPM and 0.5 gauss).The blades should begin firing in sequence within 45 seconds of turning on the rotation coil.

Turn off the rotation coil and wait for the steering blades to stop activating. Set the initial pump speed to 120 RPM. Reduce the speed to 90 RPM for 20 +/- 5 seconds and return the pump speed to 120 RPM. Wait 120 seconds and reduce the speed to 90 RPM again for 20 +/- 5 seconds. Return the speed to 120 RPM. This will put the tool in 100 % steering mode.

Turn on the rotation coil (which should be set at 40 RPM and 0.5 gauss).The blades should begin firing in sequence within 45 seconds of turning on the rotation coil.

2.5.3 Steering Disabled Mode Test

The rotation simulator must be initially turned off. Begin with the tool running at 120 RPM and in steering mode per section 5.2. Reduce the speed to 90 RPM for 20 +/- 5

seconds and return the pump speed to 120 RPM. Turn on the rotation simulator. The tool should stop steering after this down-linking command. Confirm that the steering blade do not actuate after this dip in pump speed.

2.5.4 Minimum Run Time Test

The tool should be run for a minimum of 3 hours during the acceptance testing to ensure proper operation. It the accumulated test time is less than three hours, run the tool for additional time as outlined below. Return the tool to rotary steering mode via the procedure in paragraph 3.5.2. Allow the tool to run at 100% steering mode to accumulate a total test time of at least 3 hours. Visually check for leaks during this operational test. Do not let the housing temperature exceed 120°F during this test. Shut the drive rotation off while allow cooling loop to continue circulating if the housing temperature reaches 120°F. Resume testing once the housing temperature decreases to 85°F or below.

After all the procedures of bench test, if the RSM tool works ok, can go to field test.

3. THE FIELD TEST OF RSM IN SHENGLI OIL FIELD

3.1 Field Test #1

This field test in shengli oil field was occurred during the summer of 2007, in two separate wells: well Xin 164-X6 and well DA373-X9. Between these two wells, the RSM tool accumulated 63 hours downhole, with 31.5 hours circulating time. Recorded downhole memory data indicated limited steering blade actuation. Directional performance data are not available. After this field test, a complete disassembly of tool was performed. Although it could not be confirmed from the available information, it was surmised that the failure of the tool to either take the downlinked commands or to steer may have likely been the result of 1) effects of magnetic interference caused by the inner rotating steel drive shaft; 2) loss of power from the battery pack (which would have prevented the steering mode instruction being maintained by the electronics board. It was also found during tool disassembly that four (4) of twelve (12) vane pump leaf springs had broken.

3.2 Field Test #2

Improve the RSM tool aim at the problems depicting in section 4.1,the second field test in shengli oil field was occurred on March 24, 2008 in wellYing2-XG16. The objectives of the test were to drill an essentially vertical section in VDM mode, then switch to Rotary Steerable mode and kick off the well. The RSM went into the hole at a measured depth of 1709.51 meters (5608.6 feet) and was successfully downlinked to VDM mode. Drilling proceeded to 1775.95 meters (5826.6 feet) with inclination progressively declining from 0.5 °to 0.3°. The tool was then downlinked to Rotary Steerable mode and attempted to kick off at 223°azimuth. The angle building ability of the tool is lower than plan. A second attempt was then made to downlink to Rotary Steerable mode, and again the angle building ability is lower. It was then tripped out of the hole. Upon post-field test inspection, it was found that an alternator driveshaft key had sheared, thereby causing the loss of electrical power to the tool.

3.3 Field Test #3

After a replacement alternator drive assembly was installed, the third field test in shengli oil field was occurred on the second week of May 2008, The RSM went into hole for well N35-X7 at a measured depth of 2434.1 meters. At 2443.69 meters, the tool was downlinked into VDM mode. Drilling proceeded to 2462.68 meters, where the tool was downlinked to Rotary Steerable mode. Drilling continued to 2539.15 meters, with no appreciable build in hole inclination; hole inclination increased slightly, from an average 0.7°at 2435 meters to1.2 °at 2493 meters. With approximately 12 hours circulating time, standpipe pressure was observed to sharply increase, indicating a possible plugged bit nozzle. It was then determined to trip the assembly out of the hole and stop the test.

CONCLUSIONS

（1）In RSM system, the bit is driven by both mud motor and rotary table, string rotates constantly, less sticking, more power to bit than present Rotary Steerable Systems let this system has more dominance to drill extended reach well and multilateral horizontal well.

（2）Each blade is controlled by using independent electromagnetic valves, pump and alternator get power from mud motor by drive shaft is the feature of RSM system.

（3）The RSM tool must be tested per field test, the final acceptance tests include functional testing of the assembled system and leak testing to ensure the integrity of all the oil to ambient seals and the Delay Time less than 5ms.

（4）The bench tests and field tests show this system can autonomously drill a planned, controlled well path, but the angle building ability is lower than plan, we think with improvements this system will be used in practical application soon.

REFERENCES

[1] Thorogood, J., Aldred, W., & Florence, F., Iversen, F. (2009). Drilling Automation: Technologies, Terminology and Parallels with Other Industries. *SPE/IADC Drilling Conference and Exhibition*, *17-19 March 2009*, *Amsterdam*, *The Netherlands*.

[2] Xiong, J. Y., Wen J. W., & Rong J. G., et al. (2010). New

Progress in the Research of Rotary Steerable Drilling Technology. *Natural Gas Industry*, *30*(4), 87-90.

[3] Poli, S., & Donaco, F., Joachim, O., & Detlef, R. (1998). Advanced Tools for Advanced Wells: Rotary Closed-Loop Drilling System-Results of Prototype Field Testing. *SPE Drilling & Completion*, *13*(2), 67-72.

[4] Xie, H. M., Zhou, J., & Yue, Y. Z. (2010). Research on the Power System Used for Rotary Navigation Drilling Device. *Drilling & Production Technology*, *33*(4), 5-7.

[5] Yang, Q. J., Han, L. J., & Ge, P., et al. (2008). A Discussion on Controlling Accuracy of Rotary Steering Motor. *Oil Drilling & Production Technology*, *30*(4), 21-23.

[6] Tang, N., Huo, A. Q., & Wang, Y. L. et al. Development of Downward Communication Receiving Function in Rotary Steerable Drilling System. *Acta Petrolei Sinica*, *31*(1), 157-160.

[7] Zhang, S. H., & Di, Q. F. (2000). Petroleum Engineering Drilling Extended Reach Well with Rotary Steering Drilling System. *Acta Petrolei Sinica*, *21*(1), 76-80.

[8] Xie, H. M., Zhou, J., & Yue Y. Z. (2010). Research on the Power System Used for Rotary Navigation Drilling Device. *Drilling & Production Technology*, *33*(4), 5-7.

[9] Han, L. J., Sun, M. X., & Li, Z. H. (2003). Introduction of Static Bias Push-The-Bit Rotary Naviyational System. *Oil Field Equipment*, *32*(6), 4-7.

[10] Downton, G., Hendricks, A., Klausen, T. S., Pafitis, D. (2000). New Directions in Rotary Steerable Drilling. *Oilfield Review*, *12*(1), 18-29.

ABOUT CSCanada

CSCanada includes 14 international non-profit Journals dedicated to advance academic achievements and research information around the world. The host organizations of our journals are *Canadian Academy of Oriental and Occidental Culture (CAOOC), Canadian Research & Development Center of Sciences and Cultures (CRDCSC)*, with their headquarter in Montreal, Canada. Registered in Quebec in March, 2005, CAOOC and CRDCSC are committed to scientific research and spreading eastern and western cultures.

CSCanada enables discovery, access, and preservation of scholarly content by serving as an educator, leader, spokesperson and professional association to achieve the following goals:

- Help scholars, researchers, and students discover, use, and build upon a wide range of scholarly content on a dynamic platform that increases productivity and facilitates new forms of scholarship
- Help libraries connect patrons to vital content while increasing shelf-space savings and lowering costs
- Help academic databases connect patrons to vital content so that persons can inquire and use the information conveniently and duly
- Help various academic institutions reach new audiences and preserve their scholarly content for future generations.

It will be a wise decision to choose our journals because of the quality and value we provide and promise as following:

► Promoting International Cooperation

CSCanada is working with over 1000 scholars, researchers, professors and students. As authors, readers, editorial board members, professionals who have accomplished in various academic fields all over the world work together to rich and improve the contents of our journals. *CSCanada* also cooperates with internationally renowned academic databases, libraries, academies, associations and other institutions to maximize the global reach of our journals.

► Comprehensive and Recognized Subject Category

CSCanada includes 14 journals, diversifying in most disciplines currently used in academic circle, which makes our journals provide a complete picture of worldwide influential research. In the future, *CSCanada* will ceaselessly increase and refine its subject category so that more academic voices can be heard.

► Easy and Convenient to Inquire and Use

All journals of *Cscanada* use Open Journal Systems (OJS). It's very convenient for everyone to view articles or journals for free by directly visit *CSCanada* website: www.*cscanada*.org and www.cscanada.net.

► Databases

All journals of *Cscanada* have been indexed by famous academic databases that readers and users can easily find.

OPEN ACCESS JOURNALS

One key request of researchers across the world is unrestricted access to research publications. Open Access gives a worldwide audience larger than that of any subscription-based journal and thus increases the visibility and impact of published work. It also enhances indexing, retrieval power and eliminates the need for permissions to reproduce and distribute content. All *CSCanada* journals are fully committed to the Open Access Initiative and will provide free access to all articles as soon as they are published.

SUBMISSION OF MANUSCRIPTS

We strongly recommend you read this in full if you have not previously submitted a contribution to *CSCanada*. We also suggest that before submission you familiarize yourself with *CSCanada*'s style and content by reading the journals, either in print or online, especially if you have not submitted to our journals recently.

Formats

All manuscripts should be sent by email as attachments to relative email address or submitted via the online system and should be typed in single line spacing and 10 pt.

► **Research Articles**

Research Articles are innovative reports whose conclusions represent a substantial advance in the understanding of a significant problem and have directly, far-reaching implications.

Research Articles include an abstract, an introduction, up to 20 figures or tables, sections with brief subheadings. Materials and Methods should usually be included, which will also be needed to support the paper's conclusions.

► **Reports**

Reports are short articles of creative research focused on an outstanding finding whose importance means that it will be of interest to scientists in other fields. They should have less than 30 references.

They begin with a fully referenced paragraph, of about 200 words, (definitely no more than 300 words) aimed at readers in other disciplines. The letters (up to ~ 5000 words including references, notes and captions or ~ 5 printed pages) should include an abstract, an introductory paragraph, up to six figures or tables. Materials and Methods should usually be included, which should be needed to support the paper's conclusions.

► **Reviews**

Reviews describe new developments of interdisciplinary significance and highlight future directions. They include an abstract, an introduction that outlines the main theme, brief subheadings, and an outline of important unresolved questions. A maximum of 50 references is suggested. Most Reviews are solicited by the editors, but unsolicited submissions may also be considered.

► **Other contributions to *CSCanada***

CSCanada also publishes News and Comment, Correspondence, Opinion, Book & Arts, Futures, News and Views, Perspectives, Insights, Outlooks, Analyses, Hypotheses, and Technology Features. Please visit www.cscanada.net for more information.

Manuscript Selection

Manuscripts should be clear and simple so that they are accessible to readers in other disciplines and to readers for whom English is not their first language. Authors are notified of decisions by e-mail. Repeated submissions of the same manuscript will not be acknowledged. *CSCanada* treats all submitted manuscripts as confidential documents. Our peer review process is also confidential and identities of reviewers are not released. Research papers that are selected for in-depth review are evaluated by at least two outside referees. Reviewers are contacted before being sent a paper and asked to return comments within 1 to 2 weeks for most papers. We are able to expedite the review process significantly for papers that require rapid assessment. Selected papers are edited to improve accuracy and clarity and for length. Papers cannot be resubmitted over a disagreement on interest or relative merit. If a paper was

rejected on the basis of serious reviewer error, resubmission may be considered. In some cases, reviewers are satisfied that a paper's conclusions are adequately supported by the data presented, but the general interest of the findings is not sufficient to justify publication in *CSCanada*. In such a case, the authors will be offered the opportunity for publication with additional review required when reviewers have asked for supplementary experiments during revision. In this case again, reviewers and editors may find an appropriately worded version of the paper to be acceptable for publication without further in depth review.

CSCanada makes decisions about submitted papers as rapidly as possible. All manuscripts are handled electronically throughout the consideration process. Authors are usually informed within a week if the paper is not being considered.

MANUSCRIPT PREPARATION

Manuscripts are preferred to be presented in the following order:

- Title
- Abstract and Keywords
- Text
- End Notes
- References
- Appendices
- Figure Legends
- Tables (each table complete with title and footnotes)
- Figures

Title

Titles do not exceed two lines in print. This equates to 90 characters (including spaces) for Letters or 75 characters (including spaces) for Research Articles. Titles do not normally include numbers, acronyms, abbreviations or punctuation. They should include sufficient detail for indexing purposes but be general enough for readers outside the field to appreciate what the paper is about.

Abstract

We suggest each manuscript should accompany a structured abstract to explain to the general reader why the research was done and why the results are significant. A structured abstract should include such contents: the purpose of the research, the materials and methods and the results. Please do not include citations or undefined abbreviations in the abstract. The preferred length of the abstract is less than 300.

Text

Research articles should fill no more than 30 pages, and Letters no more than 5 pages. A typical Letter to *CSCanada* contains about 5000 words of text (including the first paragraph of Letters, figure legends, reference list and the methods section if applicable) and four small display items (figures and/or tables) with brief legends. A composite figure (with several panels) usually needs to take about half a page, equivalent to about 600 words, in order for all the elements to be visible. Our preferred format for is APA and MLA is also acceptable. We prefer the use of a 'standard' font, preferably 10-point Times New Roman. For mathematical symbols, Greek letters and other special characters, use normal text or Symbol font. Word Equation Editor/Math Type should be used only for formulae that cannot be produced using normal text or Symbol font. When you quote some paper in your article please follow the APA format. For detail information please visit http://www.apastyle.org/

End Notes

End notes are brief and follow the reference list. Papers containing supplementary information contain a statement after the reference list:

Acknowledgements should be brief, and should not include thanks to anonymous referees and editors, inessential words, or effusive comments. Acknowledgements can contain grant and contribution numbers.

Author Contributions: authors are required to include a statement to specify the contributions of each co-author. The statement can be up to several sentences long, describing the tasks of individual authors referred to by their initials.

References

References are each numbered, ordered sequentially as they appear in the text, methods summary, tables, boxes, figure legends, online-only methods in our nature science and engineering journals. When cited in the text, reference numbers are superscript, not in brackets unless they are likely to be confused with a superscript number. Only one publication can be listed for each number. We preferred articles that have been published or submitted to a named publication in the reference list; papers in preparation should be mentioned in the text with a list of authors (or initials if any of the authors are co-authors of the present contribution). Published conference abstracts, numbered patents and preprints on recognized servers may be included in reference lists, but text, grant details and acknowledgements may not. Please follow the style below in the published edition of *CSCanada* in preparing reference lists.

We advise the authors to use the APA style to write the references list. You can visit http://www.apastyle.org for detail information. There are some examples for APA style.

► **Books**

One author:

Gardner, H. (1993). *Frames of Mind: The Theory of Multiple Intelligences*. New York: Basic Books.

Two to seven authors:

Cargill, O., Charvat, W., & Walsh, D. D. (1966). *The Publication of Academic Writing*. New York: Modern Language Association.

More than seven authors:

Cooper, L., Eagle, K., Howe, L., Robertson, A., Taylor, D., Reims, H., . . . Smith, W. A. (1982). *How to Stay Younger While Growing Older: Aging for All Ages*. London: Macmillan.

No author given:

Experimental Psychology. (1938). New York: Holt.

No publication date given:

Smith, J. (n.d.). *Morality in Masquerade*. London: Churchill.

An organization or institution as "author":

University of Minnesota. (1985). *Social Psychology*. Minneapolis: University of Minnesota Press.

U.S. Census Bureau. (2000). *Statistical Abstract of the United States.* Washington, DC: U.S. Government Printing Office.

An editor as "author":

Updike, J. (Ed.). (1999). *The Best American Short Stories of the Century*. Boston: Houghton Mifflin

An edition of an author's work:

Brockett, O. (1987). *History of the Theatre* (5th ed.). Boston: Allyn and Bacon.

A translation:

Freud, S. (1970). *An Outline of Psychoanalysis* (J. Strachey, Trans.). New York: Norton (Original work published 1940)

A work in a series:

Cousins, M. (1984). *Michel Foucault. Theoretical Traditions in the Social Sciences*. New York: St. Martin's Press.

A work in several volumes:

Wilson, J. G., & Fraser, F. C. (Eds.). (1977-1978). *Handbook of Teratology* (Vols. 1-4). New York: Plenum Press.

Conference proceedings:

Schnase, J. L., & Cunnius, E. L. (Eds.). (1995). *Proceedings of CSCL '95: The First InternationalConference on Computer Support for Collaborative Learning*. Mahwah, NJ: Erlbaum.

Chapter in an edited book:

Rubenstein, J. P. (1967). The Effect of Television Violence on Small Children. In B. F. Kane (Ed.), *Television and Juvenile Psychological Development* (pp. 112-134). New York: American Psychological Society.

► **Articles**

Journal / periodical (continuous pagination):

Prasart Nuangchalerm (2011). In-service Science Teaches' Pedagogical Content Knowledge, *Studies in Sociology of Science*, *2*(2), 35-39.

Journal / periodical (non-continuous pagination):

Sawyer, J. (1966). Measurement and Prediction, Clinical and Statistical. *Psychological Bulletin, 66*(3), 178-200.

Journal article with three to seven authors:

Huang, Yanbo, Lan, Yubin, Hoffmann,W. C., & Lacey, R. E.(2011). A Pixel-Level Method for Multiple Imaging Sensor Data Fusion through Artificial Neural Networks. *Advances in Natural Science*, *4*(1), 1-13.

Journal article more than seven authors:

Akaria, Z., Hussin, Z. H., Zakaria, Z., Noordin, N. B., Hilmie M.Z., Sawal, B.M., Saad, S. F.,...Kamil, S. B. O. (2009). E-Filing System Practiced by Inland Revenue Board (IRB): Perception Towards Malaysian Taxpayers. *Cross-Cultural Communication*, *5*(4). 10-20.

Newspaper:

Monson, M. (1993, September 16). Urbana Firm Obstacle to Office Project. *The Champaign-Urbana News-Gazette*, pp. 1, 8.

Magazine:

Raloff, J. (2001, May 12). *Lead Therapy Won't Help Most Kids*. Science News, 159, 292.

Review:

Gleick, E. (2000, December 14). The Burdens of Genius [Review of the book *The Last Samurai* by H. DeWitt]. *Time,* 156, 171.

Article in a reference book or encyclopedia - signed and unsigned:

Sturgeon, T. (1995). Science Fiction. In *The Encyclopedia Americana* (Vol. 24, pp. 390-392). Danbury, CT: Grolier.

Islam. (1992). In *The New Encyclopedia Britannica* (Vol. 22, pp. 1-43). Chicago: Encyclopedia Britannica.

A work in a collection or anthology:

Jesrani, P. J. (1998). Working Turn Tables. In N. Bhatia, S. Dhand, & V. Rupaleria (Eds.), *Throwing a Great Party* (pp. 19-48). Chicago: NT Publishers.

Shapcott, T. (1980). Margaret Atwood's Surfacing. In K. L. Goodwin (Ed.), *Commonwealth Literature in the Curriculum* (pp. 86). South Pacific Association of Common-wealth Literatures and Language Studies.

Paper published as part of the proceedings of a conference:

Nicol, D. M., & Liu X. (1997). The Dark Side of Risk (What Your Mother Never Told You About Time Warp). In *Proceedings of the 11th Workshop on Parallel and Distributed Simulation, Lockenhaus, Austria*, *10–13 June 1997* (pp. 188–195). Los Alamitos, CA: IEEE Computer Society.

► **Dissertation**

Obtained from university:

Carlson, W. R. (1977). *Dialectic and Rhetoric in Pierre Bayle*. (Unpublished doctoral dissertation).Yale University, USA.

Obtained from Dissertations and Theses database:

Mancall, J. C. (1979). *Resources Used by High School Students in Preparing Independent Study projects: A bibliometric Approach* (Doctoral dissertation). Retrieved from ProQuest Dissertations and Theses database. (UMI No. AAT 7905069)

An abstract from DAI:

Delgado, V. (1997). An Interview Study of Native American Philosophical Foundations in Education. *Dissertation Abstracts International: Section A. Humanities and Social Sciences*, 58(9), 3395.

► **Other materials**

Patent:

Islam. (1992). In The New Encyclopedia Britannica (Vol. 22, pp. 1-43). Chicago: Encyclopedia Lemelson, J. H. (1981). *U.S. Patent No. 4, 285,338*. Washington, D.C.: U.S. Patent and Trademark Office.

Video or DVD (motion pictures):

Jesrani, P. J. (1998). Working Turn Tables. In N. Bhatia, S. Dhand, & V. Rupaleria (Eds.), Mass, J. B. (Producer), & Gluck, D. H. (Director). (1979). *Deeper into Hypnosis* [Motion picture]. Englewood Cliffs, NJ: Prentice Hall.

Television program:

Pratt, C. (Executive Producer). (2001, December 2). *Face the Nation* [Television broadcast]. Washington, DC: CBS News.

Personal communications (email messages, interviews, lectures, and telephone conversations):

Because the information is not retrievable it should not appear in the reference list. In your paper they should look as follows: J. Burnitz (personal communication, September 20, 2000) indicated that.… or In a recent interview (J. Burnitz, personal communication, September 20, 2000).

► **Books (Online)**

An entire electronic book retrieved from a database:

Murray, T. H. (1996). *The Worth of a Child*. Berkeley: University of California Press. Retrieved from netLibrary database.

An entire electronic book with direct link to item:

Bryant, P. (1999). *Biodiversity and Conservation*. Retrieved from http://darwin.bio.uci.edu/~sustain/bio65/Titlpage.htm

An article or chapter in an electronic book

Symonds, PM. (1958). Human drives. In C. L. Stacey & M. DeMartino (Eds.), *Understanding Human Motivation* (pp. 11-22). Retrieved from PsycBOOKS database.

Entire electronic technical or research report - available on the web:

Russo, A. C., & Jiang, H. J. (2006). Hospital Stays among

Patients with Diabetes, 2004 (Statistical Brief #17). Retrieved from Agency for Healthcare Research & Quality: http://www.hcup-us.ahrq.gov/reports/statbriefs/sb17.jsp

Paper from the proceedings of a conference:

Miller, S. (2000). Introduction to Manufacturing Simulation. In *Proceedings of the 2000 Winter Simulation Conference*, (pp. 63-66). Retrieved from http://www.informs-sim.org/wsc00papers/011.PDF

► **Journal Articles (Online)**

New style guidelines use the DOI (Digital Object Identifier) which is an assigned alpha-numeric code that usually appears on the article or in the database record. If the DOI is not provided, enter the citation information using Cross/Ref Simple Text Query <http://www.crossref.org/SimpleTextQuery/>. The retrieval date is no longer required.

Article with DOI assigned:

Demir, Müge (2011). Using Nonverbal Communication in Politics. *Canadian Social Science*, 7(5), 1-14. DOI:10.3968/J.css.1923669720110705.19

Article from electronic journal (no print version):

Phouphet KYOPHILAVONG,Jeff BENNETT(2011). Willingness to Pay for Cleaning up Road Dust in Vientiane. Retrieved from *International Business and Management*, http://www.cscanada.net/index.php/ibm/article/view/j.ibm.1923842820110302.070

Article with no DOI: (include URL for journal website not database)

Tyrer, Pat (2011). Food and Fantasy as Reflection of Female Repression in Like Water for Chocolate. *Studies in Literature and Language*, 3(2), 1-5. Retrieved from http://www.cscanada.net/index.php/sll/article/view/1992

Article - preprint version

Shi,Guangren (in press). Finite Volume Method for Solving a Modified 3-D 3-Phase Black-Oil. *Journal of Advances in Petroleum Exploration and Development*. Retrieved from http://cogprints.org/6305/1/NRC-50738.pdf

Newspaper article from an online database:

Altman, L. K. (2001, January 18). Mysterious Illnesses often Turn Out to be Mass Hysteria. *New York Times*. Retrieved from the ProQuest Newspapers database.

A newspaper article from newspaper's website:

Cary, B. (2001, June 18). Mentors of the Mind. *Los Angeles Times.* Retrieved from http://www.latimes.com

company information from a database:

Ingersoll-Rand Company Limited. (2004). *Company Profile.* Retrieved July 29, 2008 from Hoovers in Lexis-Nexis.

An article posted on an open-access or personal website:

Cain, A., & Burris, M. (1999, April). *Investigation of the Use of Mobile Phones while Driving.* Retrieved from http://www.cutr.eng.usf.edu/its/mobile_phone_text.htm

Archer, Z. (n.d.). *Exploring Nonverbal Communication*. Retrieved from http://zzyx.ucsc.edu/~archer

A cd-rom publication:

Reporter, M. (1996, April 13). Electronic Citing Guidelines Needed [CD-ROM]. *New York Times*, (late ed.), p. c1. Retrieved from New York Times Ondisc.

► **Websites**

Website of an organization or government:

Wisconsin Department of Natural Resources. (2001). *Glacial Habitat Restoration Areas*. Retrieved from http://www.cscanada.net/index.php/hess

Midwest League. (n.d.). *Pitching, Individual Records*. Retrieved from http://www.cscanada.net/index.php/hens

A personal homepage: (retrieval date is included due to possibility of change)

Duncan, D. (1998, August 1). *Homepage*. Retrieved July 30, 2007 from http://www.cscanada.net/index.php/ibm

A posting to an online discussion group or listserv:

Marcy, B. (1999, April 3). Think They'll Find any Evidence of Mallory & Irvine [electronic mailing list message]. Retrieved from http://www.cscanada.net/index.php/mse

A blog post:

MiddleKid. (2007, January 22). The Unfortunate Prerequisites and Consequences of Partitioning Your Mind [Web log message]. Retrieved from http://www.cscanada.net/index.php/pam

An online video:

Norton, R. (2006, November 4). *How to Train a Cat to Operate a Light Switch* [Video file]. Retrieved from http://www.cscanada.net/index.php/sll

NOTE: The URL should not be underlined. Sometimes underlining appears automatically when a URL is displayed in a browser or in Word. Remove the underlining before submitting your paper.

Footnotes

Content footnotes are occasionally used to support substantive information in the text (or to acknowledge copyright permission status). They begin on a separate page with a heading centered on the first line below the manuscript page header. The first line of each footnote is indented 5-7 spaces and they are numbered with Arabic superscript numerals following punctuation marks within the text.

Tables

Tables should each be presented portrait (not landscape) direction and upright on the page, not sideways. Tables have a short, one-line title in bold text. Tables should be no larger than one page (140mm*180mm). Symbols and abbreviations are definite immediately below the table, followed by essential descriptive material as briefly as possible, all in double-spaced text. We also use APA format on tables you can visit http://www.apastyle.org/ for detail information. Here is the example. We strongly advise you to put your tables at the relevant places in your article not in the end of your article.

Table 1
Error Rates of Older and Younger Groups

Number	Group1	Group 2	Total	Older 1	Younger 1
1	A11	A21	A31	A51	Y1
2	A12	A22	A32	A52	Y2
3	…	…	…	...	5
…	…	…	…	…	…
n	A1n	A2n	A3n	A5n	Yn

Top line: 1.5 pt
Middle line: 0.25 pt
Bottom line: 2.25 pt

Figures

CSCanada requires figures in electronic format. Figures should be as small and simple as is compatible with clarity. The goal is for figures to be comprehensible to readers in other or related disciplines, and to assist their understanding of the paper. Unnecessary figures and parts (panels) of figures should be avoided. Avoid unnecessary complexity, colorful and over amount of details. For instruction, *CSCanada* standard figure sizes are 95mm (single column) and 190mm (double column) and the full depth of the page is 283mm. We strongly advise you to put your figures at the relevant places in your article **not** in the end of your article. The figures also are suggested in APA format you can visit http://www.apastyle.org/ for detail information.

• Units should have a single space between the number and the unit, and follow SI nomenclature or the nomenclature common to a particular field. Thousands should be separated by commas (1,000). Unusual units or abbreviations are defined in the legend. Scale bars should be used rather than magnification factors. Where possible, text, including keys to symbols, should be provided in the legend rather than on the figure itself. At initial submission, figures should be at good quality to be assessed by referees, ideally as JPEGs, PNGs, and BMPs.

Editorial

Editorials are the voice of the journal and are written by the journal's editorial-writing team and usually present commentary and analysis concerning an article in the issue of the journal in which they appear. They may include 3 figures or tables. They are nearly always solicited, although unsolicited editorials may occasionally be considered. Editorials are limited to 1500 words, with up to 30 references.

RECRUITMENT

We are seeking qualified researchers and scholars to join our editorial team as editors, sub-editors or reviewers. For more information, please send an email to: caooc@hotmail.com, office@cscanada.net, office@cscanada.org.

CALL FOR PAPERS

All *CSCanada* journals welcome innovative contributions. The host organizations of our 14 journals are *Canadian Academy of Oriental and Occidental Culture, Canadian Research & Development Center of Sciences and Cultures* with their headquarter in Montreal, Canada registered in Quebec and are committed to scientific research and spreading eastern and western cultures. Please submit your paper according to our guide on the website www.cscanada.org.

PUBLICATION FEE

All *CSCanada* journals are international, peer-reviewed, Open-Access journals. Articles published by our journals are distributed under the terms of the Creative Commons Attribution Non-commercial License, provided the original work is properly cited, the use is non commercial and is otherwise in compliance with the license. Authors of accepted articles must pay a publication fee. The related standards are as follows. Publication fee in 2012: $300 USD per article. After the payment is done, authors have to send the proof of payment to related email address.

Advances in Petroleum Exploration and Development

ISSN 1925-542X [Print]
ISSN 1925-5438 [Online]

Subscriptions Form

Name_____

Title_____

Company_____

Address 1_____

Address 2_____

Country_____

Postal Code_____

Telephone_____

Fax_____

E-mail_____

Website_____

All correspondence concerning subscriptions should be sent to:
Canadian Research & Development Center of Sciences and Cultures

Address:

758, 77e AV, Laval, Quebec, H7V 4A8, Canada

Contact with us by:
Http://www.cscanada.org Http://www.cscanada.net
E-mail: aped@cscanada.net aped@cscanada.org caooc@hotmail.com

APED

Advances in Petroleum Exploration and Development

Volume 3
Number 1
31 March 2012

Peer Reviewed Journal

Canadian Research & Development Center of Sciences and Cultures
www.cscanada.net www.cscanada.org

Indexed by
Chemical Abstracts Service (CAS, a division of The American Chemical Society)
Gale
ProQuest
EBSCO Publishing
Ulrich's
AMICUS
CNKI
DOAJ
Journal TOCs
Open J-gate

Filed by
Library and Archives Canada
Bibliothèque nationale du Québec

ISSN 1925-542X